ISTANBUL TECHNICAL UNIVERSITY ★ GRADUATE SCHOOL

DEVELOPMENT OF SUPRAMOLECULAR HYDROGELS WITH ADJUSTABLE VISCOELASTIC, MECHANICAL AND SELF-RECOVERING PROPERTIES

Ph.D. THESIS

Esra SU

Department of Chemistry

Chemistry Programme

OCTOBER 2021

ISTANBUL TECHNICAL UNIVERSITY ★ GRADUATE SCHOOL

DEVELOPMENT OF SUPRAMOLECULAR HYDROGELS WITH ADJUSTABLE VISCOELASTIC, MECHANICAL AND SELF-RECOVERING PROPERTIES

Ph.D. THESIS

Esra SU
(509152005)

Department of Chemistry

Chemistry Programme

Thesis Advisor: Prof. Dr. Oğuz OKAY

OCTOBER 2021

İSTANBUL TEKNİK ÜNİVERSİTESİ ★ LİSANSÜSTÜ EĞİTİM ENSTİTÜSÜ

AYARLANABİLİR VİSKOELASTİK, MEKANİK VE KENDİ-KENDİNİ ONARMA ÖZELLİKLERİNE SAHİP SUPRAMOLEKÜLER HİDROJELLERİN GELİŞTİRİLMESİ

DOKTORA TEZİ

Esra SU
(509152005)

Kimya Anabilim Dalı

Kimya Programı

Tez Danışmanı: Prof. Dr. Oğuz OKAY

EKİM 2021

Esra SU, a Ph.D. student of ITU Graduate School student ID 509152005, successfully defended the thesis entitled "DEVELOPMENT OF SUPRAMOLECULAR HYDROGELS WITH ADJUSTABLE VISCOELASTIC, MECHANICAL AND SELF-RECOVERING PROPERTIES", which she prepared after fulfilling the requirements specified in the associated legislations, before the jury whose signatures are below.

Thesis Advisor :	**Prof. Dr. Oğuz OKAY** İstanbul Technical University	.....
Jury Members :	**Prof. Dr. Nermin ORAKDÖĞEN** Istanbul Technical University	.....
	Prof. Dr. Yıldırım ERBİL Gebze Technical University	.....
	Prof. Dr. Orhan GÜNEY Istanbul Technical University	.....
	Assoc. Prof. Deniz C. TUNCABOYLU Bezmialem Vakif University	.....

Date of Submission : 10 September 2021
Date of Defense : 05 October 2021

To my family,

FOREWORD

I am excited to complete my doctoral thesis, which I have prepared with serious effort and dedication over the years. I will use this section as an opportunity to thank the people who have stood by me and supported me during this difficult process.

First of all, I would like to thank my advisor, Oğuz OKAY, who took me as my advisor by including me in the research group and did not limit me in any way, including the choice of subject and conducting the studies, but on the contrary, allowed the doctoral student to demonstrate his competence.

I would like to thank my thesis monitoring juries, Prof. Dr. H. Yıldırım ERBİL, Prof. Dr. Nermin ORAKDÖĞEN, who participated in my thesis defenses and helped shape the thesis with their constructive criticisms and valuable opinions.

Thanks to Polymeric Gels Research Lab (PGRL) former and current members, and my colleagues from the department.

I can't find the words to express my gratitude to my family, especially my father, who have always loved and cared for me all my life.

I would also like to thank the Scientific and Technical Research Council of Turkey for its general domestic doctorate scholarship (TUBITAK 2211-A) and for the financial support it provided during the project studies (218M502).

September 2021

Esra SU
(M.Sc. Chemist)

TABLE OF CONTENTS

Page

ABBREVIATIONS

µ-CT	**:** Micro-computed tomography
2D	**:** Two-dimensional
3D	**:** Three-dimensional
AMPS	**:** 2-acrylamido-2-methylpropane sulfonic acid
AMPS-Na	**:** Sodium salt of AMPS
BAAm	**:** N,N'-methylene(bis)acrylamide
BSSE	**:** Basis set superposition error
CV	**:** Crystal violet
DMAA	**:** N,N-dimethylacrylamide
DSC	**:** Differential scanning calorimetry
GPC	**:** Gel permeation chromatography
IRGACURE	**:** 2-Hydroxy-4′-(2-hydroxyethoxy)-2-methylpropiophenone
KPS	**:** Potassium persulfate
NaOH	**:** Sodium hydroxide
PAMPS	**:** Poly(AMPS)
PEG	**:** Polyethylene glycol)
PEO	**:** Polyethylene oxide
PLA	**:** Poly(lactic acid)
PNIPA	**:** Poly(N-isopropylacrylamide)
QMC	**:** Quantum mechanical calculation
SEM	**:** Scanning electron microscopy
TEMED	**:** N,N,N',N'-tetramethylethylenediamine
UV	**:** Ultraviolet
VOI	**:** Volume of interest

SYMBOLS

ΔH_m	: Melting enthalpy of ice
$\dot{\varepsilon}$	: Strain rate
ε_f	: Strain at break
ε_{eff} *or* ε_h	: Healing efficiency
ε_{max}	: Maximum strain
ε, λ *or* γ	: Strain
λ	: Deformation ratio
λ_f	: Deformation ratio at break
λ_s	: Elongation ratio at break in equilibrium swollen state
$\dot{\gamma}$	: Shear rate
γ_c	: Critical shear rate
γ_o	: Strain amplitude
η	: Viscosity
η_o	: Zero-shear viscosity
σ_f	: Fracture stress
$\sigma_{\mathbf{nom}}$	: Nominal stress
$\sigma_{\mathbf{true}}$	: True stress
ω	: Angular frequency
τ	: Lifetime
χ_{DMAA}	: Mol fraction of DMAA
a_s	: Chain expansion at equilibrium degree of swelling
A	: Counterion distance
b	: Bond length
$\mathbf{C_o}$	: Monomer concentration
$\mathbf{C_{true}}$	: True monomer concentration
d_1	: Density of ice
d_{Ace}	: Density of acetone
D	: Average pore diameter
D_{dry}	: Diameter of gel in dried state
D_s	: Diameter of equilibrium swollen gel

E : Young's modulus

E_i : Instantaneous modulus

f_{diss} : Ratio of dissipated energy

$f_{H\text{-}bonds}$: Fraction of crosslink

f_{unf} : Fraction of unfrozen water

f_v : Fraction of broken bonds

G' : Storage modulus

G'' : Loss modulus

G_R : Rouse modulus

$G(t)$: Relaxation modulus

H_2O % : Water content

l : Layer spacing

m : Mass of equilibrium swollen gel

m_{Ace} : Mass of equilibrium swollen gel in acetone

m_{dry} : Mass of equilibrium swollen gel

m_o : Mass of dry gel

m_{rel} : Relative weight swelling ratio

M_n : Number-average molecular weight

n : Shear thinning index

q_v : Equilibrium volume swelling ratio

q_w : Equilibrium weight swelling ratio

$q_{v,t}$: Volume swelling ratio

$q_{w,t}$: Weight swelling ratio

Q : Bjerrum length

R : Resilience

R_f : End-to-end distance of network chain at the point of fracture

R_o : End-to-end distance of network chain in as-prepared

R_s : End-to-end distance of network chain in equilibrium swollen state

t : Time

$\tan \delta$: Loss factor

T_m : Melting temperature

U_{hys} : Hysteresis energy

U_{xl} : Average dissociation energy

v_e : Cross-link density

$v_{e,dry}$: Cross-link density of dry polymer

ν_2^o : Volume fraction of crosslinked polymer

V_{ice} : Volume of ice

V_P : Pore volume

w_{AMPS} : Weight fraction of AMPS

W : Toughness

W_g : Gel fraction

LIST OF TABLES

Page

LIST OF FIGURES

Page

DEVELOPMENT OF SUPRAMOLECULAR HYDROGELS WITH ADJUSTABLE VISCOELASTIC, MECHANICAL AND SELF-RECOVERING PROPERTIES

SUMMARY

Biological systems are living systems with unique features such as self-healing, reorganization, and being able to respond to external stimuli. The production of synthetic materials with similar properties by imitating biological systems will prevent the loss of both raw material and energy and will increase the quality of life. Thanks to the new generation hydrogels with these features, soft and smart materials, underwater adhesives, wound dressings, actuators, sensors and many more will be used in daily life to replace the living tissues. Today, many research groups continue their studies for the production of hydrogels with a double network structure, nanocomposite hydrogels, cryogels, tough and shrinkable gels, as well as cost-effective soft devices. Despite all these efforts, the design of autonomous self-healing soft materialswith a high mechanical strength is still a big problem.

In the first part of the thesis, self-healing hybrid crosslinked poly(2-acrylamido-2-methylpropanesulfonic acid) (PAMPS)-based hydrogels with a high mechanical strength were synthesized by solution polymerization of AMPS without using any initiator. Although PAMPS hydrogels have been in use for many years due to their large swelling capacities, they are brittle and exhibit no self-healing behavior limiting their applications. Recently, PAMPS hydrogels were prepared without an initiator by thermal polymerization. However, these hydrogels were easily soluble in water and their use was also limited due to their poor mechanical properties. To develop high mechanical strength in PAMPS hydrogels and hinder their water solubility, three strategies were applied in the first part of the thesis, namely, clay nanoparticles and a chemical crosslinker were included into the reaction system both separately and together to produce nanocomposite, chemically cross-linked, and hybrid cross-linked PAMPS hydrogels, respectively. Although both nanocomposites and chemically cross-linked hydrogels up to 2 mol% crosslinker content PAMPS hydrogels were weak and easily soluble in water, hybrid crosslinked ones formed using both clay nanoparticles and chemical crosslinkers were water insoluble, and exhibited good compressive mechanical properties with a Young's modulus of around 0.7 MPa together with a sel-healing ability. The hybrid strategy thus developed within the framework of the thesis is a novel and general approach for the production of nanocomposite ionic hydrogels with self-healing ability.

The synthesis of water-stable PAMPS hydrogels formed by only H-bonding interactions has not reported before. This is due to the 100-fold weaker strength of H-bonds compared to the covalent bonds, leading to the dissociation of H-bonds between the PAMPS chains in water. However, cooperativity of H-bonds similar to those in double-stranded DNA would create H-bonded physical hydrogels of high mechanical strength. This was the idea behind the experiments conducted in the

second part of the thesis. UV photopolymerization of AMPS in water was conducted in the presence of 2-hydroxy-4'-(2-hyroxyethoxy)-2-methylpropiophenone (Irgacure 2959) photoinitiator at a high AMPS concentration without using any chemical crosslinkers. As compared to the thermal polymerization at 80 °C leading to water soluble PAMPS hydrogels, UV polymerization at 23±2 °C produces water-insoluble hydrogels exhibiting an equilibrium swelling ratio of 1013±53, i.e., the mass of the hydrogel around 1013-fold increases upon swelling in an excess of water. Although the hydrogels are stable in water, they all could be dissolved in aqueous urea solutions due to the breaking of H-bonds. The network chains of PAMPS hydrogels formed by UV polymerization was found to have a much higher molecular weight as compared to those obtained by thermal polymerization. This reflects strengthening of H-bonds with increasing chain length due to the so-called proximity effect. Moreover, the addition of N,N-dimethylacrylamide (DMAA), a non-ionic monomer, to the UV polymerization system further improved both the mechanical properties and self-healing behavior of PAMPS hydrogels. The results could be explained with the hydrogen donor-acceptor relationship between DMAA-AMPS units. Because the hydrogels are physically cross-linked by H-bonds, they heal completely within minutes without any external stimuli. In addition to self-healing, the combination of supramolecular crosslinks also imparted shape-memory properties to the PAMPS hydrogels.

Cryogelation is a simple and environmentally friendly technique for the production of macro-porous hydrogels, called cryogels, which exhibit extraordinary properties such as a large porosity, full squeezability, high toughness, and super-fast responsiveness. Cryogelation reactions are usually conducted at 10 to 20 °C below the freezing temperature of the reaction solution and hence, the reactions proceed in the unfrozen domains of the apparently frozen reaction system. Because of the cryoconcentration, the concentrations of the reactants in the unfrozen domains significantly deviate from those in the initial reaction system. Therefore, the cryogel studies reported so far are incomplete as they consider the initial conditions instead of the real conditions of the cryogelation system. Within the scope of the third part of the thesis, the relationship between the real conditions of the cryogelation, that is, the conditions in the unfrozen domains, and the cryogel properties were investigated. For this purpose, cryogelation of AMPS in the presence of N,N'-methylene(bis)acrylamide (BAAm) as a crosslinker was conducted in aqueous solutions at 18 °C. Two series of experiments were carried out to highlight the effects of the chemical crosslinker BAAm, and the initial monomer concentration C_0 on the cryogel properties. In the first series, the amount of BAAm was changed in the range of 1.2-9.1 mol% while the monomer concentration, C_0 was fixed at 10%. It was found that the swelling capacity of the cryogels decreases with the increasing amount of the crosslinker while, their mechanical strength increases. This improvement was reflected in a 7-fold increase in Young's modulus and 4-fold increase in the fracture stress of the cryogels. In the second series, the initial monomer concentration C_0 was changed between 10 and 25 wt% at a crosslinker content of 1.2 mol%. The mechanical properties of the cryogels remained almost unchanged by varying C_0 while their swelling capacity decreased as C_0 is increased. It was also observed that the cryogels formed at 10 and 15 wt% monomer concentration were transparent when swollen in water, while those formed at 20 and 25 wt% were opaque indicating the onset of a phase separation during reactions. As mentioned above, the main aim of this last section was to determine the actual reaction condition under which cryogelation took place and to examine its reflection

on the final cryogel properties. For this purpose, the real monomer concentration (C_{true}) in the unfrozen domains, and the volume of ice V_{ice} acting as a template for the pores were determined by DSC measurements conducted on apparently frozen reaction solutions. Although the real monomer concentration C_{true} was independent on the actual concentration C_o, both the ice volume V_{ice} and the ratio C_{true}/C_o decreased with increasing C_o. These changes determined both the morphology and mechanical properties of PAMPS cryogels. In short, the experiments carried out in this section have shown that it is possible to control the structure of the final cryogels by controlling the real synthesis conditions during cryogelation.

AYARLANABİLİR VİSKOELASTİK, MEKANİK VE KENDİ-KENDİNİ ONARMA ÖZELLİKLERİNE SAHİP SUPRAMOLEKÜLER HİDROJELLERİN GELİŞTİRİLMESİ

ÖZET

Biyolojik sistemler; kendini onarma, yeniden düzenlenme ve dış uyarılara cevap verebilme gibi eşsiz özelliklere sahip sistemlerdir. Biyolojik sistemleri taklit ederek benzer özellikler gösteren malzeme üretimi hem ham madde hem de enerji kaybını önleyecek, yaşam kalitesini yükseltecektir. Bu özelliğe sahip hidrojel malzemeler sayesinde günlük hayatta esneyebilir yumuşak malzemeler, sualtı yapıştırıcılar, yara örtüleri, harekete geçiriciler, sensörler ve daha birçokları günlük hayatta kullanılabilir hale gelecek ve canlı dokuların yeri doldurulabilecektir. Günümüzde birçok araştırma grubu; çift ağ yapılara sahip hidrojeller, nanokompozit hidrojeller, kriyojeller, tok ve elastik jeller veya uygun maliyetli yumuşak robotların üretimi için çalışmalarını sürdürmektedir. Bütün bu çabalara rağmen hala otonom olarak kendini onarabilen ve aynı zamanda mekanik dayanımı yüksek yumuşak malzeme tasarımı büyük bir problemdir.

Bu sorunlara çözüm üretebilmek adına yürütülen tez çalışmaları 3 ana kısma ayrılmıştır. Çalışmalar kapsamında başlıca 2-akrilamido-2-metilpropan sulfonik asit (AMPS) monomeri kullanılmış ve çeşitli stratejiler uygulanarak kendini onarabilen poli(AMPS) (PAMPS) hidrojelleri elde edilmiştir. Yüksek derecede su emme kapasiteleri ve geniş potansiyel uygulama alanlarına karşın mekanik dayanımlarının düşük oluşu, dolayısıyla kolaylıkla parçalanması ve kendini onaramaması nedeniyle tez kapsamında PAMPS hidrojeli seçilmiştir. İlk kısımda yüksek sıkıştırma direnci gösteren, tok ve kendini onarabilen hibrit çapraz bağlı PAMPS hidrojeller kil nanopartikülleri ve çapraz bağlayıcı içeren AMPS sulu çözeltilerinden elde edilmiştir. İkinci kısım çalışmaları kapsamında ise H-bağlarından oluşan 3-boyutlu bir polimer ağyapıya sahip suda 1000 katı şişebilen ve %1000 çekilebilir, aynı zamanda da kendini %100 onarabilen PAMPS temelli hidrojeller geliştirilmiştir. Son kısım çalışmaları ise PAMPS temelli kriyojellerin gerçek sentez koşulları ve yapı-morfoloji ilişkisinin aydınlatılmasına ayrılmıştır. Aşağıdaki paragraflarda her bir bölüm içinde gerçekleştirilen çalışmaların ayrıntıları verilmiştir.

Tez çalışmasının ilk kısmında herhangi bir başlatıcı kullanmadan PAMPS temelli ve mekanik dayanımı yüksek, kendini onarabilen hidrojeller termal polimerizasyon ile sentezlenmiştir. Bu tip bir malzeme daha önce elde edilmemiş olup geliştirilen hidrojel ürünler tezin ilk kısmının özgün değeridir. Son yıllarda yayınlanmış bir makalede termal polimerizasyonla başlatıcı olmaksızın kendini onarabilen PAMPS hidrojeli eldesi rapor edilmiştir. Ancak, bu jelin zayıf mekanik özellikleri ve suda çözünebilir olması nedeniyle kullanımı sınırlıdır. Buradan yola çıkarak yapıya kimyasal çapraz bağlayıcı ve nanokil ilavesiyle mekanik dayanımı yüksek hibrit çapraz bağlı PAMPS hidrojeller geliştirilmeye çalışılmıştır. Kimyasal çapraz bağlayıcı ve nanokilin (Laponit) ayrı ayrı eklendiği çalışmalar sonucu elde edilen

hidrojellerin suda kolaylıkla çözündüğü, mekanik özelliklerinde ise herhangibir iyileşme olmadığı gözlenmiştir. Buna karşılık kimyasal çapraz bağlayıcı ve Laponit'in birarada kullanımı ile yüksek mekanik dayanım, suda çözünmezlik ve kendini onarma özelliğine sahip hibrit çapraz bağlı PAMPS hidrojelleri sentezlenmiştir. Deneysel bulgular, yüksek derişimde Laponit'in 'iskambil kağıt evi' yapısı oluşturması ve hidrojelde mevcut kimyasal çapraz bağ noktalarının yapı bütünlüğünün korunmasına yardımcı olması ile açıklanmıştır. Yapılan çalışmalar sonucunda 45 MPa'a kadar varan sıkıştırma gerilimine dayanan ve kendini onaran hidrojeller elde edilmiştir. Kil nanopartiküllerini ve kimyasal çapraz bağlayıcıyı bir arada kullanilarak tez kapsamında geliştirilen hibrit stratejisi aynı zamanda iyonik nanokompozit hidrojellerin üretimi için yeni, özgün ve genel bir yaklaşım olarak literatüre kazandırılmıştır.

Termal polimerizasyonla sentezlenen PAMPS hidrojelinin kendini onarma özelliğinin yanı sıra yüksek sıkıştırma direnci göstermesine rağmen çekilebilir olmaması geliştirilen malzemenin bir dezavantajı olarak ortaya çıkmıştır. Diğer yandan hidrojel sentezlerinde kil nanopartikülleri ile kimyasal çapraz bağlayıcısı da kullanılmaktadır. Hiçbir katkı olmadan, sadece AMPS monomeri kullanılarak suda kararlı, sadece H-bağı etkileşimleri yardımıyla fiziksel PAMPS hidrojel sentezi daha önce literatürde yayınlanmamıştır. Bunun nedeni, H-bağlarının kovalent bağlara oranla yaklaşık yüz misli zayıf oluşu, dolayısıyla su ortamında PAMPS zincirleri arasındaki H-bağlarının kolaylıkla parçalanmasıdır. Ancak, çift-sarmal DNA moleküllerinde olduğu gibi kooperatif H-bağlarının oluşturulması suretiyle mekanik dayanımı yüksek ve suda kararlı H-bağlı PAMPS hidrojelleri elde edilebilir. Tezin ikinci kısmında yapılan deneysel çalışmalarının arkasında bu fikir bulunmaktadır. Yapılan denemelerde AMPS'nin termal polimerizasyonu yerine fotopolimerizasyonu uygulanmış olup ilk etapta her iki polimerizasyon tekniğinin hidrojel ürün üzerine etkileri kıyaslanmıştır. Bu amaçla yapılan denemelerde ağırlıkça % 50 AMPS monomerinin sulu çözeltisi başlatıcı veya çapraz bağlayıcı olmaksızın etüvde 80°C'de ve 24 saat termal polimerizasyonu, buna paralel olarak 365 nm'de UV ışık altında 2-hydroxy-4'-(2-hydroxyethoxy)-2-methylpropiophenone (Irgacure 2959) fotobaşlatıcısı varlığında 23±2 °C'de ve 24 saat fotopolimerizasyonu yapılmıştır. Termal polimerizasyonla sentezlenen PAMPS hidrojeli suda kolayca çözünürken UV fotopolimerizasyon sentezi sonucu elde edilen hidrojelin suda şiştiği ama şeklini koruduğu saptanmıştır. Bunun nedenini anlayabilmek için elde edilen hidrojeller olası H-bağlarını koparacak üre çözeltisinde (5 M) çözülmüş, saf suya karşı diyaliz edilmiş, ardından jel geçirgenlik kromatografisi (GPC) yardımıyla molekül ağırlıkları tayin edilmiştir. UV ve termal polimerizasyon ile elde edilen hidrojellerdeki polimer zincirlerinin molekül ağırlıklığının sırasıyla 750.000 ve 8.300 g/mol olduğu, yani UV polimerizasyonu ile yaklaşık 100 kat daha uzun zincirlerin oluştuğu saptanmıştır. GPC ölçümleri sonuçları UV polimerizasyonu sonucu elde edilen PAMPS hidrojellerinin suda çözünmezliğini ve yüksek mekanik performansını açıklamaktadır. PAMPS zincir uzunluğu arttıkça zincir içi ve zincirler arası H-bağı oluşturma olasılığı artmakta, dolayısıyla daha fazla sayıda fiziksel çapraz bağlar oluşturmakta, bunun sonucu olarak UV polimerizasyonu sonucu elde edilen hidrojelin %99'dan fazla su emmesine rağmen suda çözünmeden kalabilmesini sağlamaktadır.

Yukarıdaki paragrafta bahsedilen ve herhangi bir kimyasal çapraz bağlayıcı kullanmadan UV fotopolimerizasyon tekniği ile PAMPS hidrojelleri sentezi literatürde daha önce yayınlanmamıştır. PAMPS hidrojellerinin mekanik dayanımını

daha da arttırmak için başlangıç monomer derişimini arttırmaya yönelik bir dizi deney gerçekleştirilmiştir. Denemelerde, AMPS monomerinin sudaki çözünürlük sınırı nedeniyle ağırlıkça en fazla ağırlıkca % 60 konsantrasyonda polimerleştirilebilmiştir. Ancak sulu AMPS çözeltisine iyonik olmayan bir monomer olan N,N-dimetilakril amid (DMAA) ilave edilerek başlangıç monomer derişimi % 80'e kadar çıkarılmıştır. Başlangıç monomer derişiminin artırılmasıyla mekanik özelliklerde kaydedilen iyileşmenin beklenenin üzerinde olduğu anlaşılmıştır. En yüksek mekanik özelliğe sahip hidrojel, monomer karışımında DMAA miktarınının molce % 60 ve toplam monomer konsantrasyonunun ağırlıkca %75 olduğu reaksiyon çözeltisinden elde edilmiştir. Diğer yandan tüm hidrojellerin 7-10 M konsantrasyonda sulu üre çözeltilerinde çözündükleri, yani hidrojel ağyapılarının sadece H-bağları ile oluştuğu saptanmıştır. GPC ölçümleri, kopolimer ağyapı zincirlerinin molekül ağırlığının 1.400.000 g/mol olduğunu, yani homopolimer zincirlere oranla iki kat daha büyük olduğu saptanmıştır. Diğer yandan yapılan çalışmalar sonunda AMPS'nin kendiliğinden çapraz bağlanma mekanizması aydınlatılmış olup DMAA-AMPS arasındaki hidrojen verici-alıcı ilişkisi sayesinde tamamen kendini onarma davranışı gösteren PAMPS hidrojelleri geliştirilmiştir. %1000 çekilebilirliğe ve 0,6 MPa'a varan kopma gerilimine sahip olan hidrojeller, herhangi bir kimyasal çapraz bağ içermemelerine rağmen suda çözünmemekte ve kendi ağırlıklarının 1000 katından fazla su tutma kapasitesine sahiptirler. Dolayısıyla bu bölüm çalışmaları sonunda fiziksel çapraz bağlı süperabsorban polimer (SAP) malzemeler geliştirilmiştir. Tüm PAMPS hidrojelleri tamamen tersinir hidrojen bağları ile çapraz bağlandığından, hidrojel dakikalar içinde ve herhangi bir dıştan uyarıya gerek olmadan %100'e yakın bir etkinlikle kendilerini onarabilmektedir. Buna ek olarak supramoleküler çapraz bağların kombinasyonu malzemeye şekil-hafıza özelliği de kazandırmıştır. Sonuç olarak tez çalışmalarının ikinci kısmında sadece komplementer H-bağları ile neler yapılabileceğini ortaya koymuş olup ileride bu konuda yapılacak çalışmalara yön verecektir.

Tezin ilk iki kısmında yapılan çalışmalar bütünüyle yeni nesil PAMPS hidrojellerin geliştirilmesine yönelik olup kendini onarabilen ve aynı zamanda yüksek mekanik performans gösteren hidrojeller sentezlenmiştir.

Tezin son kısmında ise PAMPS kriyojellerin geliştirilmesi ve kriyojelleşme sisteminin gerçek koşullarını aydınlatmak amaçlanmıştır. Kriyojelleşme, geniş gözeneklilik, tamamen sıkılabilirlik, yüksek tokluk, uyaranlara super hızlı yanıt verme gibi olağanüstü özellikler gösteren ve kriyojel olarak adlandırılan makro-gözenekli hidrojellerin üretimine yönelik basit ve çevre dostu bir uygulamadır. Şimdiye kadar raporlanan kriyojel çalışmaları, kriyojelleşme sisteminin gerçek koşullarını açığa çıkarmada eksik kalmıştır. Tez çalışmaları kapsamında kriyojelleşmenin, yani donma noktasının altındaki reaksiyon sisteminin gerçek koşulları ile kriyojel özellikleri arasındaki ilişki incelenmiştir. Bu kısımda gerçekleştirilen deneyler sadece sentez koşulları kontrol edilerek nihai ürünün yapısını kontrol edebilmenin mümkün olduğunu göstermiştir.

Kriyojel çalışmaları iki ana grupta gerçekleştirilmiştir. İlk grupta başlangıç monomer derişimi ağırlıkça % 10 olacak şekilde sabit tutularak kimyasal çapraz bağlayıcı (BAAm) etkisi incelenmiştir. Bunun için monomere oranla BAAm miktarı molce % 1,2 ve 9,1 aralığında değişitirilerek elde edilen kriyojellerin mekanik özellikleri incelenmiştir. İkinci seride ise BAAm miktarı molce %1,2 olacak şekilde sabit tutularak başlangıç monomer derişimi C_o % 10-25 aralığında değiştirilmiştir. Sentez sırasında hazırlanan çözeltiler sıvı azota daldırılarak ön-soğutma işlemine tabi

tutulmuştur. Bu ön soğutma işlemi, reaksiyon çözeltisinin polimerizasyon reaksiyonları başlamadan önce donmasını sağlamak amacıyla uygulanmıştır. Diğer yandan bu işlem sonucunda polimerizasyon öncesi oluşan buz kristalleri reaktörün dış yüzeyinden içe doğru yönlenmiş olup, buna bağlı olarak da yönlenmiş ve tabakalı yapıya sahip kriyojeller elde edilmiştir. Sıklıkla biyolojik sistemlerde iskelet görevi için hazırlanan kriyojellerin bu şekilde tabakalı olması hücre tutunma kabiliyetini arttıracağından deneyler bu koşullarda sürdürülmüştür. Çalışmalar sonunda gerçek kriyojelleşme koşulları aydınlatılmış olup, kriyojelleşme koşulları ve yapı-mekanik özellik ilişkisi açıkça ortaya konmuştur. Elde edilen sonuçlara göre başlangıç monomer derişimi ne olursa olsun kriyo-konsantrasyon sonucu donmamış bölgelerdeki monomer konsantrasyonu, diğer bir ifade ile gerçek monomer konsantrasyonu sabit kalmaktadır. Bu ilginç bulgu gelecek çalışmalar için oldukça önem arz etmektedir. Ayrıca başlangıç monomer konsantrasyonunun artması ile donabilecek su miktarı da azaldığından sıvı azot etkisiyle elde edilen yönlenme artan monomer konsantrasyonu ile azalmaktadır. Tezin son kısmında yürütülen çalışmalar sonunda kriyojelleşme sırasındaki gerçek sentez koşulları açığa çıkarılarak, nihai ürün özelliklerindeki değişim de aydınlatılmıştır. Kısacası bu bölümde gerçekleştirilen denemeler sonunda oldukça kolay ve erişilebilir DSC ölçümleri ile kriyojelleşme sisteminin optimum koşullarının belirlenebileceği ve istenen malzeme özelliklerine seri denemeler yerine nokta atışı olarak ulaşılabileceği gösterilmiştir. Tezin son kısmında edinilen bulguların kriyojeller konusundaki yeni araştırmalara öncülük edeceği düşünülmektedir.

1. INTRODUCTION

Hydrogels are water-swollen three-dimensional hydrophilic polymer networks with physical properties similar to soft biological tissues. The hydrophilicity of the polymer network is due to its hydrophilic groups such as amine ($–NH_2$), carboxyl (–COOH), hydroxyl (–OH), amide (–CONH–) and sulfonic acid ($–SO_3H$). The characteristic features of smart hydrogels such as functionality, reversible swelling/shrinkage behavior, high environmental sensitivity, sterilizability, ionic conductivity, high absorption capacity and biocompatibility make them biosensors, contact lenses, drug carriers, metal and dye adsorbent, controlled release agents, etc., and provide many application areas. In addition, these properties make it possible to use hydrogels in organ and tissue applications, artificial muscles and wearable devices.

In the literature, hydrogels have been classified differently according to their source, type of crosslinking, and the stimuli to which they react. According to the way of crosslinking, hydrogels can be divided into two main categories: covalent (chemically crosslinked) hydrogels and supramolecular (physically crosslinked) hydrogels. Generally, synthetic hydrogels are formed through irreversible covalent bonds, that is, with permanent chemical crosslinking points between polymer chains. Supramolecular hydrogels are a new class of non-covalent cross-linked polymeric materials that perfectly combine the advantages of supramolecular polymers and synthetic chemically crosslinked hydrogels.

Although synthetic hydrogels formed via chemical crosslinks have many applications, they are often brittle, opaque, and incapable of self-healing. However, the dynamic nature of supramolecular hydrogels gives them tunable mechanical properties; It gives the ability to respond to physical (temperature, light, electric and magnetic field) and chemical (pH, ionic strength, enzymes, etc.) external stimuli. This adjustability gives the material a wide range of applications, including drug delivery carriers and tissue engineering. Compared to chemically crosslinked hydrogels, supramolecular hydrogels also show properties such as injectability or

easily processability for biomedical applications. One of the most attractive properties of supramolecular polymeric networks is their ability to self-repair when damaged.

Self-healing is one of the remarkale properties of biological materials such as skin, bone, and wood. Inspired by the ability of natural materials to heal cracks without disrupting the integrity of the structure, thanks to the energy distribution mechanism, studies are carried out to bring this ability to synthetic materials. For synthetic materials, this phenomenon was first noticed by Leibler and co-workers [1]. They synthesized a mixture of oligomers containing hydrogen-bonding urea groups from materials of natural origin such as aliphatic diacids and triacids. The supramolecular arrangement of these components enables the material to self-heal within minutes of being damaged. However, the problem of poor mechanical performance of self-healing hydrogels has not been resolved. These poor mechanical properties limit the use of self-healing hydrogels in cartilage and tissue engineering applications. In short, the demand for the development of tough self-healing hydrogels is huge. However, the main problem for self-healing hydrogels has still not been solved because, it requires the combination of two opposite characters, namely the mobility of the network chains and the mechanical toughness of the water-swollen polymer network.

The preferred monomer used in this thesis is 2-acrylamido-2-methyl-1-propanesulfonic acid (AMPS), which can be used to obtain highly swollen hydrogels in water. AMPS is an ionic monomer frequently used in the synthesis of polyelectrolyte hydrogels with a high water holding capacity. The combination of the twin dimethyl group and the sulfomethyl group provides hydrolytic and thermal stability to AMPS-containing polymers. The fully ionizable sulfonate group of AMPS causes the linear polymers derived from it to dissolve completely over a wide pH range. While in the 1970s there were patents for the use of this monomer only for the production of acrylic fiber, today there are thousands of patents and publications covering its use in various fields such as water treatment, personal care products, adhesives and medical applications. In recent years, researchers have been working on improving the mechanical strength and creating self-healing behavior of poly(AMPS) (PAMPS) hydrogels.

In this thesis, PAMPS hydrogels and cryogels with adjustable viscoelastic and mechanical properties were prepared and characterized. The thesis work is divided into three parts. The first part aims to synthesize self-healing PAMPS hydrogels without using any initiator and to improve their poor mechanical properties. The preparation of AMPS-based hydrogels without crosslinker and initiator has not been reported before, except for one study recently published [2]. Xing et al. reported synthesis of self-healing PAMPS-based hydrogels at 80 °C by solution polymerization without the use of a crosslinker and initiator. They showed that the spontaneous cross-linking ability of PAMPS emerges from intermolecular hydrogen bonds acting as physical crosslinks while the ability of AMPS to polymerize without any initiator is due to the catalytic effect of H^+ counterions of sulfonic acid groups. However, the hydrogels reported by Xing et al were easily soluble when immersed in an excess of water and exhibited weak mechanical properties even at a water content of above 15 wt%. In order to make them water insoluble, and improve their mechanical properties, a series of experiments were carried out in the first part of the thesis. The hydrogels were synthesized from an aqueous solution of 50 wt% AMPS at 80 °C and after a reaction time of 24 h. Laponite clay nanoparticles, and the chemical crosslinker N,N‟-methylene(bis)acrylamide (BAAm) were included separately and together into the reaction system. It was found that the incorporation of Laponite nanoparticles or BAAm crosslinker alone into the hydrogel network leads to mechanical weak PAMPS hydrogels that easily dissolve in water. Interestingly, when Laponite and BAAm were added together to the gelling solution, PAMPS hydrogels thus produced exhibited a high Young's modulus (~0.7 MPa), compressive strength (45 MPa), good resilience, and a high self-healing efficiency. In addition, hybrid crosslinked PAMPS hydrogels were insoluble in water revealing existence of strong H-bonds between PAMPS network chains. This finding was explained with the strengthening of the electrostatic interactions between AMPS and Laponite due to the existence of chemical cross-linking points, as well as due to the "house of cards' structure of Laponite nanoparticles at a high concentration. The hybrid strategy thus developed within the first part of the thesis is a novel and general approach for the production of nanocomposite ionic hydrogels with self-healing ability.

The synthesis of water-stable physical PAMPS hydrogels formed by only H-bonding interactions has not been reported before. This is due to the 100-fold weaker strength of H-bonds compared to the covalent bonds, leading to the dissociation of H-bonds between the PAMPS chains in water. However, cooperativity of H-bonds similar to those in double-stranded DNA would create H-bonded physical hydrogels of high mechanical strength. This was the idea behind the experiments conducted in the second part of the thesis. UV photopolymerization of AMPS in water was conducted at a high AMPS concentration without using any chemical crosslinkers. As compared to the thermal polymerization at 80 °C leading to water soluble PAMPS hydrogels, UV polymerization at 23±2 °C produces water-insoluble hydrogels exhibiting an equilibrium swelling ratio of 1013±53, i.e., the mass of the hydrogel around 1013-fold increases upon swelling in an excess amount of water. Although the hydrogels are stable in water, they all could be dissolved in aqueous urea solutions due to the breaking of H-bonds. The network chains of PAMPS hydrogels formed by UV polymerization was found to have a much higher molecular weight as compared to those obtained by thermal polymerization. This reflects strengthening of H-bonds with increasing chain length due to the so-called proximity effect. Moreover, the addition of DMAA, a non-ionic monomer, to the UV polymerization system further improved both the mechanical properties and self-healing behavior of PAMPS hydrogels. The results could be explained with the hydrogen donor-acceptor relationship between DMAA-AMPS units. Because the hydrogels are physically cross-linked by H-bonds, they self-heal completely within minutes without any external stimuli. In addition to self-healing, the combination of supramolecular crosslinks also imparted shape-memory properties to the PAMPS hydrogels.

Another alternative method that will improve the mechanical properties and shorten the response time to external stimuli is the cryogelation method. The cryogelation technique is a simple and environmentally friendly method used in the production of macroporous hydrogels called cryogels. With this technique, free-radical crosslinking copolymerization is carried out below the freezing point of the reaction system. As water freezes, the monomer and initiator come out of the ice, resulting in the formation of unfrozen microdomains containing a high concentration of monomer and initiator due to cryoconcentration. On the other hand, ice crystals form interconnected frozen regions forming macropores after drying of the final cryogels.

The cryoconcentration effect accelerating the cryogelation reactions generally overcomes the reduced reaction rates due to low temperature, and cryogels can be obtained even at very low initial monomer concentrations. After cryogelation, the resulting gel is brought to room temperature and dried, resulting in the appearnce of pores in the μm scale in place of the ice crystals interconnected by a 3D polymer network.

It should be particularly noted that cryoconcentration is a unique feature that distinguishes cryogelation from the freeze-drying process. This is because the pore walls are composed of a dense polymer originating from cryoconcentrated monomers around the ice crystals during cryogelation. On the other hand, the pore walls formed by the freeze-drying process of a conventional hydrogel are weakly cross-linked. As a result, the porous structures obtained by cryogelation are mechanically stable that can withstand even large strains, while those produced by freeze-drying is fragile. Thus, the cryogelation technique provides a significant improvement in the mechanical properties of first-generation conventional hydrogels. Almost complete compressibility, high toughness, rapid response to stimuli are not observed in hydrogels but are some of the characteristic features observed in cryogels.

Although a lot of work has been done on cryogels, some details are still missing regarding the actual cryogelation conditions. In the third part of this thesis, the relationship between the real conditions of the cryogelation, that is, the conditions in the unfrozen domains and the cryogel properties were investigated. For this purpose, cryogelation of AMPS in the presence of BAAm crosslinker was conducted in aqueous solutions at 18 °C. The variation of the morphology and mechanical properties of PAMPS cryogels depending on the amount of BAAm and the total monomer concentration was invesigated. Additionally, the real monomer concentration (C_{true}) in the unfrozen domains, and the volume of ice V_{ice} acting as a template for the pores were determined by DSC measurements conducted on apparently frozen reaction solutions. Although the real monomer concentration C_{true} was independent on the actual concentration C_o, both the ice volume V_{ice} and the ratio C_{true} / C_o decreased with increasing C_o. These changes were found to determine both the pore morphology and mechanical properties of PAMPS cryogels. In short, the experiments carried out in this section have shown that it is possible to control

the structure of the final cryogels by controlling the real synthesis conditions during cryogelation.

1.1 Purpose of The Thesis

The purpose of the present thesis is to create mechanically strong PAMPS hydrogels able to absorb a large amount of water without dissolving. Another purpose is to create such hydrogels via non-covalent bonds such as H-bonding interactions to generate autonomous self-healing behavior. Thus, the thesis covers a series of studies aimed at synthesizing viscoelastic and mechanically strong PAMPS hydrogels and cryogels with tunable properties. The thesis work is divided into three parts. In the first part, self-healing hybrid crosslinked PAMPS-based hydrogels with a high mechanical strength were synthesized by solution polymerization without using any initiator. It was shown that, although both nanocomposite and chemically crosslinked PAMPS hydrogels are weak and easily soluble in water, hybrid crosslinked ones formed using both clay nanoparticles and chemical crosslinkers are water insoluble, and exhibit good compressive mechanical properties and self-healing ability. The hybrid strategy thus developed is a novel approach for the production of nanocomposite ionic hydrogels with self-healing ability. The manuscript entitled 'Hybrid cross-linked poly(2-acrylamido-2-methyl-1-propanesulfonic acid) hydrogels with tunable viscoelastic, mechanical and self-healing properties', which constitutes the first part of the thesis was published in a SCI indexed journal in 2018.

Considering the fact that the H-bonds are 100-fold weaker than the covalent bonds, it seems impossible to produce H-bonded hydrogels remaining stable in water. However, the results of the second part of the thesis show that this prediction is incorrect. By adjusting the synthesis conditions, we were able to increase the molecular weight of the primary chains of PAMPS so that multiple H-bonds could be created leading to water-insoluble H-bonded PAMPS hydrogels with a high swelling capacity and mechanical strength. Moreover, the incorporation of DMAA, a non-ionic monomer, into the network chains further improved both the mechanical properties and self-healing behavior of PAMPS hydrogels. Because the hydrogels are physically cross-linked by H-bonds, they self-heal completely within minutes without any external stimuli. The results of the second part of the thesis was

published in an SCI-Expanded indexed journal in 2019 under the title ‘A Self-Healing and Highly Stretchable Polyelectrolyte Hydrogel via Cooperative Hydrogen Bonding as a Superabsorbent Polymer’.

Cryogelation is a simple and environmentally friendly technique for the production of macroporous hydrogels, called cryogels, with extraordinary properties. Because cryogelation reactions are usually conducted at 10 to 20 °C below the freezing temperature of the reaction solution, the concentrations of the reactants in the unfrozen domains significantly deviate from those in the initial reaction system. Therefore, the cryogel studies reported so far are incomplete as they consider the initial conditions instead of the real conditions of the cryogelation system. In the third part of this thesis, the relationship between the real conditions of the cryogelation, that is, the conditions in the unfrozen domains and the cryogel properties were investigated. For this purpose, the real monomer concentration in the unfrozen areas, and the volume of ice acting as a pattern for the pores were determined for the cryogelation reactions of AMPS under various experimental conditions. It was shown that both the ratio of real-to-actual monomer concentration and the ice volume changes depending on the experimental parameters, and these changes determine both the morphology and mechanical properties of PAMPS cryogels. In short, the experiments carried out in this section have shown that it is possible to control the structure of the final cryogels by controlling the real synthesis conditions during cryogelation. The last part of the doctoral thesis was published under the title ‘Cryogenic formation-structure-property relationships of poly(2-acrylamido-2 -methyl-1-propanesulfonic acid) cryogels’ in a SCI-Expanded index journal.

2. HYBRID CROSS-LINKED POLY(2-ACRYLAMIDO-2-METHYL-1-PROPANESULFONIC ACID) HYDROGELS WITH TUNABLE VISCOELASTIC, MECHANICAL AND SELF-HEALING PROPERTIES[1]

2-Acrylamido-2-methyl-1-propanesulfonic acid (AMPS) is an ionic monomer widely used for the synthesis of polyelectrolyte hydrogels possessing a large water sorption capacity [3–6]. AMPS has received attention due to its strongly ionizable sulfonate group (Figure 2.1); it dissociates completely in the overall pH range [7–9], and therefore, chemically cross-linked hydrogels derived from AMPS exhibit pH independent swelling behavior and good electro-responsive property making them attractive material in a wide range of applications, such as in soft-biomimetic actuators, superabsorbents, biomaterials, bioengineering, water purification, agriculture, and food industry [5,10–13]. However, such hydrogels have a low strength and toughness due to the lack of an effective energy dissipation mechanism [14–17].

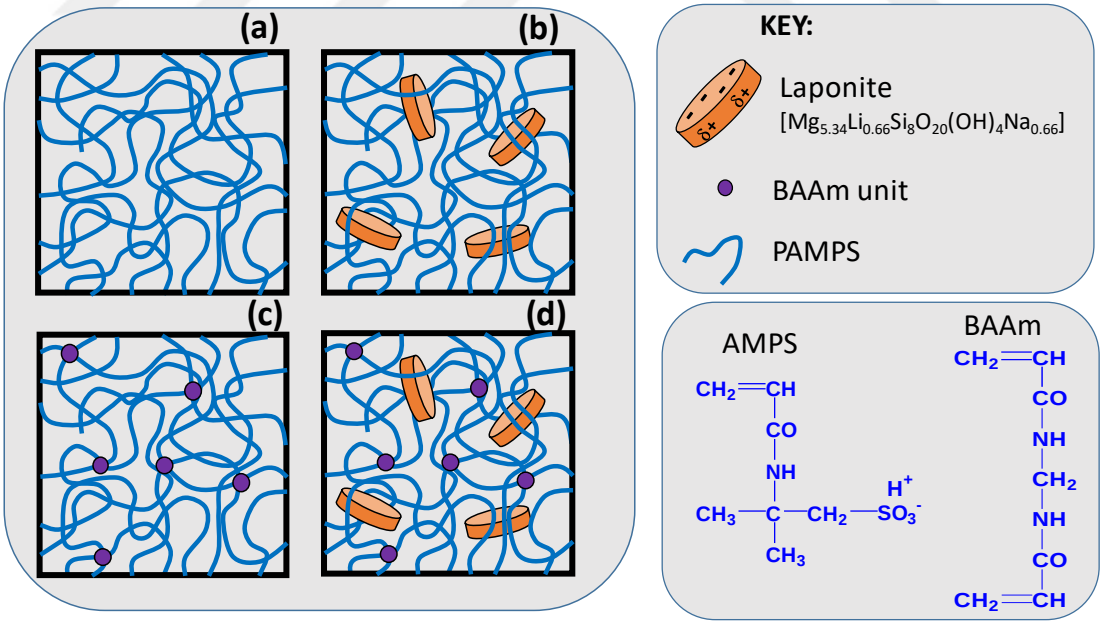

Figure 2.1 : Scheme of pure PAMPS (a), nanocomposite- (b), chemically-cross-linked- (c), and hybrid-cross-linked PAMPS hydrogels (d).

[1] This chapter is based on the paper "Su, E. and Okay, O. (2018). Hybrid cross-linked poly(2-acrylamido-2-methyl-1-propanesulfonic acid) hydrogels with tunable viscoelastic, mechanical and self-healing properties. *Reactive and Functional Polymers*, 123, 70-79."

Xing et al. recently reported preparation of a self-healing hydrogel based on PAMPS using initiator-free polymerization of AMPS in aqueous solutions in the absence of a cross-linker [2]. Their results indicate that the polymerization ability of AMPS in the absence of an external initiator is due to the catalytic effect of H^+ counterions of the sulfonic acid groups, while its self-cross-linking ability arises due to the intermolecular hydrogen bonds acting as physical cross-links [2]. This simple, inexpensive, and one-pot synthetic procedure leads to the formation of PAMPS hydrogels with mechanical properties strongly dependent on their water contents. For instance, the hydrogels containing less than 10% water exhibit a Young's modulus approaching to 400 MPa, while increasing water content above 15% produces mechanically weak hydrogels with a modulus of around 22 kPa [2]. Our preliminary experiments showed that PAMPS hydrogels prepared as described by Xing et al. completely dissolve in excess of water indicating that the inter-chain hydrogen bonds are too weak to resist the expansion of PAMPS chains in water due to the osmotic pressure of AMPS counterions.

In this study, we attempt to improve the mechanical performance of physical PAMPS hydrogels using three strategies, as schematically illustrated in Figure 2.1. First, Laponite nanoparticles were incorporated into the physical network of PAMPS chains to increase the strength of intermolecular interactions. Laponite is a synthetic hectorite clay and, when suspended in water, it forms disk-like particles with a thickness of 1 nm, a diameter of about 25 nm, carrying strongly negative charge on the surface and weakly positive charge on the rim (Figure 2.1) [18,19]. At a low concentration, Laponite forms a clear colloidal suspension in water due to the repulsive electrostatic interactions between particle surfaces. Increasing Laponite concentration leads to the formation of a clay hydrogel with so-called house-of-cards structure due to the electrostatic bonds between the positively charged rim and the negatively charged surfaces. Laponite nanoparticles have been used in many studies along with in-situ produced hydrophilic non-ionic polymers to form nanocomposite hydrogels with improved mechanical properties [20–23]. The surface of the nanoparticles provides an interface on which polymer chains can physically absorb, thus acts as multifunctional cross-link zones of nanocomposite hydrogels. Hydrogen bonding, ionic, dipole interactions and polymer entanglements seem to be responsible for the formation of nanocomposite hydrogels. As a second strategy, we

included the classical chemical cross-linker N,N′-methylenebis(acrylamide) (BAAm) into the gelation solution to improve the elastic properties of the hydrogels.

As will be seen below, incorporation of Laponite (1 – 15 wt.%) or BAAm (0.5 – 1.3 mol%) into the gelation system leads to the formation of water-soluble gels, as the pure PAMPS hydrogel, due to the weak inter-chain hydrogen bonds. However, simultaneous incorporation of Laponite and BAAm into the network structure strengthens hydrogen bonding interactions and provides formation of water-insoluble, hybrid cross-linked PAMPS hydrogels with excellent mechanical properties. For instance, they exhibit a high modulus (~700 kPa), compressive strength (45 MPa at ~90% strain), good resilience, and self-healing. Because nanocomposite polyelectrolyte hydrogels are hard to prepare due to agglomeration of the particles, the hybrid-cross-linking approach presented here might enable preparation of a variety of mechanically strong nanocomposite hydrogels consisting of charged polymer chains of different architecture.

2.1 Experimental Part

2.1.1 Materials

The monomer 2-acrylamido-2-propane-1-sulfonic acid (AMPS, Aldrich), chemical cross-linker N,N′-methylenebis(acrylamide) (BAAm, Merck), and the synthetic hectorite clay, Laponite XLG ($Mg_{5.34}Li_{0.66}Si_8O_{20}(OH)_4Na_{0.66}$) provided by Rockwood Ltd. were used without further purification. The hydrogels were prepared by solution polymerization of AMPS at 80 °C in the absence of an external initiator. AMPS concentration was fixed at 50 wt.%, with respect to water, while various amounts of Laponite and BAAm separately or together were added into the solution to obtain nanocomposite-, chemically cross-linked-, and hybrid-cross-linked hydrogels, respectively (Table 2.1). The concentration of Laponite is expressed as wt.% of the solution while BAAm content is given by mol % with respect to the monomer AMPS. Typically, AMPS (5 g) was dissolved in 5 mL distilled water at 24±2 °C. Laponite (0.10 – 1.765 g) was then added and stirred 2 h to obtain a homogeneous solution. We have to note that Laponite dissolved easier in the AMPS solution than in water, which is in accord with the dispersion effect of AMPS on Laponite aggregates [24]. After addition of BAAm (20 – 78 mg) and bubbling

nitrogen, the solution was transferred into plastic syringes of 20 mm in diameter and the polymerization was conducted at 80 °C for 18 h.

2.1.2 Rheological experiments

Rheological measurements were performed on Gemini 150 Rheometer system, Bohlin Instruments, equipped with a Peltier device for temperature control. Hydrogel samples after preparation were cut into thin slices of 20 mm in diameter and about 3 mm in thickness and then placed between the parallel plates of the rheometer. The upper plate (diameter 20 mm) was set at a distance of 2950±150 μm. During all measurements, a solvent trap was used to minimize the evaporation. The frequency-sweep tests at a strain amplitude γ_o = 0.01 were carried out at both 25 and 40 °C over the frequency range 0.1 to 300 rad·s^{-1}. The hydrogels were also subjected to stress-relaxation experiments at 25°C. A shear deformation of predetermined strain amplitude γ_o was applied to the hydrogel samples and the resulting stress σ (t, γ_o) was monitored as a function of time. Here, we report the relaxation modulus G (t) as functions of the relaxation time t and strain amplitude γ_o. The experiments were conducted with increasing strain amplitudes γ_o from 0.01 to 1. For each hydrogel, stress-relaxation experiments at various γ_o were conducted starting from a value of the relaxation modulus deviating less than 10 % from the modulus measured at γ_o = 0.01.

2.1.3 Mechanical tests

Uniaxial compression and elongation tests were performed at 24±2 °C on a Zwick Roell Z0.5 TH test machine using a 500 N load cell. Load and displacement data were collected using flat hydrogel samples with dimensions of 4×3 mm and a thickness of 3 mm. For uniaxial compression measurements, the hydrogel samples were compressed at various strain rates between 0.1 and 4 min^{-1}. Before the test, an initial compressive contact to 0.01 N was applied to ensure a complete contact between the gel and the plates. For uniaxial elongation measurements, the initial sample length between jaws and the strain rate were 10±1 mm and 1 min^{-1}, respectively. The stress was presented by its nominal σ_{nom} and true values σ_{true} (= λ σ_{nom}), which are the forces per cross-sectional area of the undeformed and deformed specimen, respectively, while the strain is given by λ, the deformation ratio (deformed length/initial length). The strain ε is also defined as the change in the

length of the gel specimen relative to its initial length, i.e., $\varepsilon = \lambda - 1$ or $\varepsilon = 1 - \lambda$, for elongation and compression, respectively. The Young's modulus E was calculated from the slope of nominal stress–strain curves between 5-15% deformations. The compressive strength σ_f was calculated from the maxima in true stress-strain curves [25]. Cyclic compression experiments were conducted with a compression step performed at a strain rate $\dot{\varepsilon}$ of 1 min^{-1} to a maximum strain σ_{max} (increased from 0.2 and 0.8), followed by immediate retraction to zero displacement and a waiting time of 5 min, until the next cycle of compression.

To quantify the healing efficiency, tensile testing experiments were performed using cylindrical gel samples of 4.6 mm in diameter and 1 cm in length. The samples were cut in the middle and then, the two halfs were merged together within a plastic syringe (of the same diameter as the gel sample) by slightly pressing the piston plunger. The healing time was fixed at 24 h. Healing efficiency ε_{eff} was estimated from the ratio of the Young's modulus and fracture stress of the healed samples to those of the virgin sample.

2.1.4 Swelling and gel fraction measurements

The hydrogel samples after preparation were cut into specimens of about 3 mm in length. Then, each specimen was immersed in a large excess of distilled water at 24±2 °C for at least 6 days by replacing water every hour during the first 6 h of the swelling period and then every day to extract any soluble species. The swelling equilibrium was tested by weighing the gel samples. The equilibrium swollen hydrogel samples in distilled water were than taken out of water and freeze dried. The gel fraction W_g, that is, the fraction of AMPS, BAAm, and Laponite incorporated into the water-insoluble polymer was calculated from the masses of dry polymer network and from the comonomer feed. The relative weight swelling ratio m_{rel} was calculated as $m_{rel} = m/m_o$ where m is the mass of the equilibrium swollen gel sample, and m_o is its mass after preparation. The water content H_2O % of the hydrogels was calculated as $H_2O\ \% = 10^2 \times (1 - m_{dry} / m)$ where m_{dry} is the dry mass of the hydrogel.

2.2 Results and Discussion

2.2.1 Rheological properties

Three series of gelation experiments were conducted by fixing the amount of AMPS at 50 wt.%, as compiled in Table 2.1. In the 1st set, Laponite nanoparticles between 1 and 15 wt.% were added into the AMPS solution while in the 2nd set, BAAm instead of Laponite was included as a chemical cross-linker. In the 3rd set, both 15 wt.% Laponite and BAAm at various amounts were added to generate hybrid cross-linked PAMPS hydrogels. In the following, gel-forming systems prepared using Laponite or BAAm are denoted as NC-x and BAAm-y, respectively, where *x* and *y* are Laponite (in wt.%) and BAAm (in mol%) contents in the feed, respectively (Table 2.1). Moreover, the systems prepared using both Laponite and BAAm are denoted as hybrid-*x*/*y*.

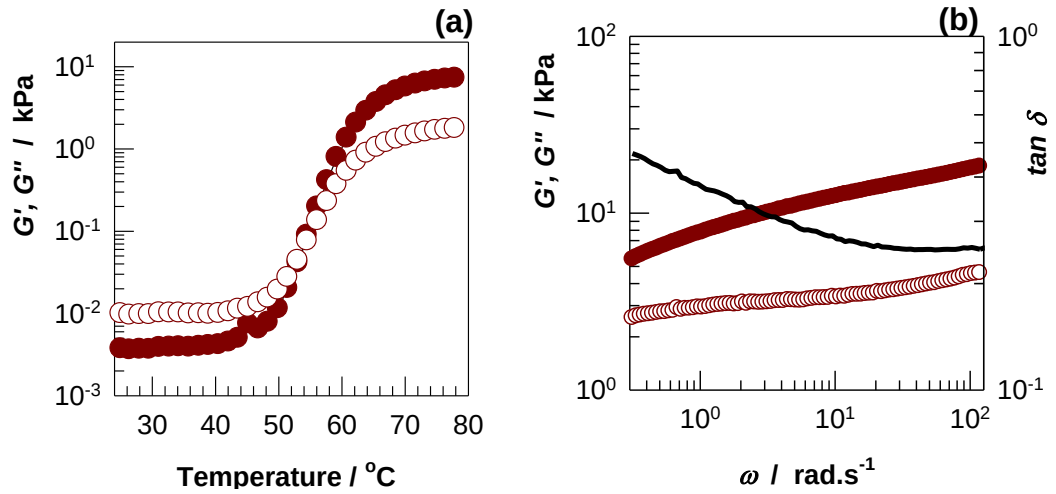

Figure 2.2 : (a) *G′* (filled symbols) and *G″* (open symbols) of 50 wt.% AMPS solution during heating from 25 to 80 °C shown as a function of temperature. ω = 6.3 rad·s^{-1}. γ_o = 0.01. (b) *G′* (filled symbols), *G″* (open symbols), and *tan δ* (lines) of PAMPS hydrogel after a reaction time of 24 h shown as a function of frequency ω. Temperature = 25 °C (c). γ_o = 0.01.

We first conducted initiator-free polymerization of AMPS without any additive by heating aqueous 50 wt.% AMPS solution from 25 to 80 °C at a rate of 1.8 °C·min^{-1}, and then keeping at this temperature for 18 h. Figure 2.2a shows the storage *G'* and loss moduli *G''* of the AMPS solution during the heating period plotted against the temperature. Above 45 °C, *G'* rapidly increases with increasing temperature and becomes equal to *G''* at 54 °C indicating a transition from dilute to semi-dilute regime of PAMPS solution. Thus, in accord with the previous report [2],

polymerization of AMPS could be initiated without an external initiator. Previous works show that some acrylic monomers such as acrylic acid and methacrylic acid undergo self-initiated photopolymerization or thermal polymerization [26,27]. Because AMPS does not self-polymerize when its H^+ is substituted by Na^+ [2], the presence of H^+ ions seems to be responsible for initiator-free polymerization of AMPS. After a reaction time of 24 h, frequency sweep tests were conducted on PAMPS hydrogels at 25 °C. Figure 2.2b shows *G'*, *G''* and the loss factor *tan* δ (= *G''*/*G'*) at a strain amplitude γ_0 of 0.01 plotted against the angular frequency ω. *G'* is larger than *G''* over the entire range of frequency while *tan* δ is above 0.1, which is typical for a weak gel. Indeed, PAMPS hydrogel exhibited poor mechanical properties, e.g. its tensile strength and Young's modulus were 11±1 and 9±2 kPa, respectively, and it easily dissolved in water.

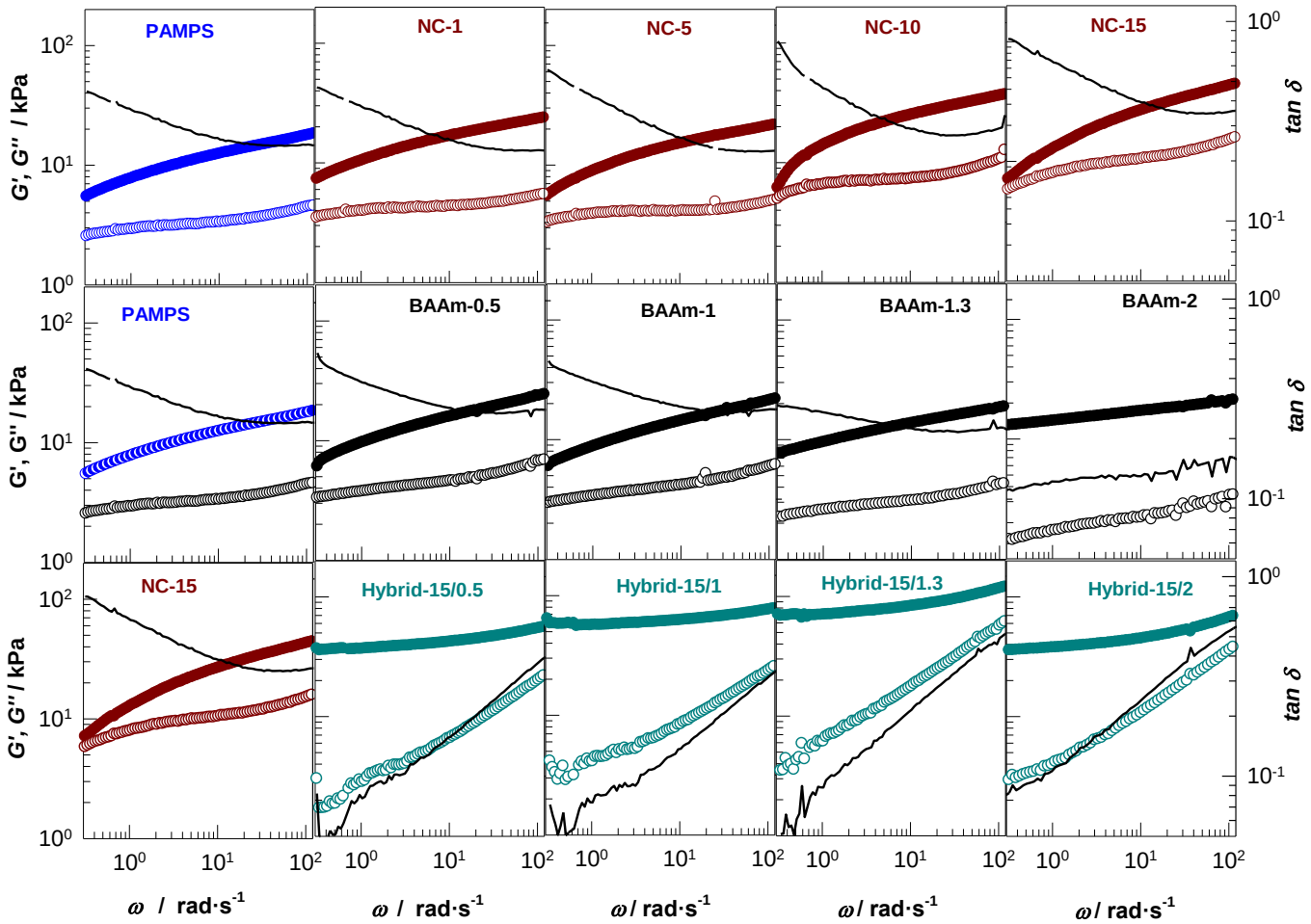

Figure 2.3 : *G′* (filled symbols), *G″* (open symbols), and *tan δ* (lines) of NC-*x*, BAAm-*y*, and hybrid-15/*y* hydrogels at 25 °C shown as a function of frequency *ω*. $\gamma_o = 0.01$.

To render PAMPS hydrogel water-insoluble and to increase its mechanical strength, we included Laponite nanoparticles and the chemical cross-linker BAAm separately or together into the reaction system. Figure 2.3 shows frequency dependences of *G'* (filled symbols), *G''* (open symbols), and *tan* δ (lines) of NC-*x*, BAAm-*y*, and hybrid-15/*y* hydrogels, respectively, prepared at various Laponite and BAAm contents. Although the storage modulus *G'* and hence the cross-link density of NC's slightly increases with increasing amount of Laponite (Figure 2.3, Table 2.1), the loss factor *tan* δ also increases indicating that the physical PAMPS gel becomes more viscous after incorporation of the nanoparticles into the physical network. Indeed, all NC's were soluble in water as those prepared in the absence of Laponite. This unexpected behavior could be related to the repulsive interactions between the negatively charged surface of the nanoparticles and PAMPS chains, as observed before in hydrogels formed by in-situ copolymerization of AMPS and acrylamide in Laponite dispersions [24,28]. Similar to the NC's, gel forming systems containing BAAm cross-linker lead to the formation of weak gels (Figure 2.3b) and, except the one prepared using 2 mol% BAAm, they all are soluble in water (Table 2.1). We have to mention that, below a critical cross-linker (divinyl monomer) concentration, cross-linking copolymerization of vinyl/divinyl monomers results in water soluble polymers [29,30]. This critical concentration is generally much higher than the theoretical one due to the effects of cyclization and multiple cross-linking reactions as well as due to the reduced reactivity of pendant vinyl groups on the growing radicals. For the present gelation system, 2 mol% BAAm is needed to obtain a chemically cross-linked PAMPS hydrogel, while at lower BAAm contents, BAAm does not form elastically effective cross-links between PAMPS chains and hence, water-soluble physical gels could be obtained.

However, hybrid-cross-linked hydrogels prepared by the addition of both Laponite and BAAm exhibit significantly improved elastic properties (Figures 2.3 and Table 2.1). The storage modulus *G'* shows a plateaulike behavior in the low-frequency range and the height of the plateau increases with increasing BAAm concentration. Plateau storage modulus *G'* of hybrids is about one order of magnitude higher than that of their components, i.e., NC- and BAAm-hydrogels, and the loss factor *tan* δ attains values below 0.1 at low frequencies. Moreover, all hybrids were insoluble in water with a gel fraction W_g around unity (Table 2.1), indicating that the cross-

links in hybrid hydrogels resist the expansion of PAMPS chains in water. The results thus reveal that Laponite and BAAm separately are ineffective for the improvement of PAMPS hydrogel properties while their combination produces water-insoluble hydrogels with a high modulus.

The results can be explained by considering the interactions between the components of the gelation system. Previous work shows that non-ionic monomers such as N-isopropylacrylamide, N,N-dimethylacrylamide, and acrylamide effectively surround the surface of Laponite particles in aqueous suspensions [20–23,31]. After gelation, a large number of non-ionic polymer chains are aggregated on the surface of clay particles forming multiple hydrogen bonding with clay, which is responsible for the extraordinary mechanical properties of nanocomposite hydrogels. In contrast, anionic monomer AMPS cannot surround the particles due to its repulsive interactions with the negatively charged particle surfaces, which prevents hydrogen bonding between PAMPS and clay. Thus, because Laponite surfaces do not act as multi-functional cross-link zones of PAMPS chains, weak physical gels could be obtained from AMPS monomer. However, when BAAm is added in the gelation system containing Laponite and AMPS, non-ionic BAAm molecules surrounding the particles act like bridges between the particle surfaces and AMPS and hence enhance clay-polymer interactions leading to improved mechanical properties of hybrid hydrogels.

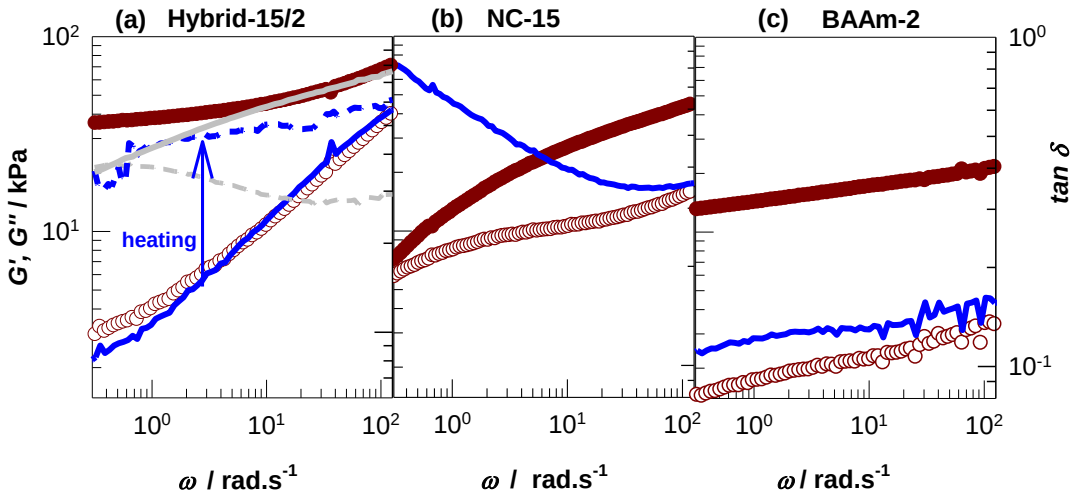

Figure 2.4 : *G'* (filled symbols), *G''* (open symbols), and *tan δ* (solid blue lines) of hybrid-15/2 (a), NC-15 (b), and BAAm-2 hydrogels (c) shown as a function of frequency ω. $\gamma_o = 0.01$. The solid and dashed gray curves in Figure 2.4a are *G'* and *tan δ*, respectively, calculated by summing up *G'* and *G''* of NC-15 and BAAm-2 hydrogels. Temperature = 25 °C. Dashed blue curve in Figure 3a represents *tan δ* values measured at 40 °C.

This finding is also highlighted in Figure 2.4a-c where the frequency dependences of *G'*, *G''*, and *tan* δ of hybid-15/2 hydrogel together with its component hydrogels, namely NC-15 and BAAm-2 are shown. Solid and dashed gray curves in Figure 2.4a represent the theoretical *G'* and *tan* δ of hybrid-15/2, respectively, calculated by summing up the dynamic moduli of its component hydrogels. At $\omega > 6$ rad·s^{-1}, calculated *G'* is close to its experimental value indicating that both the physical and chemical cross-links are effective in the hybrid network structure. At lower frequencies, a positive deviation from the calculated *G'* appears which can be attributed to the reduced mobility of chemically cross-linked PAMPS chains increasing the lifetime of H-bonds between PAMPS and Laponite. This explanation is in accord with much lower *tan* δ of the hybrids as compared to its calculated value (Figure 2.4a). For instance, at $\omega = 0.3$ rad·s^{-1}, *tan* δ is 0.05, indicating that the hybrid hydrogel at this time scale belongs to the category of strong gels, while the calculated value of *tan* δ is 0.4, typical for a weak gel (Figure 2.5).

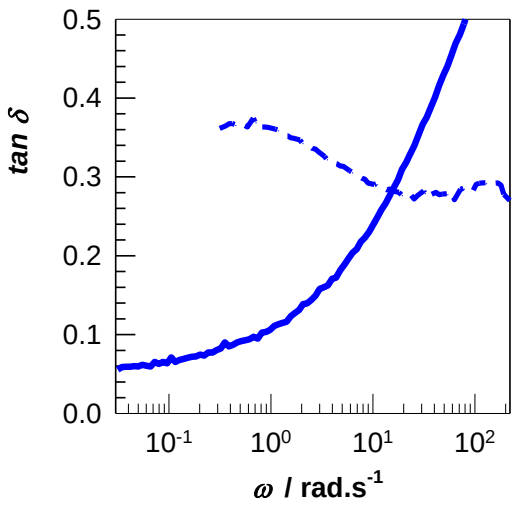

Figure 2.5 : *tan* δ of hybrid-15/2 hydrogel (solid line) plotted against the frequency ω. The dashed curve represents calculated *tan* δ from *G'* and *G''* of the precursor hydrogels. $\gamma_0 = 0.01$.

Another point seen in Figure 2.4a is increasing *G''* and *tan* δ (solid blue line) with increasing frequency revealing energy dissipation at short experimental time scales. Such a significant increase of *G''* with rising frequency has been reported before in polysaccharide gels with strong hydrogen bonding interactions, such as sodium alginate - poly(N-isopropylacrylamide) (PNIPA) [32], hyaluronic acid-graft-PNIPA [33], methyl cellulose [34], and hyaluronic acid [35]. The appearance of a similar viscoelastic behavior in hybrid-PAMPS hydrogels is attributed to the strong

intermolecular hydrogen bonding interactions between chemically cross-linked PAMPS and Laponite nanoparticles contributing to the gel elasticity at a low frequency. Increasing frequency progressively breaks H-bonds so that strong hydrogel transforms into a weak one. This also means that heating the hybrid hydrogels would break H-bonds existing at short frequencies. The dashed blue curve in Figure 2.4a representing ω-dependence of *tan* δ measured at 40 °C indeed reveals that *tan* δ is close to the calculated value indicating that most of H-bonds are broken at the elevated temperature.

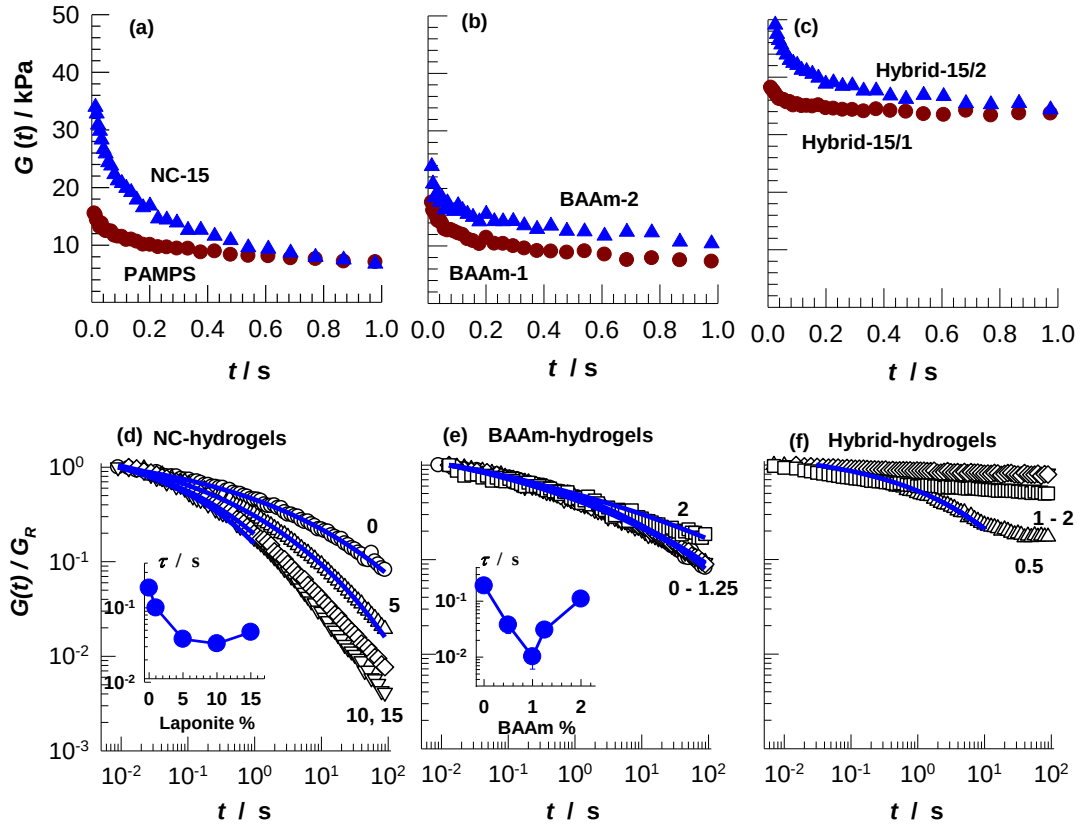

Figure 2.6 : (a-c): Relaxation modulus *G(t)* during a relaxation time of 1 s for PAMPS, NC-15, BAAm-1, BAAm-2, and resulting hybrid-hydrogels. Strain = 5%. **(d-f):** *G(t)* normalized with respect to the Rouse modulus G_R as a function of time *t* for NC- (d), BAAm- (e), and hybrid-hydrogels (f). (d) Laponite = 0 (○), 5 (△), 10 (▽), and 15 wt.% (◇). (e, f) BAAm = 0 (○), 0.5 (△), 1.0 (▽), 1.25 (◇), and 2 mol% (□). Strain = 5%. The curves are the best fits to equation (2.1). The insets show the lifetime τ of physical cross-links as functions of Laponite and BAAm contents.

Stress-relaxation experiments are another mean of studying the dynamic properties of the hydrogels. Figures 2.6a-c show the relaxation modulus *G(t)* of the hydrogels during the first second of relaxation following a step strain of 5%. The hydrogels exhibit a two-step relaxation response consisting a fast relaxation at time *t* shorter

than 0.2 s and slow relaxation at longer times. The fact that all hydrogels exhibit relaxation reveals finite lifetimes of their apparent cross-links and energy dissipation. Figures 2.6d-f show double-logarithmic plots of *G(t)*, normalized with respect to the modulus G_R at $t = 0$, as a function of time t up to 100s for NC-, BAAm-, and hybrid-hydrogels, respectively, formed at various Laponite and BAAm contents. The measurements were performed at 5% strain which is in the linear regime for all hydrogels (Figure 2.7). For all hydrogels, *G(t)* decreases with time but never goes to zero over the duration of the relaxation tests.

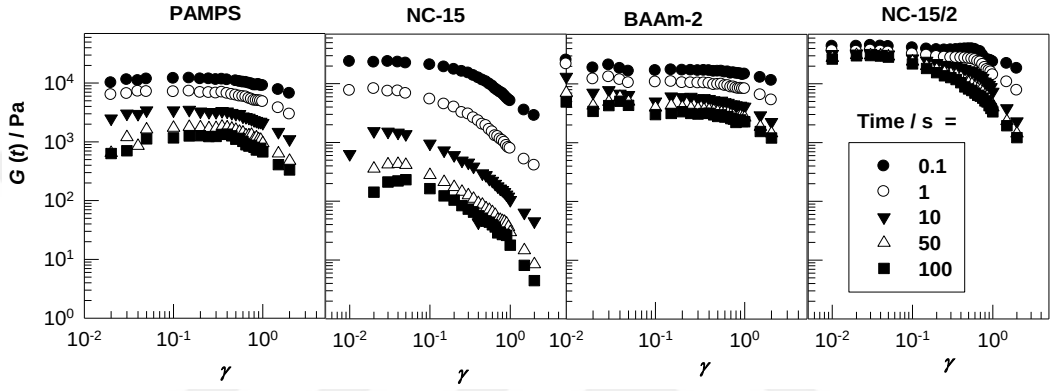

Figure 2.7 : Relaxation modulus *G(t)* of PAMPS, NC-15, BAAm-2, and NC-15/2 hydrogels shows as a function of strain γ at times scales indicated.

The strongest time-dependence of the relaxation modulus *G(t)* was observed in NC-hydrogels, with *G(t)* being a mirror image of *G'(w)* (Figure 2.3a). For Laponite contents below 10 wt.%, all data could be fitted using the stretched exponential function [36–39]:

$$G(t) = G_R \exp\left(-(t/\tau)^{\beta}\right) \tag{2.1}$$

with an exponent $\beta = 0.25 \pm 0.05$, where τ is the lifetime of the physical crosslinks. At larger amount of Laponite, the data below 1 s could also be fitted to the stretched exponential function with the same exponent while at longer time scales a power law behavior similar to the critical gel appears, $G(t) \sim t^n$ where $n = -0.83 \pm 0.05$. The solid red curves in Figures 2.6d-f are best fit curves using equation 2.1. The inset to Figure 2.6d showing the lifetime τ of the physical cross-links calculated using equation (2.1) reveals formation of H-bonds with shorter lifetimes as the amount of Laponite is increased. A similar behavior was observed in BAAm-hydrogels (inset to Figure 2.6e). Increasing amount of BAAm up to 1 mol% decreases the lifetime τ while it again increases at higher BAAm contents. In contrast, the hybrids with >0.5 mol%

BAAm exhibit only a slight time-dependent relaxation modulus supporting the existence of long-lived H-bonds in hybrid network structure.

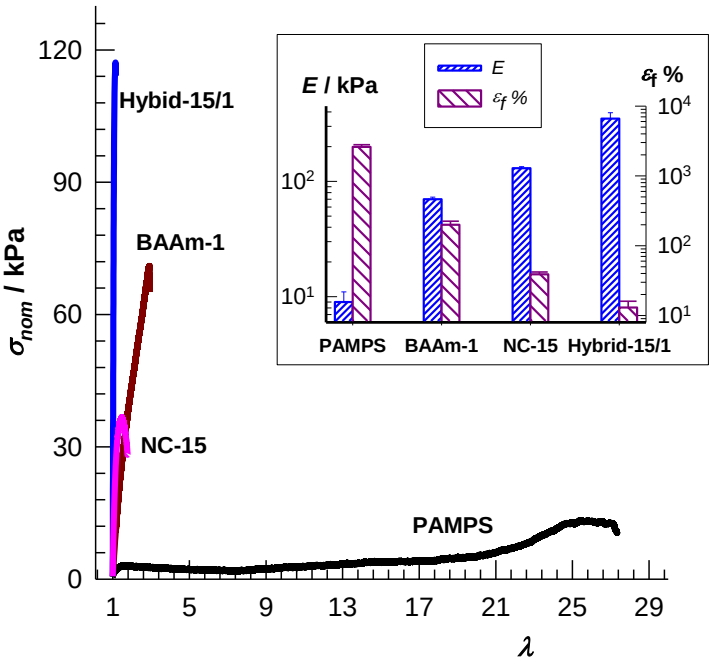

Figure 2.8 : Tensile stress – strain curves of PAMPS, NC-15, BAAm-1 and hybrid-15/1 hydrogels as the dependence of the nominal stress σ_{nom} on the deformation ratio λ. $\dot{\varepsilon}$ = 1 min^{-1}. The inset shows the Young's modulus E and stretch at break ε_f of the hydrogels.

Table 2.1 : Synthesis conditions, gel fractions W_g, storage modulus *G'* and loss factor *tan δ*, both measured at 1 and 100 rad.s^{-1}, and water contents of equilibrium swollen hydrogels. Standard deviations in the water contents are less than 1% while for *G'* and *tan δ*, they are less than 5%.

Code	AMPS / g	H_2O / g	Laponite / g	BAAm / mg	AMPS wt%	Laponite wt%	BAAm mol%	W_g	H_2O wt.%	*G'* / kPa		*tan δ*	
										1 rad.s^{-1}	100 rad.s^{-1}	1 rad.s^{-1}	100 rad.s^{-1}
PAMPS	5	5	0		50	0		0	-	8	18	0.38	0.25
NC-1	5	5	0.10		50	1		0	-	10	23	0.38	0.23
NC-5	5	5	0.53		50	5		0	-	9	21	0.44	0.23
NC-10	5	5	1.10		50	10		0	-	14	36	0.47	0.30
NC-15	5	5	1.765		50	15		0	-	13	43	0.62	0.35
BAAm-0.5	5	5		20	50		0.5	0	-	10	24	0.39	0.28
BAAm-1	5	5		39	50		1	0	-	9	21	0.39	0.28
BAAm-1.3	5	5		49	50		1.3	0	-	10	19	0.27	0.23
BAAm-2	5	5		78	50		2	1.0±0.1	99.7	14	21	0.12	0.16
Hybrid-15/0.5	5	5	1.765	20	50	15	0.5	0.90±0.01	93	37	55	0.077	0.37
Hybrid-15/1	5	5	1.765	39	50	15	1	0.90±0.01	90	57	77	0.079	0.31
Hybrid-15/1.3	5	5	1.765	49	50	15	1.3	0.95±0.01	87	70	117	0.095	0.49
Hybrid-15/2	5	5	1.765	78	50	15	2	0.96±0.03	86	38	67	0.11	0.54

Table 2.2 : Compressive modulus *E* and the fracture stress σ_f of hybrid-15/1.3 and -15/2 hydrogels together with their component hydrogels at two strain rates. Standard deviations are given in parenthesis.

Code	***E* / kPa**		**σ_f / MPa**	
	at 0.5 min^{-1}	**at 4 min^{-1}**	**at 0.5 min^{-1}**	**at 4 min^{-1}**
NC-15	95 (10)	221 (13)	10.2 (1.5)	43 (1)
BAAm-1.3	28 (2)	51 (4)	4.5 (0.2)	5.9 (0.6)
BAAm-2	49 (3)	68 (2)	6.2 (0.6)	8.1 (0.2)
Hybrid-15/1.3	416 (34)	690 (58)	19.1 (0.7)	27 (1)
Hybrid-15/2	546 (8)	583 (5)	44 (2)	41 (1)

2.2.2 Mechanical properties

Hydrogels were subjected to uniaxial tensile and compression tests at 24±2 °C. Figure 2.8 shows tensile stress-strain curves at a strain rate $\dot{\varepsilon}$ of 1 min^{-1} for PAMPS, BAAm-1, NC-15, and Hybrid-15/1 hydrogels. PAMPS hydrogel exhibits a Young's modulus of 9±2 kPa and a very high extensibility, about 2600%. The stretchability of PAMPS hydrogel decreases from 2600 to 200% after incorporation of BAAm into the comonomer feed while in hybrid one, it further reduces to 13%. Simultaneously, Young's modulus E increases from 9±2 to 70±3 and 350±44 kPa indicating increasing effective crosslink density of the hydrogels (inset to Figure 2.8). We have to mention that the hybrids formed at higher BAAm contents were mechanically stronger than Hybrid-15/1 shown in Figure 2.8 but they were too slippery to obtain meaningful tensile test results. Therefore, the mechanical properties of all hydrogels were compared by uniaxial compression tests.

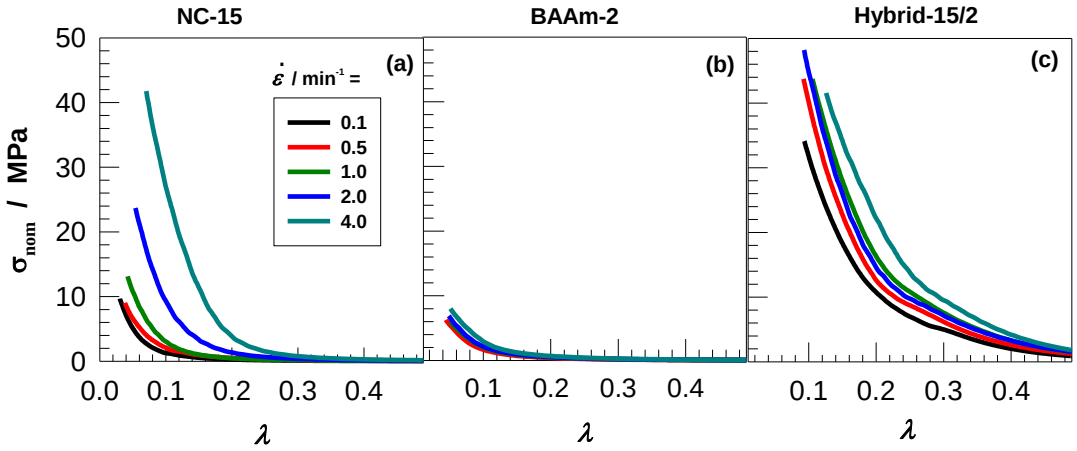

Figure 2.9 : Compressive stress – strain curves of NC-15 (a), BAAm-2 (b), and Hybrid-15/2 hydrogels (c) at various strain rates $\dot{\varepsilon}$ indicated.

Figures 2.9a-c show compressive stress-strain curves of NC-15, BAAm-2, and Hybrid-15/2 hydrogels, respectively, at various strain rates $\dot{\varepsilon}$. For NC-15 hydrogel, a strong strain rate dependence of the stress-strain curves is seen with a significant increase of the compressive strength at high rates. In contrast, BAAm-2 hydrogel exhibits a weak strain rate sensitivity and a low compressive strength. Hybrid-15/2 hydrogel which is a combination of NC-5 and BAAm-2 also exhibits a weak strain rate dependence but it is the mechanically strongest hydrogel overall rates. Figure 2.10a shows strain rate dependences of Young's modulus E and compressive strength σ_f of the precursor NC-15 and BAAm-hydrogels (left panel), and the

resulting hybrids (right panel). E and σ_f of the hydrogels at two different strain rates are also compiled in Table 2.2 Hybrid-hydrogels exhibit a modulus E between 400 and 700 kPa at strain rates $\dot{\varepsilon}$ above 0.1 min^{-1}, which is about 15- and 4-fold higher than the precursor NC- and BAAm-hydrogels indicating increasing number of effective cross-links when both Laponite and BAAm are incorporated into the physical PAMPS network. Comparison of the swelling behavior of the hydrogels also reflects significant difference in the cross-link density of BAAm-2 and hybrid-15/2 hydrogels. Figure 2.11a shows relative weight swelling ratio m_{rel} of BAAm-2, and hybrid 15/y hydrogels plotted against the time of swelling in water while Figure 2.10b shows the images of BAAm-2 and hybrid-15/2 hydrogel specimens before and after equilibrium swelling in water. The mass of BAAm-2 hydrogel sample 160-fold increases upon swelling in water which is 40 times larger than the mass increase observed in hybrid-15/2 gel sample. Moreover, increasing BAAm content of hybrids from 0.5 to 2 mol% decreases the swelling ratio m_{rel} from 7.4 to 5.3 indicating increasing cross-link density of the hydrogels.

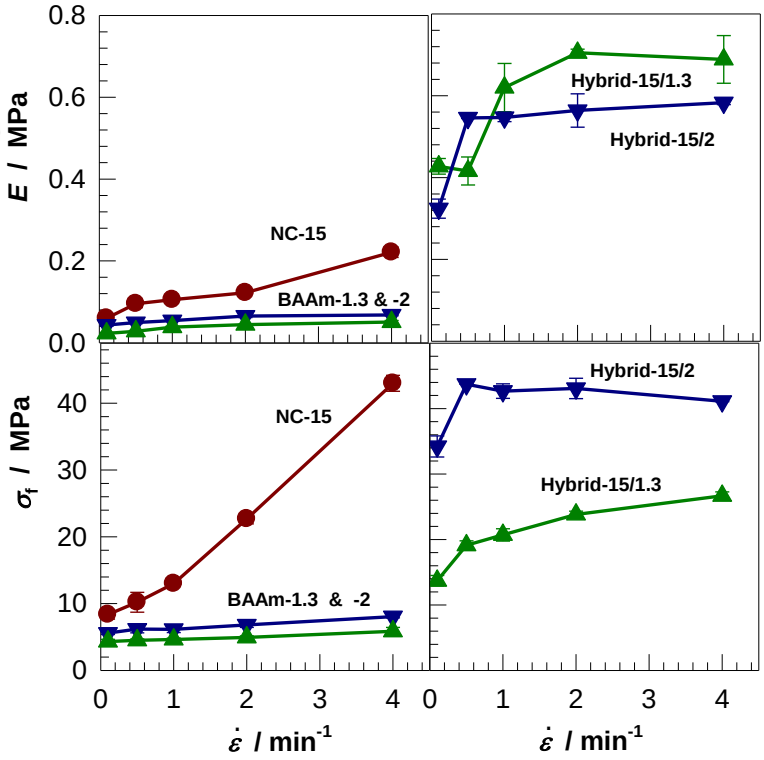

Figure 2.10 : Young's modulus E (upper panel) and compressive strength σ_f (bottom panel) of hybrid-hydrogels (right panel) and their component hydrogels (left panel) plotted against the strain rate $\dot{\varepsilon}$.

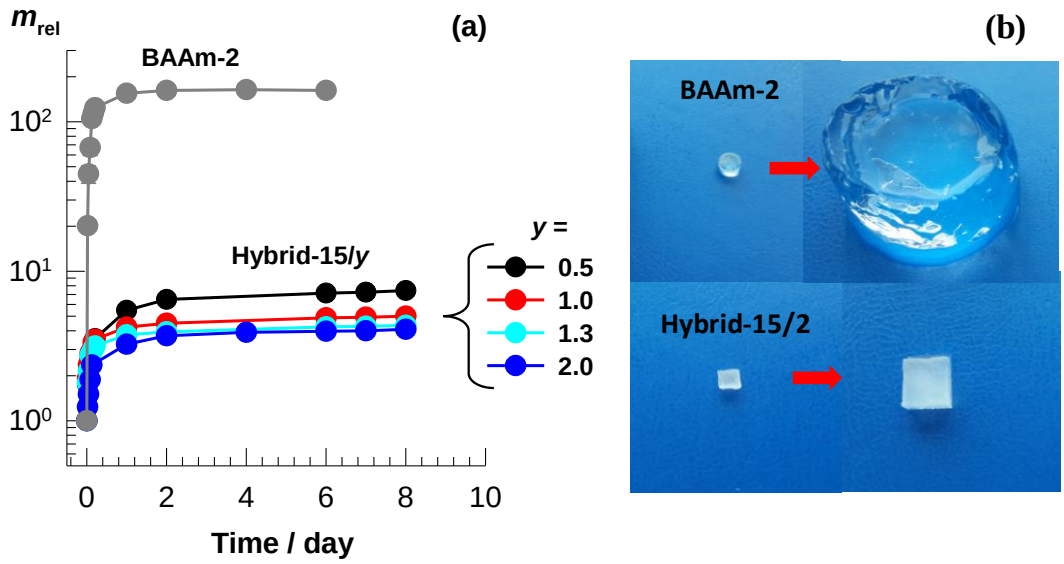

Figure 2.11 : (a): Relative weight swelling ratio m_{rel} of BAAm-2, and hybrid 15/*y* hydrogels plotted against the time of swelling in water. BAAm contents *y* (in mol%) are indicated. **(b):** Images of BAAm-2 and hybrid-15/2 hydrogel specimens before and after equilibrium swelling in water.

All the mechanical properties of the hydrogels reported so far are related to their as-prepared states. Because NC- and BAAm-hydrogels, except BAAm-2, are soluble in water (Table 2.1), we can only compare the mechanical characteristics of BAAm-2 with the resulting hybrid-15/2 hydrogel in their equilibrium swollen states in water. Figure 2.12a shows compressive stress-strain curves of swollen BAAm-2 and hybrid-15/2 hydrogels while Figure 2.12b compares their Young's modulus and compressive strength. It is seen that the mechanical performance of the hydrogels significantly decreases after their swelling due to the dilution of PAMPS chains. However, hybrid-15/2 exhibits 6-fold larger modulus (48±4 kPa) and 5-fold larger compressive strength (126±14 kPa) as compared to BAAm-2 precursor.

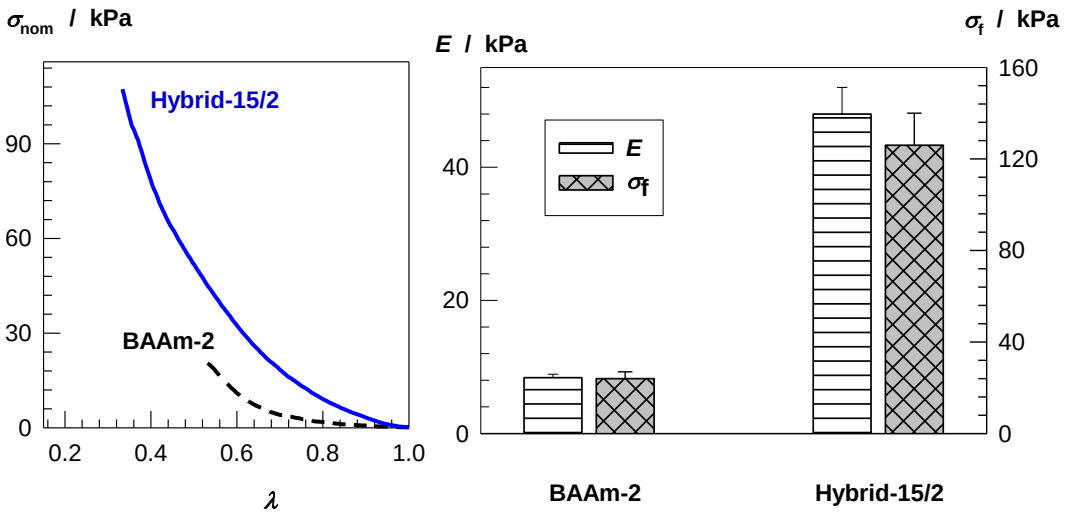

Figure 2.12 : (a): Compressive stress – strain curves of BAAm-2 and Hybrid-15/2 hydrogels in their equilibrium swollen states in water. $\dot{\varepsilon}$ = 1 min^{-1}. **(b):** Young's modulus E and fracture stress σ_f of swollen BAAm-2 and Hybrid-15/2 hydrogels.

2.2.3 Self-healing properties

Supramolecular and hybrid network structures of the hydrogels suggest that they would possess the ability to self-heal after creating a damage. To find out whether the cross-links making the hydrogel network would break reversibly or irreversibly under an external load, we performed cyclic compression tests at a strain rate $\dot{\varepsilon}$ of 1 min^{-1}. Figures 2.13a-d show loading / unloading cycles of PAMPS, NC-15, BAAm-1, and Hybrid-15/1 hydrogels, respectively, conducted under increased maximum strain ε_{max} from 20 to 80% compression with a waiting time of 5 min between cycles. Loading and unloading curves are indicated by solid and dashed lines, respectively. The general trend is that the unloading curve of each cycle follows a different path from the loading curve with a smaller area under the curve, indicating dissipation of energy due to breaking of intermolecular bonds. Below the maximum strain ε_{max} of 80%, each loading curve follows the path of the previous loading demonstrating that the intermolecular bonds broken under stress are reformed during the waiting time of 5 min. However, the loading curve for ε_{max} = 80% (solid blue line) deviates from the previous loading and the extent of deviation increases in the order of BAAm-1 < Hybrid-15/1 < PAMPS < NC-15. The results thus suggest existence of both reversibly and irreversibly broken bonds in the hydrogels.

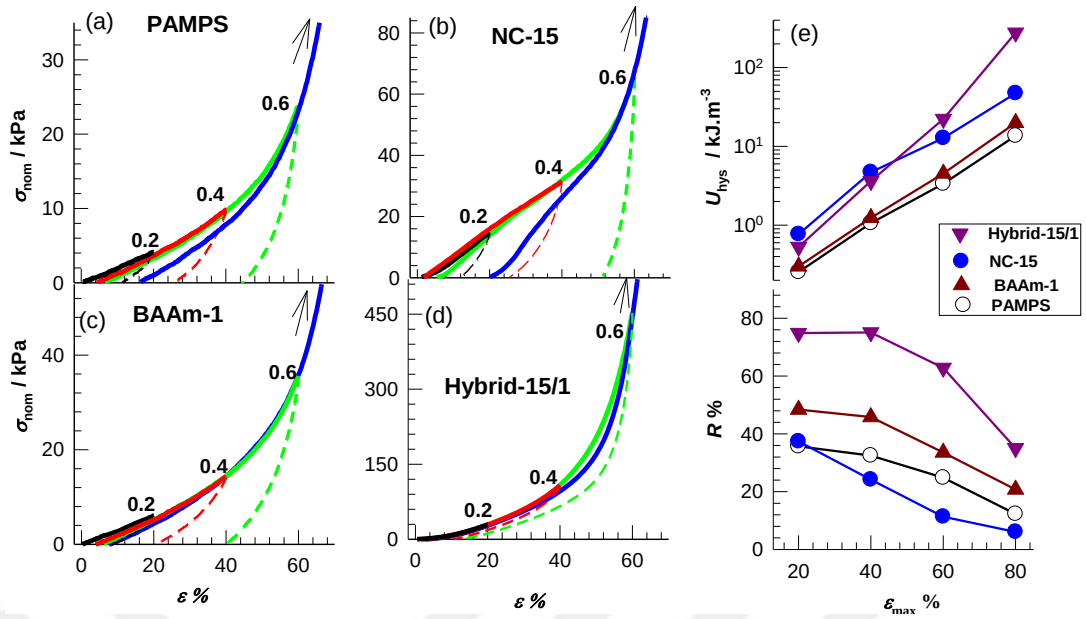

Figure 2.13 : (a-d): Loading / unloading compression cycles for PAMPS (a), NC-15 (b), BAAm-1 (c), Hybrid-15/1 hydrogels (d). The tests were conducted with increasing maximum strain ε_{max} from 20 to 80%, as indicated. Loading and unloading curves are shown by solid and dashed lines, respectively. $\dot{\varepsilon}$ = 1 min^{-1}. Wait time between cycles = 5 min. **(e):** ε_{max} dependences of the hysteresis energy U_{hys} and resilience R for PAMPS (○), NC-15 (●), BAAm-1 (▲), and Hybrid-15/1 hydrogels (▼).

The energy U_{hys} dissipated during the compression cycles was estimated from the area between the loading and unloading curves using the equation:

$$U_{hys} = \int_{0}^{\varepsilon_{max}} \sigma_{nom}\, d\varepsilon - \int_{\varepsilon_{max}}^{0} \sigma_{nom}\, d\varepsilon \qquad (2.2)$$

while the resilience R representing the ability of a hydrogel to deform reversibly without dissipation of energy was calculated from the ratio of the areas below the unloading to the loading curves, i.e.,

$$R = \frac{\int_{\varepsilon_{max}}^{0} \sigma_{nom}\, d\varepsilon}{\int_{0}^{\varepsilon_{max}} \sigma_{nom}\, d\varepsilon} \qquad (2.3)$$

Hysteresis energy U_{hys} and resilience R of the hydrogels are plotted in Figure 2.13e as a function of the maximum strain ε_{max}. Hybrid hydrogel exhibits both the highest resilience R and hysteresis energy U_{hys} among the hydrogels. Because R corresponds to the recovered energy while the dissipated energy U_{hys} is proportional to the number of broken bonds, the number of bonds broken under strain is largest in

hybrid hydrogel but most of these bonds are reformed after the cycle. Although NC-15 hydrogel also exhibits a large hysteresis, its resilience is the lowest revealing the occurrence of an irreversible damage.

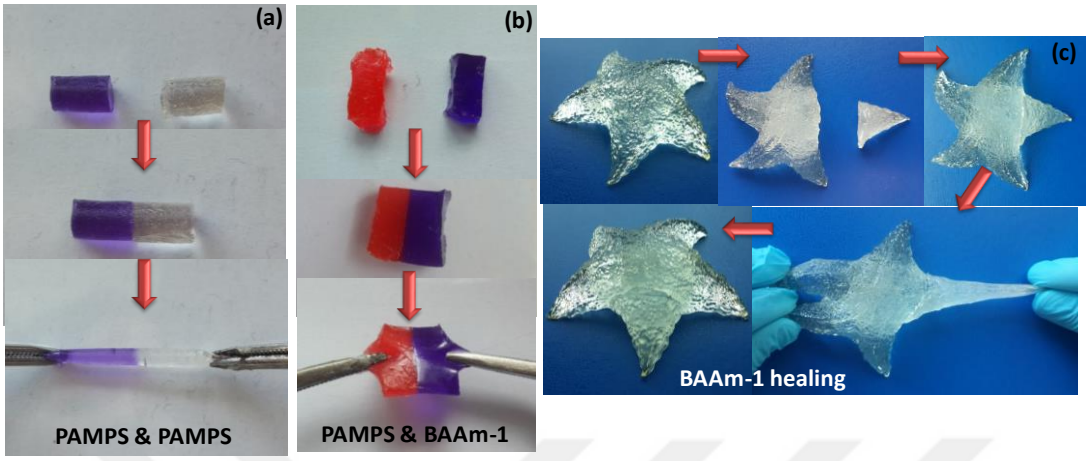

Figure 2.14 : Photographs of hydrogel samples demostrating their self-healing abilities. After pressing the fractured surfaces of PAMPS – PAMPS (a), PAMPS - BAAm-1 (b), and BAAm-1 – BAAm-1 hydrogel specimens (c) together over night at room temperature, they merge into a single piece. The samples were colored with a dye for clarity.

Self-healing ability of the hydrogels was also macroscopically investigated by cutting the gel specimens into two parts, and then merging the cut surfaces by pressing together. Self-healing tests were conducted on PAMPS, NC-15, BAAm-1, and hybrid-15/1 hydrogels. The hydrogels prepared without Laponite, that is, both PAMPS and BAAm-1 could be healed at room temperature (24±2 °C) after a healing time of 24 h (Figure 2.14). However, healing in the gel specimens containing Laponite could only be induced by heating the cut surfaces above the room temperature. In the following, healing tests of NC-15 and hybrid-15/1 hydrogels were conducted at 50 °C for 24 h. To quantify the healing efficiency, tensile tests at a strain rate of 1 min^{-1} were conducted on both virgin and healed hydrogel samples. For all hydrogels studied, we observed that the second damage always occurred in the healed region of the gel specimens revealing that the original network structure cannot be completely recovered after the healing process.

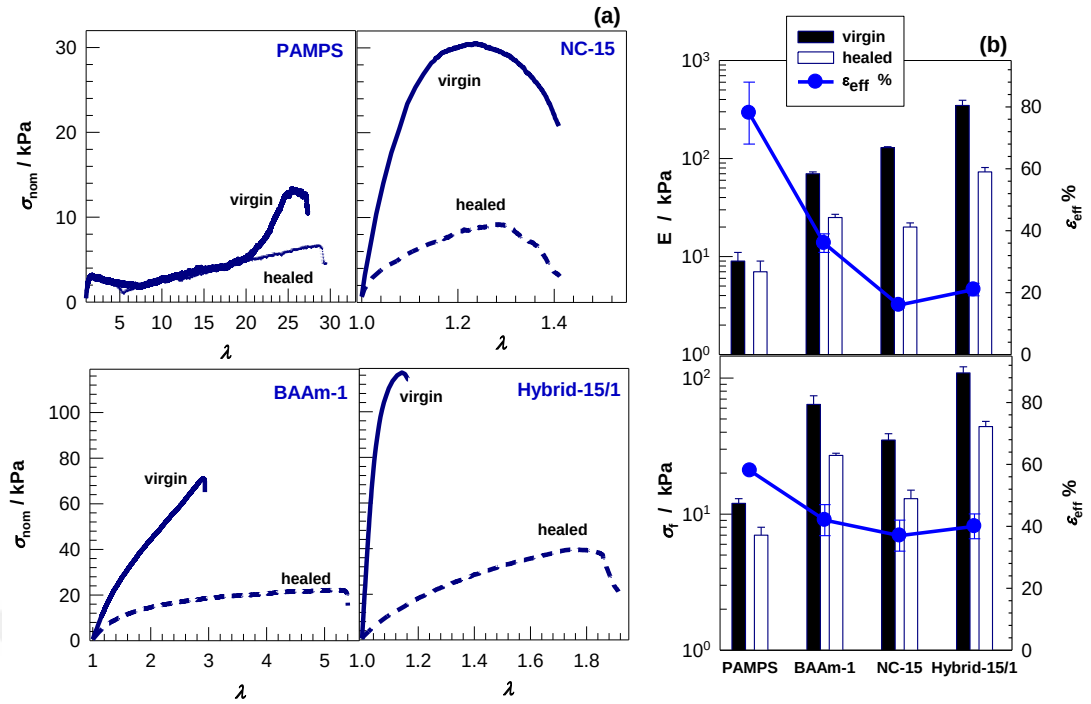

Figure 2.15 : (a): Stress-strain curves of virgin and healed PAMPS, NC-15, BAAm-1, and hybrid-15/1 hydrogels. (b): Young's modulus E and compressive strength σ_f of virgin (filled bars) and healed hydrogel samples (open bars), and their healing efficiencies ε_{eff} (symbols).

Figure 2.15a shows stress-strain curves of virgin and healed PAMPS, NC-15, BAAm-1, and hybrid-15/1 hydrogels. It is seen that the fracture stress of all healed gel samples is lower than that of the virgin ones. Moreover, healed BAAm-1 and hybrid-15/1 hydrogels exhibit larger elongation at break as compared to virgin ones, likely because of the lower cross-link density of the healed samples contributing to the extensibility of the network chains. In Figure 2.15b, Young's modulus E and compressive strength σ_f of virgin (filled bars) and healed hydrogel samples (open bars) together with the corresponding healing efficiencies ε_{eff} (line and symbols) are compiled for the hydrogels studied. The highest modulus and strength after healing was observed in hybrid hydrogels. The healing efficiencies of the hydrogels with respect to the modulus and strength are between 16-78 and 37-58%, respectively, and they decrease in the order PAMPS > BAAm-1> Hybrid-15/1> NC-15. Thus, although hybrid hydrogel exhibits a much higher modulus (348 vs 129 kPa) and strength (109 vs 35 kPa) as compared to the NC-hydrogel, it exhibits a better healing performance.

2.3 Conclusions

We described a simple strategy to prepare mechanically strong PAMPS hydrogels with self-healing ability. Initiator-free polymerization of AMPS in aqueous solutions in the presence of Laponite nanoparticles and BAAm cross-linker produces hybrid-cross-linked hydrogels with excellent mechanical prope rties. To elucidate the individual effects of Laponite and BAAm on the hydrogel properties, the hydrogels were also prepared without any additive as well as after incorporating of Laponite and BAAm alone into the physical network. AMPS polymerization without any additive leads to highly stretchable hydrogels with an elongation at break of 2600%. However, PAMPS hydrogels easily dissolve in water due to the weak inter-chain hydrogen bonds. Addition of Laponite or BAAm separately further weakens the hydrogen bonding interactions and hence produces weak and water-soluble hydrogels. In contrast, simultaneous incorporation of Laponite and BAAm into the physical network leads to hybrid cross-linked PAMPS hydrogels with superior mechanical properties. They exhibit a high modulus (~700 kPa), compressive strength (45 MPa at ~90% strain), good resilience, and self-healing. The strength of hybrid cross-linked PAMPS hydrogels is attributed to the strong interactions between chemically cross-linked PAMPS chains and nanoparticles. The hybrid approach presented here might enable preparation of mechanically strong nanocomposite hydrogels consisting of strongly or weakly charged polymer chains of different architecture.

3. A SELF-HEALING AND HIGHLY STRETCHABLE POLYELECTROLYTE HYDROGEL VIA COOPERATIVE HYDROGEN-BONDING AS SUPERABSORBENT POLYMER[2]

The classical first-generation hydrogels are chemically cross-linked hydrophilic polymers absorbing large quantities of water while maintaining their integrity [40]. Although such hydrogels display spectacular features offering a wide range of potential application areas, they encounter irreversible damage under a low strain due to the absence of an efficient mechanism for energy dissipation [17,41]. To overcome this limitation, several studies in the last decade have focused on preparing mechanically strong physically cross-linked hydrogels [42]. Although physical hydrogels can easily be prepared via non-covalent interactions such as H-bonding [43–48], or hydrophobic interactions [49–51], they generally exhibit insufficient mechanical strength or low water holding capacity due to the weak intermolecular bonds. Considering the strength of H-bonds is about 100-fold weaker than that of the covalent bonds, generation of a strong physically cross-linked polymer or gel requires H-bonding cooperativity [52,53]. Such a strengthening effect of cooperativity of H-bonds is observed in the nature, starting from water molecules up to biopolymers such as double-stranded DNA or proteins [54]. For instance, the stability of the secondary and tertiary structures of proteins and DNA arises from the cooperative effect of H-bonds between oxygen atom of the C=O and NH fragments, acting as proton acceptor and donor, respectively.

The general strategy for the preparation of mechanically strong hydrogen-bonded hydrogels is to reduce their water contents and hence, to amplify H-bonding interactions [55–63]. For instance, hydrogen-bonded physical hydrogels with moderate water contents (30-80%) were prepared using dual amide groups [54], diaminotriazine-diaminotriazine interactions [56,57], ureidopyrimidinone units [57,58], and H-bond acceptor and donor comonomer units [60–63]. To our

[2] This chapter is based on the paper "Su, E. Yurtsever, M. Okay, O. (2019). A self-healing and highly stretchable polyelectrolyte hydrogel via cooperative hydrogen-bonding as a superabsorbent polymer. Macromolecules 52, 3257-3267."

knowledge, superabsorbent hydrogels formed via entirely H-bonds that are stable in water with a swelling capacity exceeding 1000-times their original mass have not been reported before..

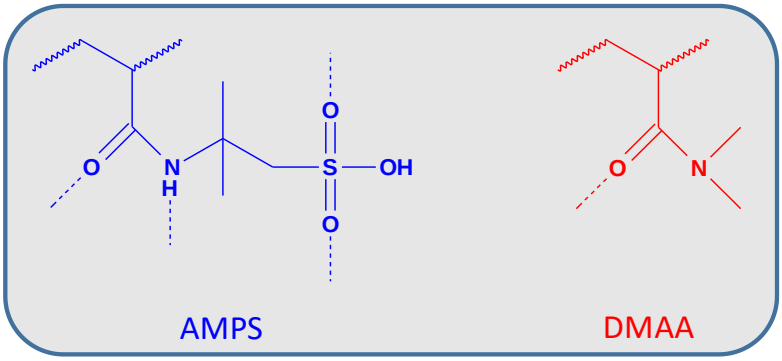

Figure 3.1 : Structure of AMPS and DMAA monomer units. Dashed lines represent H-bonding regions.

2-acrylamido-2-methyl-1-propanesulfonic acid (AMPS) is a popular strong electrolyte monomer widely used in the preparation of superabsorbent polymers exhibiting pH-independent large swelling capacity (Figure 3.1) [3,7–9,64,65]. Poly(AMPS) (PAMPS) hydrogels are also attractive materials in bioengineering, food industry, agriculture, and water purification [5,10–13]. However, because PAMPS hydrogels have generally been prepared via covalent cross-links, they exhibit poor mechanical properties limiting their application areas. Recent work shows that AMPS undergoes spontaneous, initiator-free thermal polymerization in concentrated aqueous solutions at elevated temperatures leading to the formation of physical PAMPS hydrogels [2,66]. The resulting physical gels formed via H-bonds between carbonyl and amino groups of AMPS units are highly stretchable (up to 2500% stretch at break) but they exhibit poor mechanical properties and hence, easily dissolve in aqueous media suggesting weak H-bonding interactions between PAMPS chains [2,66]. This is expected due to the strong polyelectrolyte nature of PAMPS in aqueous media, generating a high osmotic pressure exerted by the AMPS counterions. This osmotic pressure seems to dominate over the rubberlike elasticity of the physical PAMPS network leading to its disruption in water.

Here, we show that UV-polymerization of AMPS at room temperature (23±2 °C) without a chemical cross-linker leads to the formation of water-insoluble, highly stretchable hydrogels with large swelling capacities (up to 1013±53 $g \cdot g^{-1}$). Although the hydrogels are stable in water, they easily dissolve in chaotropic solvents

suggesting that they form via H-bonding interactions between PAMPS chains. The question arising is why UV-polymerized hydrogels are stable in water as compared to the water-soluble thermal-polymerized ones? In the following, we discuss and compare rheological and mechanical properties of PAMPS hydrogels prepared via UV and thermal polymerizations. As will be seen below, the molecular weight of PAMPS primary chains isolated from UV-polymerized hydrogels is around 2-orders of magnitude higher than that of thermal polymerized ones, which is responsible for their stability in water. We also hypothesized that the incorporation of N, N-dimethylacrylamide (DMAA) units into the physical PAMPS network would further enhance the mechanical strength of PAMPS hydrogels. Although DMAA units are unable to form H-bonds between one another due to their dimethyl amino groups, they exhibit enhanced proton acceptor properties of their C=O groups through the σ-donation effect of the methyl groups (Figure 3.1). This would contribute to the cooperativity of H-bonds in PAMPS/DMAA hydrogels. We indeed observed that the addition of DMAA significantly improves both the mechanical and self-healing properties of physical PAMPS hydrogels in their as-prepared states without changing their high stretchability and extraordinary swelling capacity.

3.1 Experimental Part

3.1.1 Materials

2-Acrylamido-2-methylpropane-1-sulfonic acid (AMPS, 99%, Sigma-Aldrich), N,N-dimethylacrylamide (DMAA, 99%, Sigma-Aldrich), 2-hydroxy-4′-(2-hydroxyethoxy)-2-methylpropiophenone (Irgacure 2959, 98%, N,N′-methylenebis(acrylamide) (BAAm, 99%, Merck), Sigma-Aldrich), and poly(ethylene glycol) (PEG, 10 000 g mol^{-1}, Sigma-Aldrich) were used without purification.

3.1.2 Preparation of hydrogels

Hydrogels were prepared by UV-initiated solution polymerization of AMPS at 23±2 °C without and with DMAA in water using Irgacure 2959 as a photoinitiator. No chemical cross-linker was used in the gel preparation. The total monomer concentration C_o was varied between 50-80 wt %, whereas DMAA mole fraction x_{DMAA} in the comonomer mixture was changed between 0 and 0.74 (Table 3.1). To illustrate the synthetic procedure, we give details for the preparation of a hydrogel at

C_o = 75 wt %, x_{DMAA} = 0.62, and in the presence of 0.2 mol % Irgacure initiator (with respect to the monomers). AMPS (2.50 g) and DMAA (2.00 g) were first mixed and dissolved in 1.50 mL of distilled water at 35 °C to obtain a homogeneous solution. After stirring for 10 min under bubbling nitrogen gas, Irgacure 2959 (14 mg) was added and the solution was transferred into plastic syringes of 20 mm in diameter as well as into rectangular plastic molds (20 × 1 cm) of 1 mm in thickness. The polymerization was conducted at 23±2 °C for 24 h under UV light at 360 nm. For comparison, PAMPS hydrogels were also prepared by thermal polymerization of aqueous 50 wt % AMPS solutions at 80 °C in the absence of an external initiator, as described before [2,65].

3.1.3 Swelling tests and gel fractions

The hydrogels prepared in the syringes were cut into specimens of ~3 mm in length and immersed in an excess of distilled water at 23±2 °C for at least 2 weeks by replacing water several times to wash out any soluble polymers, unreacted monomers and the initiator. After reaching swelling equilibrium, the specimens were taken out of water and freeze dried (Christ Alpha 2e4 LD-plus). The fraction of the monomers converted into water-insoluble polymer, that is, the gel fraction W_g was calculated as $W_g = m_{dry} / \left(10^{-2}\, m_o\, C_o\right)$, where m_o and m_{dry} are the masses of the specimen just after synthesis and after drying, respectively. The relative weight swelling ratio m_{rel} was calculated as $m_{rel} = m / m_o$, where m is the mass of the equilibrium swollen gel specimen. The water content H_2O % of the equilibrium swollen hydrogels was calculated as $H_2O\ \% \ = 10^2 \left(1 - m_{dry} / m\right)$.

3.1.4 Solubilization of the hydrogels and gel permeation chromatography (GPC) measurements

PAMPS gel specimens (0.39 g) after preparation were solubilized in 100 mL of aqueous 5 M urea solution by stirring at room temperature for 5 days. For AMPS/DMAA copolymer hydrogels, complete solubilization of the specimens required 7 to 10 M urea solutions and a dissolution time of 15 days under stirring. The polymer solutions containing urea were then poured into dialysis tubes (3500 MWCO, Snake Skin, Pierce) and dialyzed for 3 days against water that was changed 5 or 6 times. They were then further dialyzed for additional 1 day against PEG-10000

to concentrate the solutions. The molecular weight of the polymers isolated from the hydrogels was estimated using GPC measurements conducted on an Agilent 1260 Infinity GPC equipped with Waters Ultrahydrogel 250 and Ultrahydrogel 500 columns, and a refractive index detector. Phosphate buffer (pH = 7, NaN_3 internal standard) at a flow rate of 0.7 mL min^{-1} was the mobile phase. Linear polyethylene oxide (PEO), polyethylene glycol (PEG) standards were used to assign molecular weights.

3.1.5 Rheological experiments

The measurements were conducted at 25°C on a Gemini 150 Rheometer system, Bohlin Instruments, equipped with a solvent trap to prevent the evaporation. The temperature was controlled with a Peltier system to maintain it constant at 25 °C. The gel specimens prepared in plastic molds were cut into thin slices of about 20 mm in diameter and 3 mm in thickness and then placed between the parallel plates of the rheometer. The upper plate (diameter 20 mm) was set at a distance of 2950±150 μm. The frequency-sweep tests at a strain amplitude γ_o = 0.01 were carried out over the frequency range 0.1 to 300 rad·s^{-1}. The viscosities η of polymer solutions isolated from the hydrogels were measured with a cone-and-plate geometry with a cone angle of 4° and diameter of 40 mm over the range of shear rates $\dot{\gamma}$ 2x10^{-4} to 10^3 s^{-1}. Zero-shear viscosities η_o were estimated by fitting the viscosity data recorded at various shear rates to the Carreau model [67],

$$\eta(\dot{\gamma}) = \eta_o \left[1 + (\dot{\gamma}/\gamma_c)^2\right]^{-n/2} \tag{3.1}$$

where γ_c is the critical shear rate and n is the shear thinning index of the shear thinning region.

3.1.6 Mechanical tests

Uniaxial tensile and compression tests were performed on cylindrical and flat gel specimens, respectively, at 23±2 °C using a Zwick Roell Z0.5 TH test machine with a 500 N load cell. The stress was presented by its nominal σ_{nom} and true values σ_{true}, which are the forces per cross-sectional area of the undeformed and deformed gel specimen, respectively. Assuming constant gel volume during deformation, the true stress σ_{true} was calculated as $\sigma_{true} = \lambda \sigma_{nom}$ where λ is the deformation ratio

(deformed length / initial length). The strain ε is defined as the change in the length of the gel specimen relative to its initial length, i.e., $\varepsilon = \lambda - 1$ or $1 - \lambda$, for elongation and compression, respectively. Young's modulus E was calculated from the slope of $\sigma_{nom} - \varepsilon$ curves between 5-15% deformations. For the tensile tests, the initial sample length between jaws and the strain rate were 10±0.1 mm and 1 min^{-1}, respectively. Cyclic tensile tests were conducted by stretching gel specimens at a strain rate $\dot{\varepsilon}$ of 5 min^{-1} to a maximum strain ε_{max}, followed by immediate retraction to zero displacement and a waiting time of 1 min, until the next cycle of stretching. For the compression tests, the specimens were compressed at $\dot{\varepsilon}$ = 1 min^{-1}. The compressive fracture stress σ_f at failure was calculated from the maxima in true stress-strain curves, as detailed before [68]. For the determination of the self-healing ability of the hydrogels, cylindrical gel specimens of 4.6 mm in diameter and 9 cm in length were cut in the middle and then, the two halfs were merged together within a plastic syringe of the same diameter as the specimen by slightly pressing the piston plunger. Tensile tests were performed on both healed and virgin gel specimens. Healing efficiencies ε_h were estimated from the ratio of the modulus, fracture stress, and fracture strain of the healed samples to those of the virgin ones. The healing time was varied between 0.25 and 72 h.

3.1.7 Quantum mechanical calculations (QMCs)

QMCs were carried out to study the nature of H-bonds between AMPS monomers, $(AMPS)_2$, and AMPS/DMAA dimers in the gas phase as well as in acidic aqueous medium with implicit and explicit water. The geometries of the studied systems were optimized by using DFT methodology at M062X/6-311+g(d,p) level of the theory. In the gas phase calculations, many conformations were generated and only the data and figures belonging to the lowest energy structures were presented. The gas phase energies are the true minima confirmed by all positive frequencies. All the interaction energies are the basis set superposition error (BSSE) corrected energies using Counterpoise method obtained by single point calculations at the same level of the optimizations. In acidic medium, each sulfonyl ($-SO_3^-$) group carries a negative charge balanced by the proton, which is not naked but in the form of solvated by a water molecule, H_3O^+. To prevent hydrogen abstraction and preserve the electrostatic interactions between the sulfonyl and hydronium ions, one more extra water

molecule near hydronium ion was added. All the dimeric systems were subjected to optimization at the same level of gas phase calculations in the implicit water by adjusting the dielectric constant ε of the medium to 78. The solvent corrections were made using standard IEFPCM model.

Table 3.1 : Compositions, Swelling and Mechanical Properties of Hydrogels.[a]

Code	C_o %	χ_{DMAA}	m_{rel}	H_2O %	W_g	E / kPa	Tensile		Compression	
							σ_f / kPa	σ_f %	σ_f / MPa	σ_f %
T-50	50	0	soluble	soluble	0	9 (2)	12 (1)	2500 (360)	-	-
U-50	50	0	877 (77)	99.94	1.00	27 (2)	64 (6)	1900 (110)	-	-
U-55	55	0	962 (40)	99.95	0.93	39 (3)	95 (8)	1320 (120)	-	-
U-60	60	0	1013 (53)	99.94	0.99	65 (5)	114 (7)	1120 (90)	9 (0.3)	95
U-70/0.5	70	0.46	1662 (11)	99.99	1.11	172 (8)	303 (13)	1130 (40)	12 (0.4)	93
U-75/0.6	75	0.62	1026 (67)	99.99	1.13	407 (22)	568 (40)	1010 (80)	14 (1.3)	89
U-80/0.7	80	0.74	934 (40)	99.99	1.11	372 (14)	518 (27)	1020 (70)	-	-

[a] Standard deviations are given in parentheses. They are less than 5% for m_{rel}, W_g, and ε_f values.

3.2 Results and Discussion

3.2.1 UV- versus thermal-polymerization of AMPS

PAMPS hydrogels were synthesized by UV-initiated polymerization of aqueous AMPS solutions using Irgacure 2959 as the initiator without a chemical cross-linker. The concentration of AMPS at the gel preparation, C_o, was varied from 50 wt % up to its solubility limit of 60 wt.%. For comparison, thermal polymerization of AMPS at 80 °C without any initiator and cross-linker was also carried out. In the following paragraphs, PAMPS hydrogels formed via UV- and thermal polymerizations are denoted as U-*x* and T-*x* gels, respectively, where *x* represents the AMPS concentration C_o. Figure 3.3a shows Young's modulus *E* of U-50 gels plotted against the initiator concentration. For comparison the modulus of T-50 gel is also shown by the open triangle. The modulus of U-50 gel prepared in the absence of the UV initiator is 8.9±0.1 kPa which is close to that of the T-50 gel (9±2 kPa). Swelling tests showed that they both are easily soluble in water suggesting weak intermolecular interactions. The modulus *E* rapidly increases with increasing initiator concentration and, after passing a maximum (30±2 kPa) at around 0.5 mol % initiator, it starts to decrease continuously. All U-50 gels prepared in the presence of the initiator were stable in water for at least 8 months, and they all exhibited a gel fraction W_g close to unity indicating that AMPS in the monomer feed was completely incorporated into the water-insoluble PAMPS network (Table 3.1). In the following, the initiator concentration was fixed at 0.2 mol % with respect to the monomer.

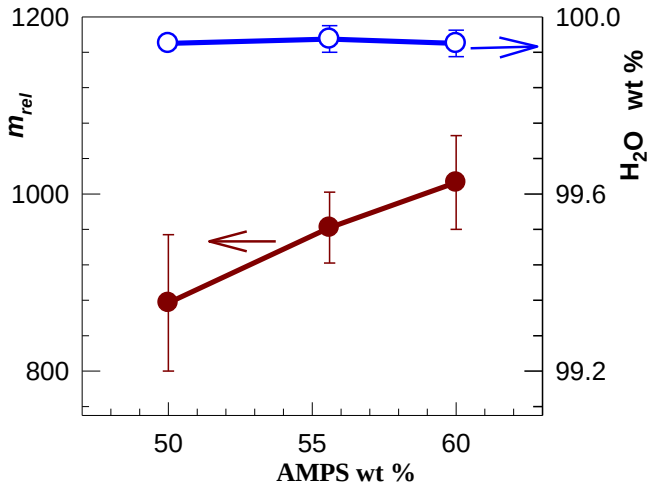

Figure 3.2 : The weight swelling ratio m_{rel} and water content of PAMPS hydrogels as a function of AMPS content.

All the U-gels exhibited large swelling capacities when immersed in water (Table 3.1). Figures 3.3b, c show the images of a U-60 gel specimen just after preparation and after equilibrium swelling in water, respectively. The equilibrium weight swelling ratio m_{rel} of the hydrogel is 1013±53 indicating that the network chains are around 10-fold stretched conformation as compared to their as-prepared states. m_{rel} slightly decreased with decreasing AMPS % and becomes 877±77 at 50 wt.% AMPS (Table 3.1, Figure 3.2).

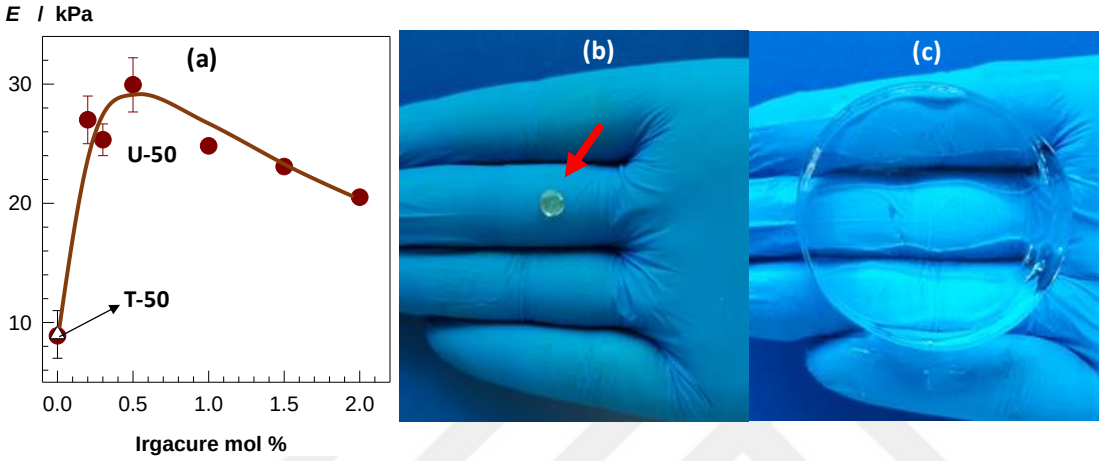

Figure 3.3 : (a): Young's modulus *E* of U-50 gels plotted against Irgacure concentration. Open triangle represents the modulus of the T-50 gel. **(b, c):** Images of a U-60 gel specimen just after preparation (b) and after equilibrium swelling in water (c).

Although U-gels are stable in water, they all could easily be dissolved in aqueous 5 M urea solution or in ethanol, which are known as chaotropic solvents disrupting H-bonds. This suggests that, similar to the T-gels, U-gels entirely form via hydrogen bonding interactions between PAMPS chains. To characterize the primary chains of the PAMPS network, we first dialyzed PAMPS/urea solutions isolated from the hydrogels against water for 3 days to remove urea, followed by dialyzing against aqueous PEG-10000 to concentrate the solutions. Figure 3.5a shows shear rate $\dot{\gamma}$ dependence of the viscosities η of 0.39 wt.% aqueous solutions of U-50 and T-50, obtained from the corresponding hydrogels. Both solutions exhibit Newtonian plateau at low shear rates and start to shear thin above a critical shear rate γ_c. U-50 solution has about 30-fold higher zero-shear viscosity η_o than the T-50 solution (23.3±0.1 vs 0.71±0.01 Pa·s) revealing that the molecular weight of PAMPS is relatively high in the former solution. Figure 3.5b shows angular frequency ω dependences of the storage *G'* (filled symbols) and loss moduli *G''* (open symbols)

of the same solutions. For the T-50 solution, G'' dominates over G' over the whole range of frequency and hence, it is a dilute polymer solution. In contrast, viscoelastic spectrum of the U-50 solution is typical for a semi-dilute polymer solution, i.e., G'' exceeds G' at low frequencies, and a crossover occurs between G' and G'' at a frequency of 2.6 rad s^{-1} corresponding to a characteristic time scale of 0.38 s for dissociation and association of non-covalent bonds. Frequency sweep tests conducted on hydrogels also show higher storage modulus G' and lower loss factor $tan\ \delta$ (=G'' / G') of U-50 as compared to T-50 (Figure 3.4).

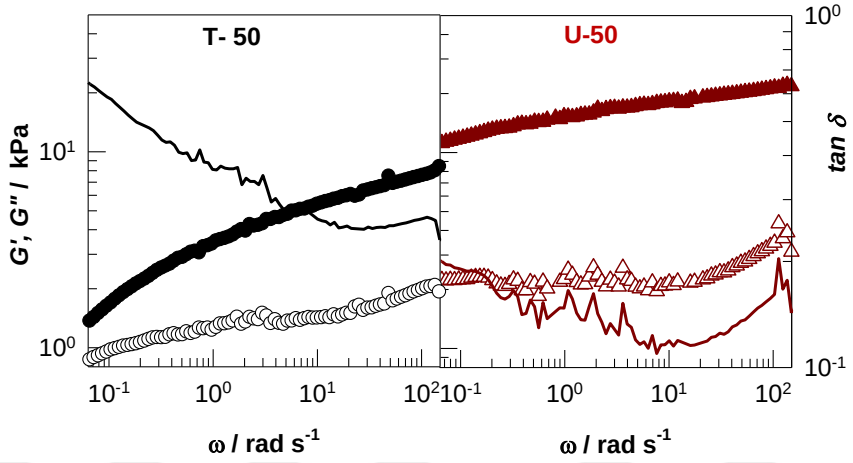

Figure 3.4 : Frequency ω dependences of the storage modulus G' (filled symbols), loss modulus G'' (open symbols), and loss factor $tan\ \delta$ (lines) of T-50 and U-50 gels at 25 °C. γ_o = 0.01.

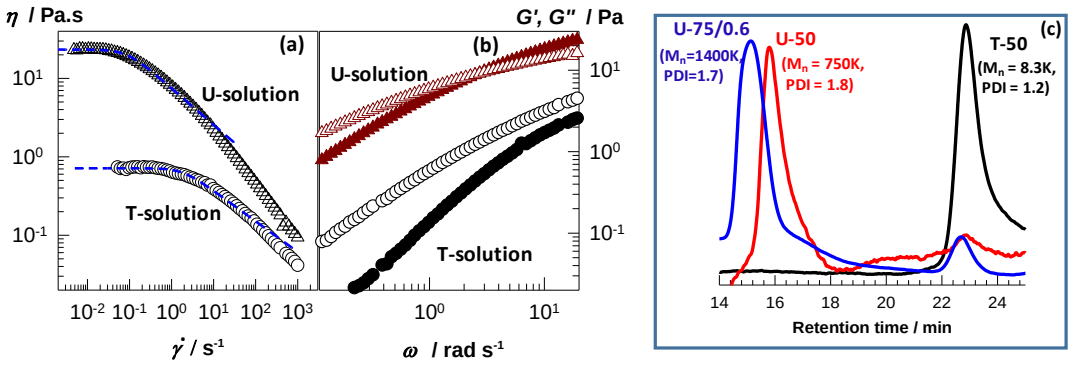

Figure 3.5 : (a): Viscosities η of aqueous 0.39 wt.% U-50 and T-50 solutions at 25 °C plotted against the shear rate $\dot{\gamma}$. The solutions were obtained from the corresponding hydrogels. The curves are the best fits to the Carreau model (equation 3.1) to estimate the zero-shear viscosity η_o. **(b):** Frequency ω dependences of the storage G' (filled symbols) and loss moduli G'' (open symbols) of 0.39 wt.% U- and T-solutions in water. γ_o = 0.1 Temperature =25 °C. **(c):** GPC curves of the polymers isolated from U-50, T-50, and U-75/0.6 hydrogels, yielding $\overline{M}_n$ values of 7.5x10^5, 8.3x10^3, and 1.4x10^6 g·mol^{-1}, with polydispersity indices of 1.8, 1.2, and 1.7, respectively.

The molecular weight of PAMPS chains isolated from the hydrogels was determined via GPC analysis with PEO standards. The number-average molecular weight $\overline{M}_n$ of the primary chains in U-gels was found to be much larger than that in T-hydrogels (Figure 3.5c). For instance, $\overline{M}_n$ of the polymers isolated from U-50 is around 90-fold higher than that of T-50 (7.5×10^5 vs 8.3×10^3 g·mol^{-1}). Thus, we may attribute the water-stability of U-hydrogels to their longer PAMPS primary chains providing formation of a larger number of H-bonds between two chains as compared to the water-soluble T-gels. Previous work indeed shows that the cooperativity of H-bonds becomes stronger as the degree of polymerization is increased [69]. This behavior was attributed to the proximity effect of the already formed H-bonds between two long polymer chains, restricting the conformations of the chain segments and hence, facilitating subsequent H-bond formation [70,71]. We should mention that the H-bonds may also trap preexisting chain entanglements and hence, increase their lifetimes to form chain-entanglement cross-links in the hydrogels. In addition, because the hydrophobic interactions and H-bonds can mutually reinforce each other [72,73], hydrophobic alkyl part of AMPS units at a high concentration (50-60%) in water contributes to the water stability of U-gels. To our knowledge, this is the first report presenting water-insoluble PAMPS hydrogels with 99.99% water content formed via entirely H-bonds.

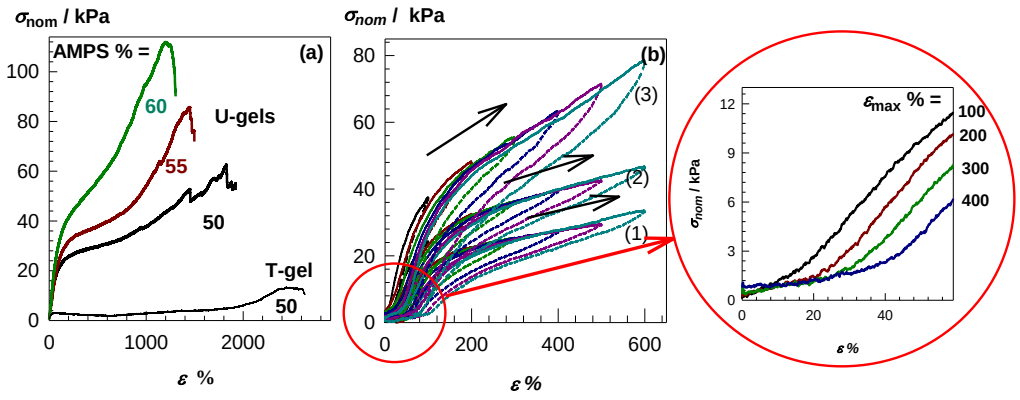

Figure 3.6 : (a): Tensile stress-strain curves of U- and T- hydrogels. AMPS contents as indicated. **(b):** Cyclic tensile tests conducted on U-gels up to a maximum strain ε_{max} of 600% with 100% steps. Loading curves are indicated by arrows. AMPS = 50 (1), 55 (2), and 60 wt % (3). The inset shows the initial portion of the loading curves.

Table 3.1 also reveals that, as compared to the T-50 gel, an improvement in the gel mechanical performances is observable after applying UV-polymerization technique without deteriorating stretch at break, which remained above 1000%. U-60 gel has the highest modulus E (65±5 kPa) and fracture strength σ_f (114±7 kPa) and sustains 1120±90% elongations. However, all U-gels exhibited plastic deformation under load, which is undesirable in many applications of tough hydrogels. For instance, successive cyclic tensile tests conducted on U-gels with increasing maximum strain from 100 to 600% resulted in a permanent deformation after each unloading step that increased with increasing maximum strain (Figure 3.6). This plastic deformation indicates that the gel elasticity of PAMPS network is insufficient to recover the original conformation. To eliminate plastic deformation and improve the elastic properties of the hydrogels, one may include a chemical cross-linker such as N,N'-methylenebis(acrylamide) (BAAm) in the monomer feed. However, experiments showed that even addition of a small amount of BAAm significantly decreases both the stretchability and swelling capacity of PAMPS hydrogels without a considerable increase in the modulus and fracture stress (Figures 3.7, 3.8). For instance, addition of 0.1 mol % BAAm reduces the strain at break from 1800 to 250%, the swelling ratio m_{rel} from 880 to 94, whereas the modulus E slightly increases from 27 to 50 kPa. Calculations show that the contribution H-bonds on the cross-link density of BAAm-cross-linked hybrid hydrogels reduces to around 50% upon incorporation of 0.1 mol % BAAm, which could be the reason for their deteriorated mechanical properties (Figure 3.7). Another strategy to improve the mechanical strength of the hydrogels is to incorporate comonomer units into the PAMPS chains strengthening H-bonding interactions, which will be discussed in the next section.

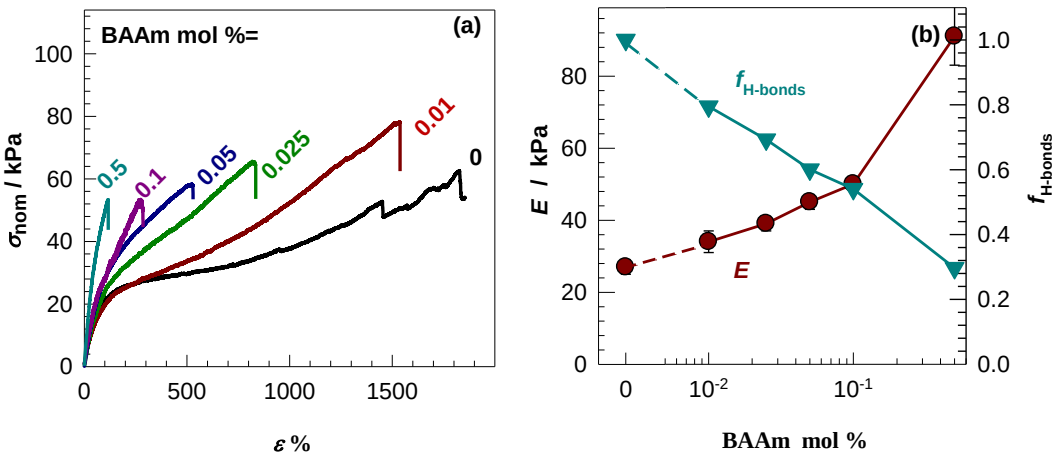

Figure 3.7 : (a): Stress-strain curves of PAMPS hydrogels prepared in the presence of various amounts of BAAm cross-linker. AMPS = 50 wt %. **(b):** Young' modulus E of PAMPS hydrogels and the fraction $f_{H\text{-bonds}}$ of cross-links contributed from the H-bonds as a function of BAAm content. AMPS = 50 wt.%. For hydrid cross-linked hydrogels containing both physical and chemical cross-links, one may calculate the fraction $f_{H\text{-bonds}}$ of cross-links contributed from the H-bonds by comparing the moduli of hydrogels prepared with and without BAAm. Because the cross-link density at a given polymer concentration is directly proportional to the modulus E, $f_{H\text{-bonds}}$ was estimated using the equation $f_{H\text{-bonds}} = E_o/E$ where E_o and E are Young's moduli of PAMPS hydrogels without and with BAAm, respectively.

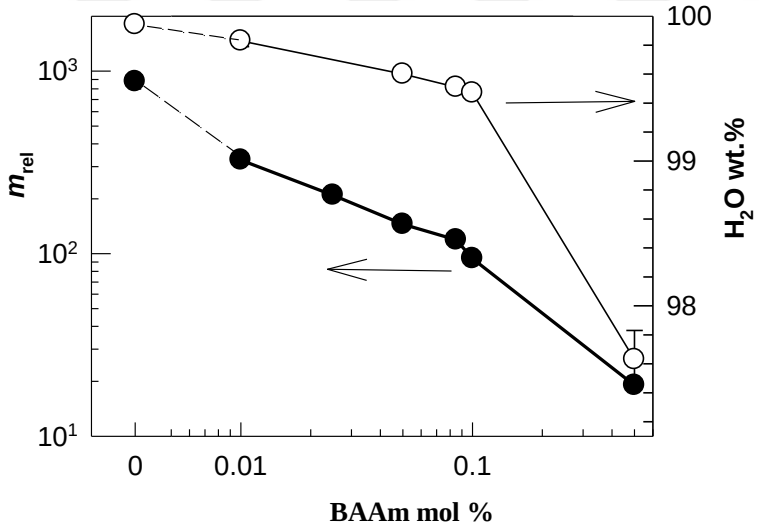

Figure 3.8 : The weight swelling m_{rel} and water contents of PAMPS hydrogels as a function of BAAm content. AMPS = 50 wt %.

3.2.2 Effect of DMAA as H-bonding acceptor

N,N-dimethylacrylamide (DMAA) monomer with its strong H-bond acceptor properties is a good candidate to strengthen H-bonding interactions in PAMPS hydrogels. Polymers derived from DMAA are also attractive for building physical gels due to their ability to form hydrophobic associations [47,74,75]. Further, we

observed that DMAA could be solubilized in saturated aqueous solution of 60 wt.% AMPS which provided formation of hydrogels with a high polymer content. By adding DMAA into 60 wt % AMPS solution, we were able to increase the total monomer concentration C_o up to 80 wt.% during which the mole fraction of DMAA (x_{DMAA}) in the feed increased up to 0.74 (Table 3.1). In the following, AMPS/DMAA hydrogels are named as copolymer hydrogels, or as U-*x/y* where *x* and *y* are the total monomer concentration C_o and DMAA mole fraction x_{DMAA} in round numbers, respectively (Table 3.1).

Similar to U-x gels, copolymer gels were insoluble in water with a gel fraction W_g of around unity, and they all exhibited large swelling ratios m_{rel} between 934 and 1622 in water (Table 3.1). An interesting point is that the incorporation of non-ionic DMAA segments into the ionic PAMPS network up to a mole fraction x_{DMAA} = 0.74 leads to an increase in the swelling ratio of the hydrogels. For instance, purely ionic U-60 hydrogel exhibits a swelling ratio m_{rel} of 1013±53, whereas incorporation of 20 wt % non-ionic DMAA segments into this hydrogel produces a hydrogel (U-70/0.5) with m_{rel} = 1662±11. This excess swelling of DMAA-containing hydrogels stands in contrast to Flory-Rehner theory predicting that the equilibrium swelling degree is directly proportional to the charge density of hydrogels [48]. We attribute this behavior to the counterion condensation in ionic gels at high charge densities leading to the formation of "osmotically passive" counterions which do not contribute to the swelling process [3,76–79]. According to Manning's theory [80], if the distance *A* between two consecutive charges on the network chains reduces to the Bjerrum length *Q*, counterions in ionic hydrogels start to condense and reduce their ionic osmotic pressure in water. For PAMPS hydrogels swollen in water, the Bjerrum length *Q* is around 0.71 nm [3], and the counterion distance *A* can be calculated as b/x_{AMPS} where *b* is the bond length which is 0.25 nm for vinyl polymers, and x_{AMPS} = 1- x_{DMAA}. The counterion distance *A* was calculated as 0.25, 0.46, and 0.66 nm for U-60, U-70/0.5, and U-75/0.6 hydrogels, respectively. Thus, incorporation of non-ionic DMAA segments into PAMPS hydrogels increases the distance *A* between charged AMPS units suppressing condensation of counterions and hence contributing to the swelling of the hydrogels in water.

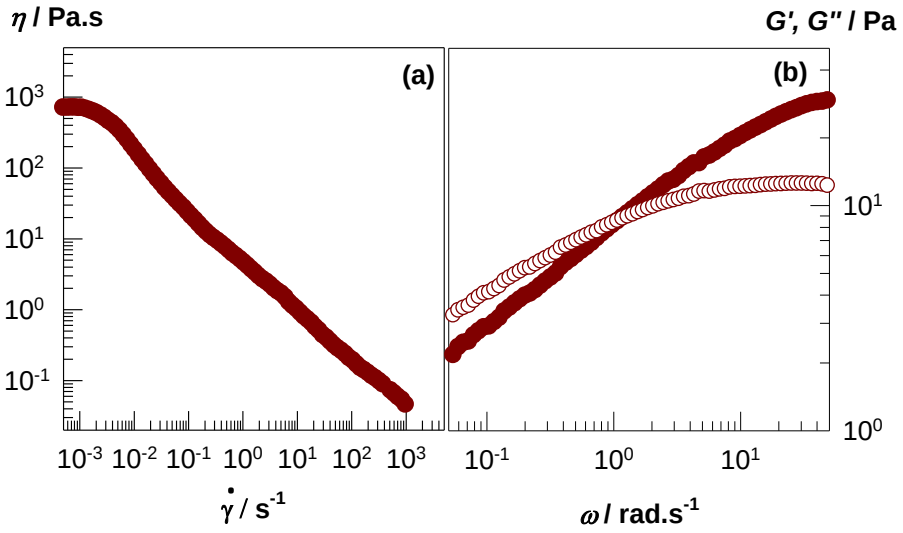

Figure 3.9 : (a): Shear rate $\dot{\gamma}$ dependence of the viscosity η of 0.39 wt.% U-75/0.6 solution. **(b):** Frequency ω dependences of *G'* (filled symbols) and *G''* (open symbols) of the same solution. $\gamma = 0.1$.

Copolymer hydrogels could also be dissolved in urea solutions revealing that they are also formed solely via non-covalent bonds. However, solubilization of the copolymer hydrogels in water required harsh conditions, e. g., a high concentration of urea (7-10 M) and a long dissolution time under stirring (15 days). Figure 3.9 shows shear-rate dependence of the viscosity η and frequency dependences of the dynamic moduli *G'* and *G''* of an aqueous 0.39 wt % U-75/0.6 solution derived from the corresponding copolymer gel. The zero shear viscosity η_o is 700±40 Pa·s, which is 30-fold larger than that of the U-50 solutions. Moreover, the crossover frequency decreases from 2.6 to 1.1 rad·s^{-1}, that is the lifetime of physical bonds increases from 0.38 to 0.91 s upon incorporation of DMAA units in the hydrogel. The number-average molecular weight of the copolymer chains isolated from U-75/0.6 was measured as 1.4x10^6 g·mol^{-1} (Figure 3.5c), which is 2- and 170-fold larger than that of DMAA-free U-50 and T-50 hydrogels, respectively. The higher molecular weight of AMPS/DMAA copolymers as compared to PAMPS formed under identical conditions could be related to the hydrophobic associations between DMAA segments [81], reduced propagation rate constant AMPS homopolymerization at high AMPS contents [6], as well as favorable reactivity ratios of AMPS and DMAA during free-radical polymerization [82,83]. Thus, DMAA significantly contributes to the strength of the H-bonds in PAMPS hydrogels by increasing the length of their primary chains.

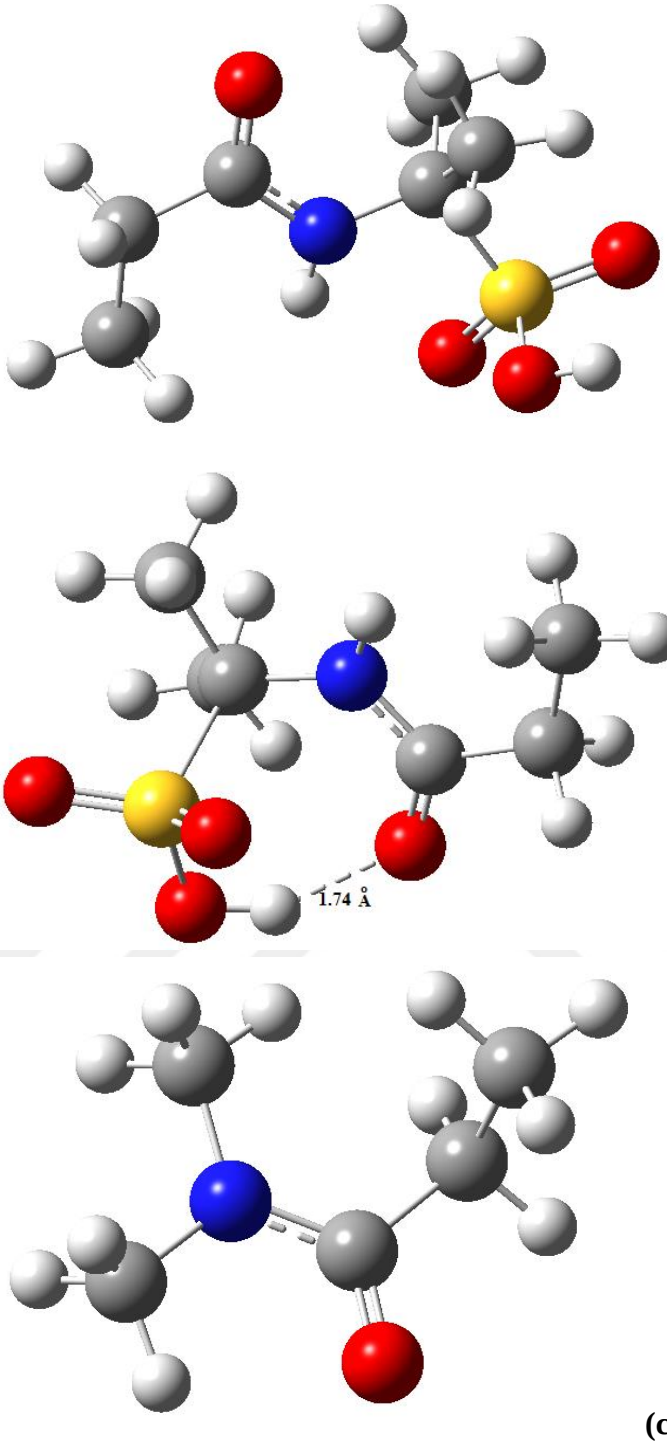

Figure 3.10 : The optimized geometries of AMPS in which C=O and N-H bonds are trans (a) and cis (b) to each other, and DMAA (c).

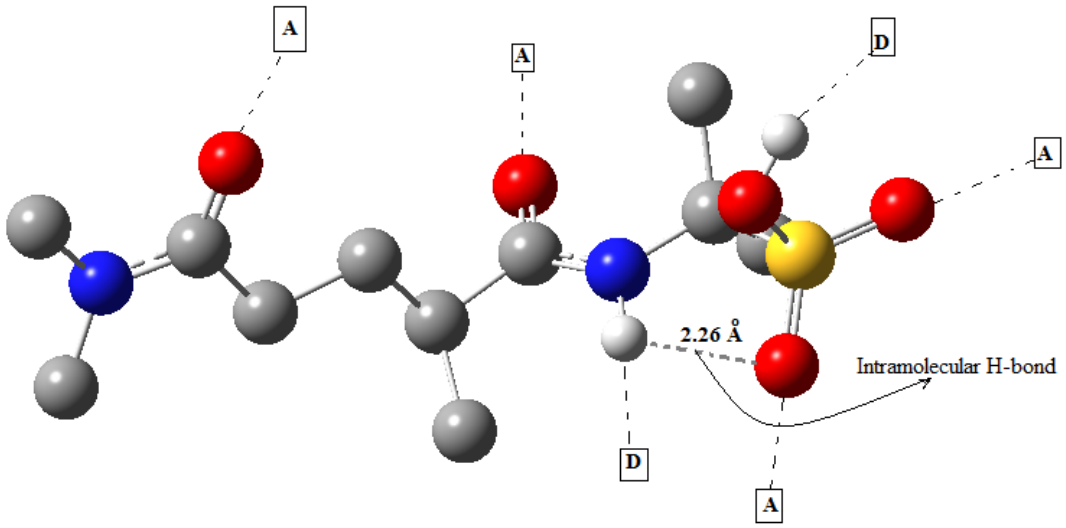

Figure 3.11 : Optimized geometry of AMPS-DMAA dimer. D and A represent H-bond donor and acceptor sites on the molecule, respectively.

Table 3.2 : BSSE-corrected Intermolecular Interaction Energies of the Dimer Molecules Obtained at M062X/6-311+g(d,p) Level, in the Gas Phase, and also with Implicit and Explicit Water.

System	**BSSE Corrected Intermolecular Interaction Energy ($kJ \cdot mol^{-1}$)**		
	Gas Phase	Implicit water	Explicit water
AMPS-AMPS	-77.4	-	-
$(AMPS)_2$-$(AMPS)_2$	-	+487.9	-28.0
AMPS/DMAA - AMPS/DMAA	-187.9	+145.6	-46.4
H_2O-H_2O	-23.8	-	Between -15.1 and -19.7 [84]

To gain more insight into the H-bonding interactions in the hydrogels, quantum mechanical calculations were carried out to study the nature of H-bonds between AMPS monomers, $(AMPS)_2$ and AMPS/DMAA dimers. The calculations were conducted in the gas phase as well as in acidic aqueous medium with implicit and explicit water. AMPS has adjacent C=O and N-H bonds which can be trans or cis to each other, where the latter conformation enables formation of an intramolecular H-bond at a distance of 1.74 Å (Figure 3.10). AMPS in the gas phase possesses three acceptor and two donor groups whereas upon incorporation of DMAA, the AMPS-DMAA dimer gains one more acceptor group (Figure 3.11). H-bonding interaction energies between AMPS monomers and AMPS/DMAA dimers in the gas phase were calculated as -77.4 and -187.9 $kJ \cdot mol^{-1}$, respectively, revealing that the H-bonds formed between copolymer chains are much stronger than those formed between PAMPS chains (Table 3.2). In aqueous medium, $(AMPS)_2$ and AMPS/DMAA dimers have 4 and 2 sulfonyl groups, respectively, and one hydronium hydrate ($H_3O^+ \cdot H_2O$) per sulfonyl group. In the absence of counterions, $(AMPS)_2$ dimers form one intermolecular H-bond between each other at a distance of 1.96 Å, whereas two intermolecular H-bonds at 1.92 and 2.34 Å distances are formed between AMPS/DMAA dimers, revealing stronger hydrogen bonding interactions between copolymers (Figure 3.12). The calculated intermolecular interaction energies for $(AMPS)_2$ and AMPS/DMAA are +487.9 and +145.6 $kJ \cdot mol^{-1}$, respectively, i.e., they are repulsive due to the negative charges, but less repulsive for the latter due to its lower negative charge. In the presence of $H_5O_2^+$ counterions, the optimization of the structures suffered from convergence problems due to the highly mobile water molecules which can adapt different conformations very easily. We have observed that the negative charges on the sulfonyl groups are distributed among the oxygen atoms bonded to sulfur atom and the positive charge on the hydronium ion is distributed over the adjacent water molecule coordinated via H-bonding to it. Between AMPS/DMAA dimers, two H-bonds form at distances between 1.9 - 2.4 Å whereas no intermolecular bonds were observed between $(AMPS)_2$ dimers (Figure 3.13). Moreover, the intermolecular interaction energies for $(AMPS)_2$ and AMPS/DMAA dimers were calculated as -28.0 and -46.4 $kJ \cdot mol^{-1}$, respectively (Table 3.2). The calculations thus confirm that the H-bonds between AMPS/DMAA copolymers are stronger than those between PAMPS polymers.

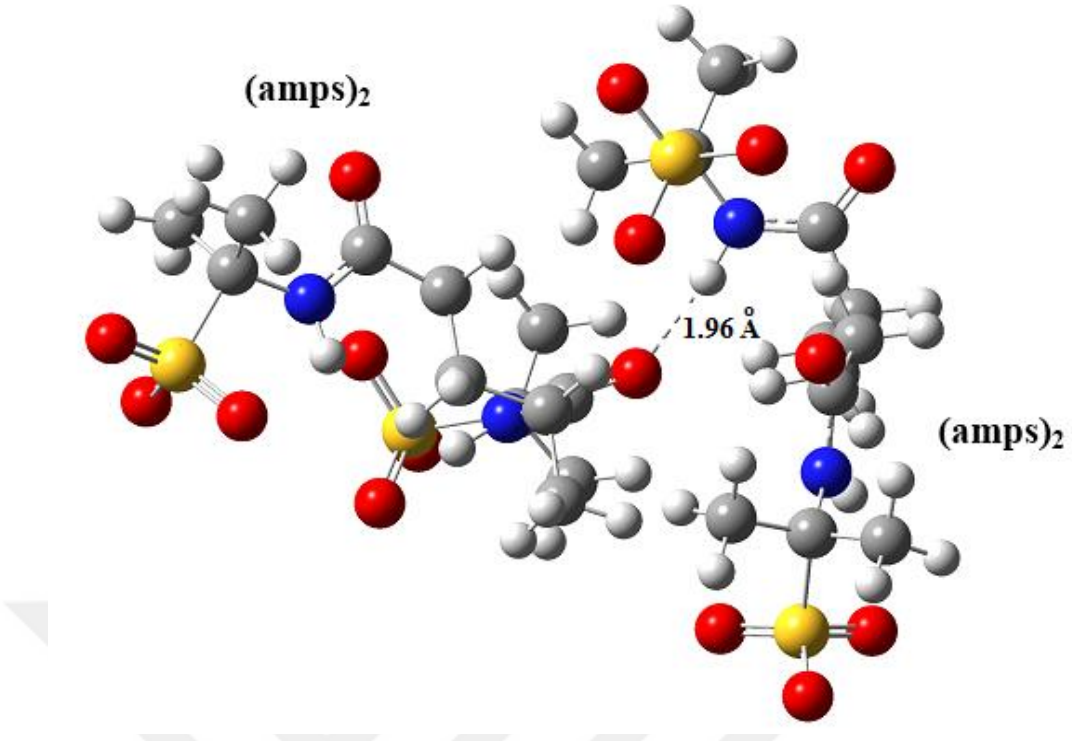

(a)

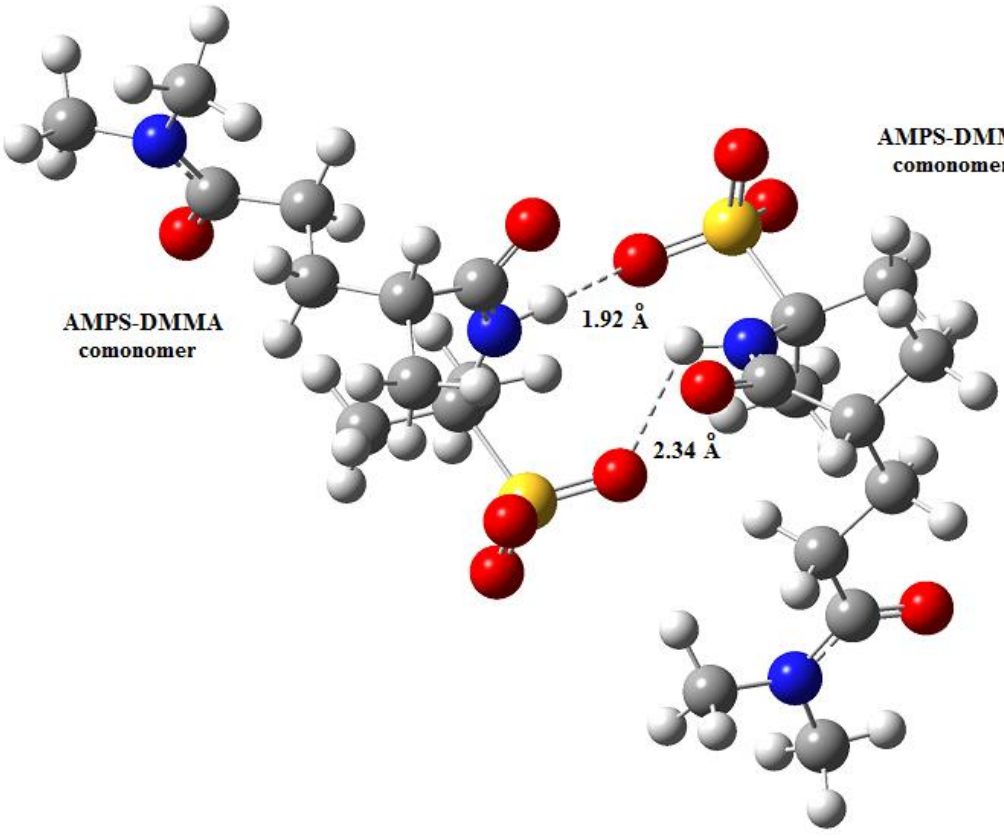

(b)

Figure 3.12 : Optimized geometries of $(AMPS)_2$ - $(AMPS)_2$ (a) and AMPS/DMAA - AMPS/DMAA dimers (b) in -4 and −2 anionic states, respectively, in implicit water medium.

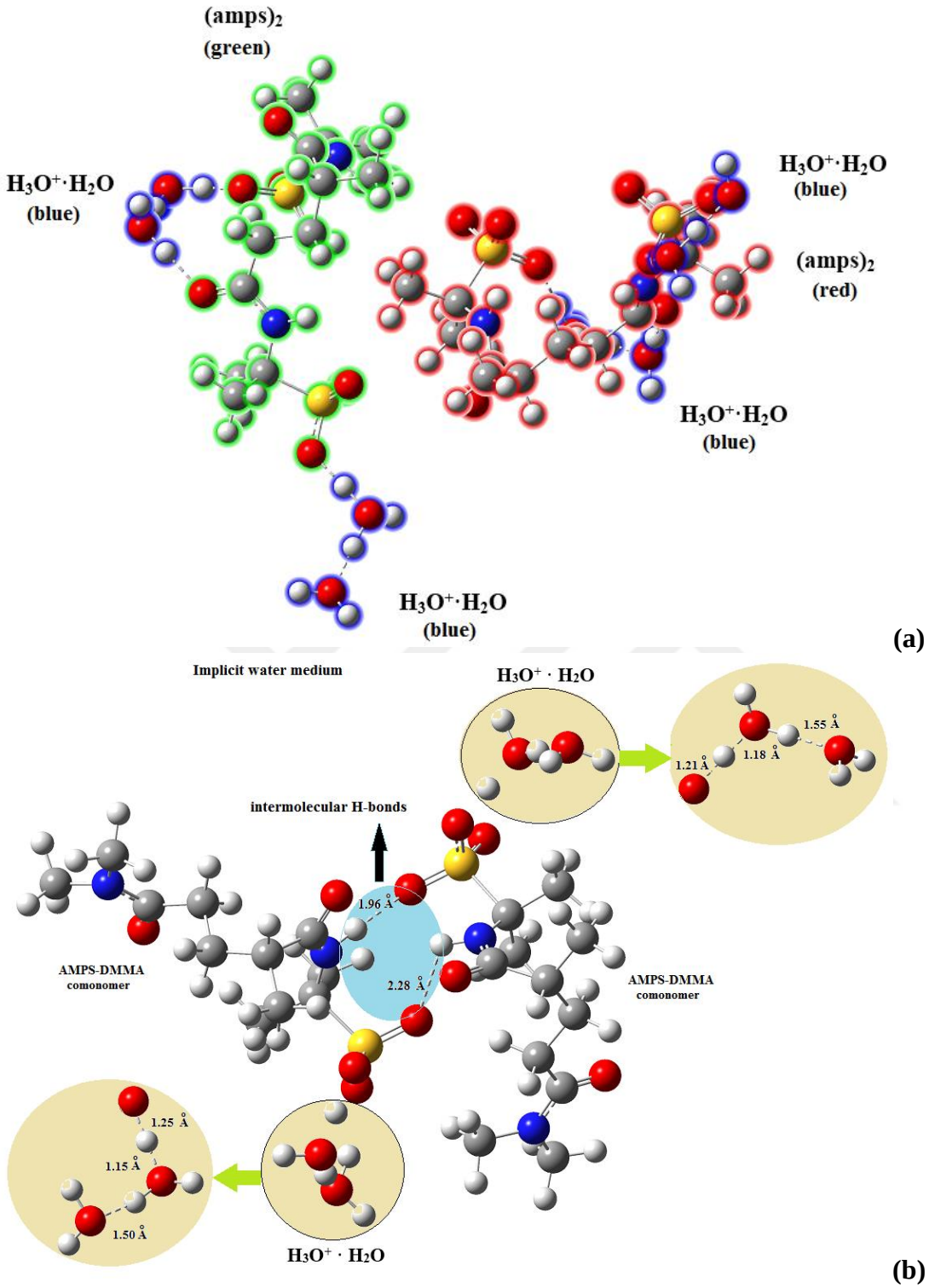

Figure 3.13 : Optimized geometries of $(AMPS)_2$ - $(AMPS)_2$ (a) and AMPS/DMAA - AMPS/DMAA dimers (b) in neutral state in explicit water medium in the presence of $H_3O^+ \cdot H_2O$ per SO_3^- group.

3.2.3. Mechanical and self-healing properties

Figure 3.14 shows tensile stress-strain curves and the mechanical parameter of the hydrogels with a mole fractions x_{DMAA} of DMAA between 0 and 0.74. Increasing x_{DMAA} up to 0.62, i.e., increasing total monomer concentration C_o from 60 to 75 wt.% significantly increases both the modulus E and the fracture stress σ_f of the hydrogels while stretch at break ε_f remains still around 1000%. At C_o = 75 wt.%, E becomes 0.41±0.02 MPa, which is in the range of the modulus of articular cartilage (0.31-0.80 MPa) [85]. One may argue that the modulus increase with increasing x_{DMAA} is due to the simultaneous increase of the polymer content of hydrogels, rather than increasing effective cross-link density, i.e., formation of additional H-bonds between AMPS and DMAA units. To investigate this point, the cross-linking density of the hydrogels was estimated from their Young's moduli E using the equation [86,87],

$$E = 3\ \nu_e\ RT \tag{3.2}$$

where ν_e is the cross-link density, i.e., the number of network chains per volume of gel, R and T are in their usual meanings. Equation 3.2 assumes affine deformation of the network chains, which is a reasonable assumption for the physical gels under study [49]. Because ν_e will increase with increasing C_o, to eliminate the concentration effect, we calculated the cross-link density ν_e^{dry} per volume of dry polymer by $\nu_e^{dry} = \nu_e / \nu_2^0$ where ν_2^0 is the volume fraction of cross-linked polymer in as-prepared hydrogels. Using the moduli E of the hydrogels (Figure 3.14b) together with the density of PAMPS (1.44 g·cm^{-3}) [3], ν_e^{dry} was calculated using equation 3.2 and plotted in Figure 3.14b against C_o. Similar to the modulus increase, ν_e^{dry} significantly increases with C_o up to 75 wt % indicating that incorporation of DMAA into PAMPS chains increases the number of non-covalent bonds acting as cross-links.

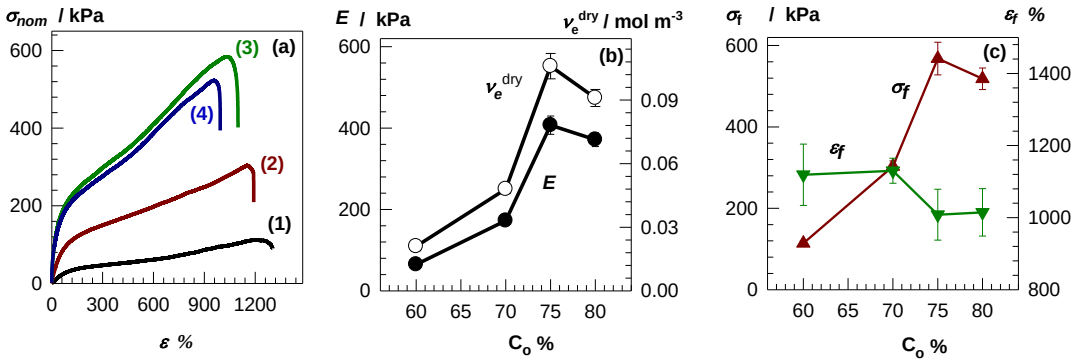

Figure 3.14 : (a): Tensile stress-strain curves of copolymer hydrogels. The concentration C_o and the mol fraction x_{DMAA} of DMAA in the comonomer feed (in parenthesis) for the curves 1, 2, 3, and 4 are: 60 (0), 70 (0.46), 75 (0.62), and 80 wt % (0.74), respectively. **(b, c):** Young's modulus E, the crosslink density ν_e^{dry}, tensile strength σ_f and stretch at break ε_f of the hydrogels plotted against C_o.

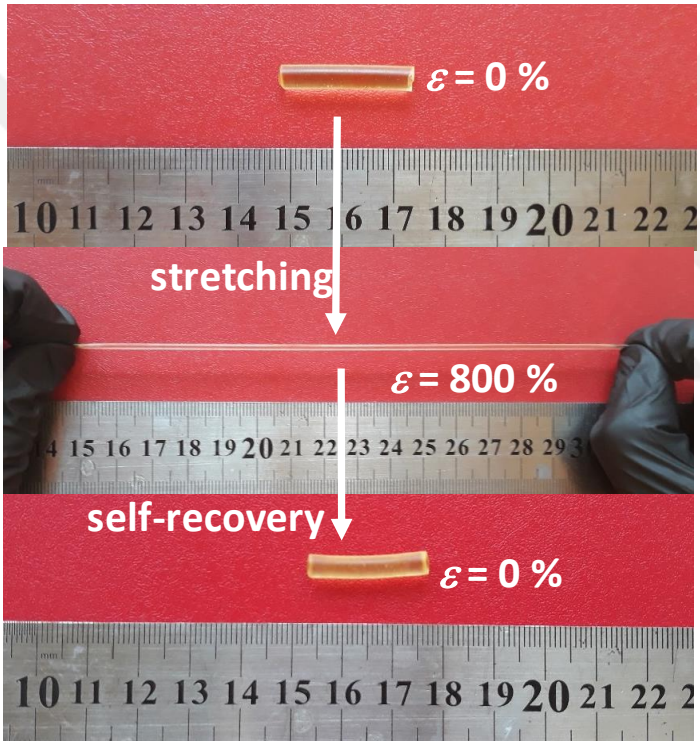

Figure 3.15 : Self-recovery behavior of a rod-shaped U-75/0.6 gel specimen after stretching to 800 % elongation ratio.

To further highlight the existence of a larger number of physical bonds in copolymer hydrogels as compared to PAMPS hydrogels, their large-strain behavior was investigated by cyclic mechanical tests. Figure 3.16a shows typical tensile cycles consisting of 8 successive loading and unloading steps conducted on a U-75/0.6 copolymer gel specimen. The tests were carried out with increasing maximum strain ε_{max} up to 800% in 8 steps, as indicated by the arrows. In contrast to pure PAMPS hydrogels exhibiting permanent deformation, the copolymer gels fully recover to

their original sizes within 1 min after unloading (inset to Figure 3.16a, Figure 3.15). This behavior is also illustrated in Figures 3.18a, 3.17, where the images of knotted and rod-shaped U-75/0.6 gel specimens are shown. After stretching the specimens to 800% elongation, they self-recover their original sizes within 1 min. Thus, DMAA significantly contributes to the elasticity of PAMPS hydrogels. Figure 3.16a also shows that, similar to PAMPS gels (Figure 3.6), each loading curve closely follows the previous loading indicating quasi-reversibility of the cycles. The filled symbols in Figure 3.16b show the hysteresis energies U_{hys} of the copolymer hydrogel calculated from the area between the loading and unloading curves plotted against the maximum strain ε_{max}. For comparison, U_{hys} data of PAMPS hydrogels with C_o between 50 and 60 wt.% AMPS are also shown in the figure by the open symbols. Incorporation of DMAA units significantly increases the hysteresis energy, i.e., the number of bonds reversibly broken under strain. For instance, at ε_{max} = 600%, U_{hys} of copolymer hydrogel is 10 to 30-fold larger than that of PAMPS hydrogels (755 vs 28-70 kJ m^{-3}).

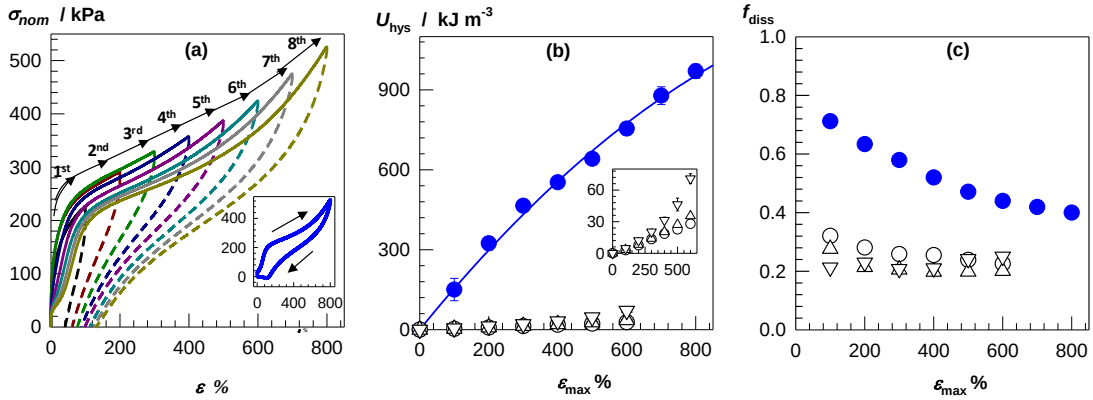

Figure 3.16 : (a): Cyclic tensile tests conducted on U-75/0.6 hydrogel with increasing maximum strain ε_{max} from 100 to 800% in 8 steps. Strain rate = 5 min^{-1}. Loading curves are indicated by arrows. The inset shows the last loading / unloading cycle with ε_{max} = 800%. **(b, c):** U_{hys} and f_{diss} of U-75/0.6 hydrogels (filled blue circles) plotted against ε_{max}. The line in Figure 3.16b is the best fit to the experimental data. For comparison, U_{hys} and f_{diss} data of U-gels prepared at C_o =50, 55, and 60 wt % are also shown by open circles, up and down triangles, respectively.

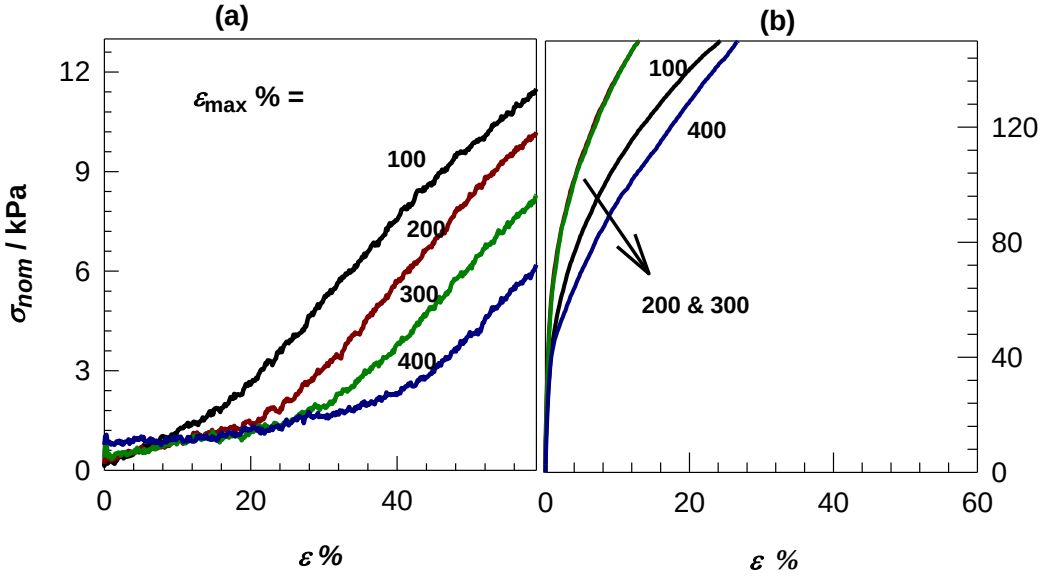

Figure 3.17 : Initial portion of the loading curves of successive cyclic tests conducted on U-50 (a) and U-75/0.6 hydrogels (b).

The ratio of dissipated energy to the loading energy (f_{diss}), that is, the amount of energy dissipated per loading energy can be regarded as a parameter presenting the extent of energy dissipation under a constant external load [4]. We calculated f_{diss} from the ratio of U_{hys} to the loading energy, i.e., the area under the loading curve. Figure 3.16c shows f_{diss} data of U-75/0.6 copolymer gel (filled symbols) and U-gels with C_o between 50 and 60 wt % (open symbols) plotted against ε_{max}. For the U-gels prepared without DMAA, this fraction is 25±4% and almost independent on ε_{max} or AMPS concentration, while, for U-75/0.6, f_{diss} is close to 80% at low strains and gradually decreases with increasing strain approaching to a limiting value of 40 % at large strains. This finding also reveals significant increase of the number of reversible bonds in PAMPS hydrogels after incorporation of DMAA segments.

U_{hys} can be regarded as the sum of the dissociation energies of intermolecular non-covalent bonds broken down during the cyclic tests, i.e. [49],

$$U_{hys} = U_{xl} \nu_e \, f_v \tag{3.3}$$

where U_{xl} is the average dissociation energy of intermolecular bonds, ν_e is, as defined above, the cross-link density of the hydrogel, that is, the total number of such bonds, and f_v is the fraction of bonds broken during the tensile cycle. The fraction f_v of broken bonds depends on the strain and hence, it increases with increasing strain ε_{max}. Thus, the initial slope of U_{hys} vs ε_{max} plots can be written as

$$\lim_{\varepsilon \to 0}\left(\frac{\partial U_{hys}}{\partial \varepsilon_{\max}}\right) = U_{xl}\nu_e \qquad (3.4)$$

The solid curve in Figure 3.16b is the best fit to the U_{hys} vs ε_{max} data yielding an initial slope of 156±6 kJ m^{-3}. From the modulus E = 407±22 kPa for U-75/0.6 hydrogel, we calculated its cross-link density ν_e using equation (3.2) as 55±3 mol m^{-3}. Substitution these values into equation (3.4), the average dissociation energy U_{xl} of the non-covalent bonds in the hydrogel was estimated as 2.9±0.2 kJ mol^{-1}. Because of the existence of a large number of H-bonds of varying strengths, one may expect that the breaking of H-bonds under strain occurs gradually so that the calculated dissociation energy corresponds to the weak H-bonds broken under 800% strain [88,89]. Thus, copolymer hydrogels are solely formed by H-bonding interactions between AMPS/AMPS and AMPS/DMAA segments.

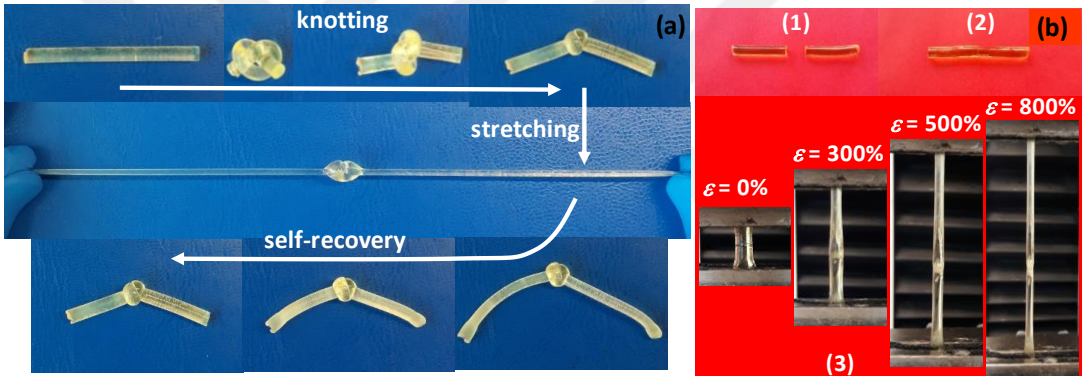

Figure 3.18 : (a): Self-recovery behavior of knotted U-75/0.6 gel specimens after stretching. (b): Self-healing of U-75/0.6 gel specimens at 23±2 °C after 24 h (1, 2), and tensile testing after healing to 800% stretch ratio (3).

The quasi-reversible manner of dissociation of H-bonds in the hydrogels under stress suggests their self-healing abilities. The images in Figure 3.18b show photographs of a gel specimen after cutting into two parts (1), and after healing at 23±2 °C by pushing the cut surfaces together for 24 h (2). The repaired sample could withstand 900% strain which is close to that of the virgin sample (Image 3). To quantify self-healing ability of the hydrogels, they were first cut into two parts and the cut surfaces were then pushed together at 23±2 °C to induce healing. Figure 3.19a shows stress-strain curves of virgin and healed U-75/0.6 gel specimens for various times. Healing efficiencies ε_h with respect to the modulus E, fracture strain σ_f, and fracture strain ε_f are shown in Figure 3.19b plotted against the healing time. After a healing time of 24 h, U-75/0.6 hydrogel sustains to a stretch ratio of 900±30 which is close to that of the

virgin hydrogel (1000±50). Moreover, the healing efficiency is significantly time-dependent and the highest healing efficiencies with respect to E, σ_f, and ε_f could be obtained after 24 h of healing time.

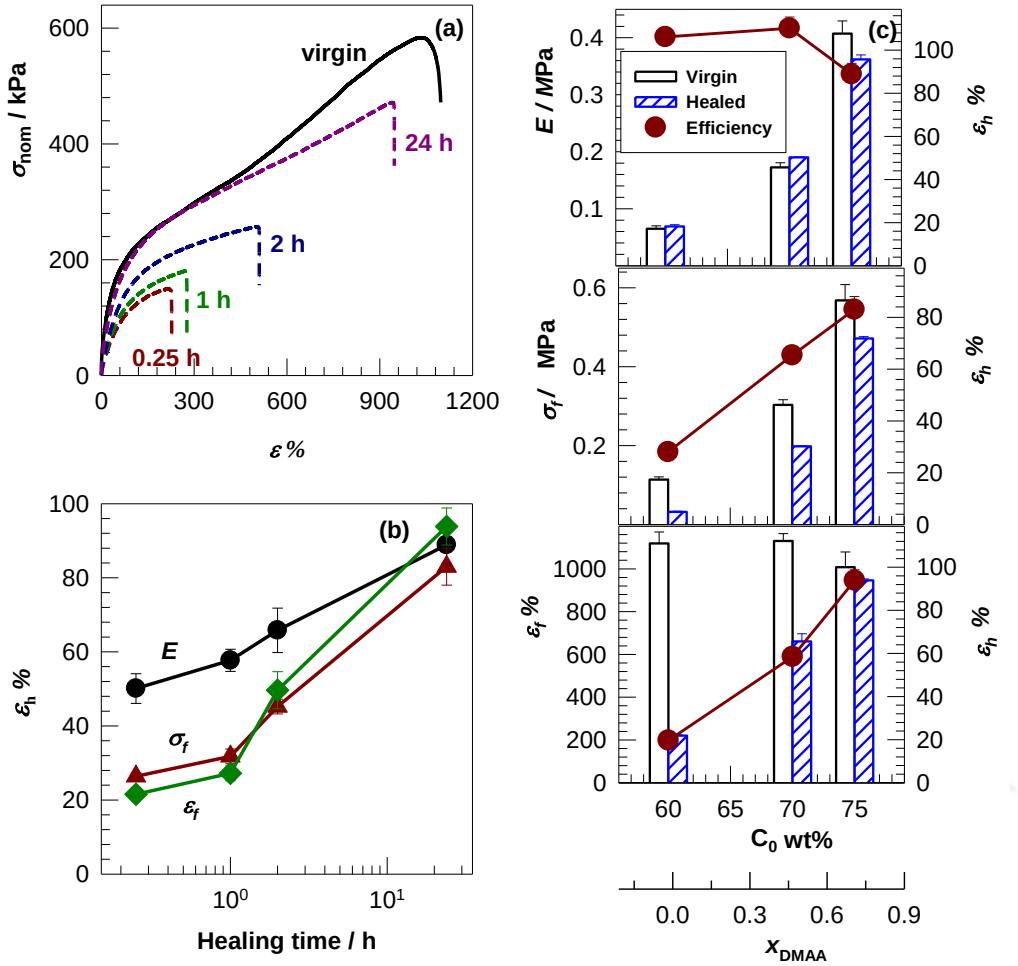

Figure 3.19 : (a): Stress-strain curves of virgin (solid curve) and healed U-75/0.6 hydrogels (dashed curves) at various healing times at 23±2 °C. **(b):** Healing efficiencies of U-75/0.6 hydrogel with respect to the modulus E, fracture stress σ_f, and strain ε_f plotted against the healing time. **(c):** The modulus E, fracture stress σ_f, and strain ε_f of virgin and healed hydrogels, and the corresponding healing efficiencies ε_h plotted against C_o and x_{DMAA}. Healing time = 24 h.

Figure 3.19c shows the mechanical parameters E, σ_f, and ε_f of virgin and healed hydrogels together with the corresponding healing efficiencies ε_h as functions of C_o and x_{DMAA}. All hydrogels prepared with or without DMAA exhibit around 100% healing efficiency with respect to the modulus revealing recovery of the original microstructure. However, healing efficiencies with respect to the fracture stress and fracture strain monotonically increase with the amount of DMAA segments in the hydrogels. For instance, U-60 gel prepared at 60 wt.% AMPS without DMAA shows healing efficiencies of 28 and 20% with respect to the fracture stress and strain,

respectively. Even after a healing time of 71 h, only 23% healing could be obtained in the fracture stress of healed gel specimens. However, incorporation of DMAA at a level of x_{DMAA} = 0.74 increases the healing efficiency to 80-90% after 24 h of healing, revealing significant contribution of DMAA segments to the recovery of the ultimate mechanical properties.

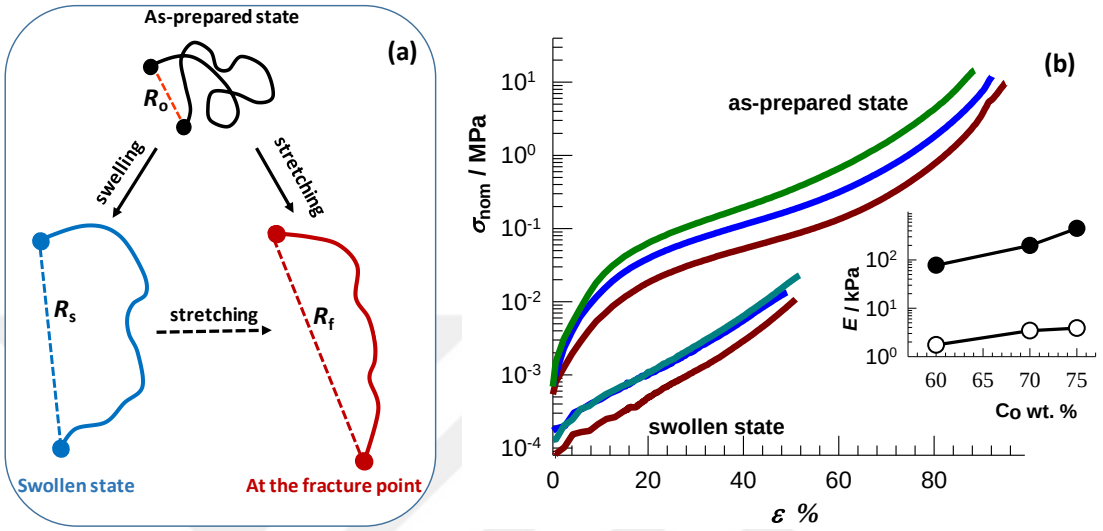

Figure 3.20 : (a): Scheme of a network chain during swelling and stretching. R_o, R_s, and R_f are end-to-end distances in as-prepared state, swollen state, and at the fracture point, respectively. (b): Compressive stress-strain curves of copolymer hydrogels in swollen and as-prepared states. C_o = 60 (dark red), 70 (blue), and 75 wt % (dark green). Inset shows Young's modulus E of the hydrogels in swollen (open symbols) and as-prepared states (filled symbols) plotted against C_o.

The mechanical performances of the physical gels discussed above were determined in their as-prepared states with water contents between 20-50 wt.%. It seems challenging to observe similar extraordinary mechanical properties in their equilibrium swollen states with water contents of around 99.99%. However, this contradicts the finite extensibility of polymer chains, as schematically illustrated in Figure 3.20a. Here, the end-to-end distances of a network chain in as-prepared and equilibrium swollen states, and at the point of fracture are denoted as R_o, R_s, and R_f, respectively. Thus, the deformation ratio λ_f at break of as-prepared hydrogels can be written as $\lambda_f = R_f / R_o$, whereas the chain expansion at equilibrium degree of swelling is given by $\alpha_s = R_s / R_o$. Although λ_f and α_s are fixed quantities for a given hydrogel, the elongation ratio at break of the hydrogels in their equilibrium swollen states ($\lambda_{s,f}$) is a dependent quantity given by,

$$\lambda_{s,f} = \frac{\lambda_f}{\alpha_s} \tag{3.5}$$

Because $\alpha_s \cong (m_{rel})^{1/3}$ and $\lambda_f = \varepsilon_f + 1$, one may estimate $\lambda_{s,f}$ of swollen hydrogels using equation 3.5 together with the values of m_{rel} and ε_f of as-prepared hydrogels (Table 3.1). For U-70/0.5, U-75/0.6, and U-80/0.7 hydrogels, their elongation ratios $\lambda_{s,f}$ at break in swollen states were calculated as 1.04±0.03, 1.10±0.08, and 1.15±0.07, respectively, revealing that they will fracture below 15% strain. Thus, as compared to around 1000 % stretchability of as-prepared hydrogels, the stretchability in their swollen states will significantly reduce due to the almost fully stretched conformation of the network chains. The tensile tests conducted on swollen gel specimens indeed showed that they all fracture in a brittle fashion at the start of the mechanical tests. Figure 3.20b shows compressive stress-strain curves of swollen and as-prepared hydrogels prepared at three different initial monomer concentrations C_o while the inset shows the Young's moduli *E* of swollen (open symbols) and as-prepared hydrogels (filled symbols) plotted against C_o. As compared to 80-93% compressibility of as-prepared hydrogels, swollen hydrogels rupture under 50% compression. Moreover, swelling causes a Young's modulus drop of 2-orders of magnitude indicating occurrence of a significant internal damage at 5-15% strains due to highly stretched conformation of the network chains. These results also indicate that the swollen copolymer hydrogels are a good candidate as sacrificial bonds, i.e., as the first-network component of double-network hydrogels to create less swollen but mechanically stronger hydrogels [90].

3.3 Conclusions

PAMPS hydrogels are attractive materials for various application areas due to their pH-independent large swelling capacities. However, their chemically cross-linked network structure prevents dissipation of energy under load leading to their fracture under low strain. We presented here, for the first-time, superabsorbent PAMPS hydrogels formed solely by H-bonding interactions that are stable in water. UV-polymerization of AMPS at 23±2 °C in aqueous solutions without a chemical cross-linker produces water-insoluble, highly stretchable physical hydrogels with swelling capacities exceeding 1000-times their original mass. The stability of the physical

gels in water is attributed to the high molecular weight of their PAMPS primary chains contributing to the H-bonding cooperativity. The molecular weight of PAMPS chains isolated from the hydrogels is around 2-orders of magnitude higher than those of thermal polymerized ones. Incorporation of DMAA segments into the physical gels further increases the molecular weight of the primary chains leading to enhanced mechanical strength of the hydrogels. PAMPS/DMAA hydrogels in their as-prepared states exhibit a high modulus (up to 0.41 MPa), tensile fracture stress (up to 0.57 MPa), and high stretchability (~1000) together with extraordinary swelling capacity (up to ~1700 $g \cdot g^{-1}$), and complete self-healing efficiency. We also show that the network chains of the hydrogels in equilibrium swollen state are almost fully stretched conformation due to the significant swelling pressure. As a consequence, swelling causes a significant drop in both stretchability and the modulus of the hydrogels.

4. CRYOGENIC FORMATION-STRUCTURE-PROPERTY RELATIONSHIPS OF POLY(2-ACRYLAMIDO-2-METHYL-1-PROPANESULFONIC ACID) CRYOGELS[3]

Hydrogels based on 2-acrylamido-2-methyl-1-propanesulfonic acid (AMPS) attract significant interest in the past decades due to their strong polyelectrolyte behavior that provides a pH-independent large water uptake capacity [3,7–9,64,65]. Poly(AMPS) (PAMPS) hydrogels have various potential application areas for the use in water purification, food industry, agriculture, energy and environmental fields, and bioengineering [5,10–13,91]. PAMPS hydrogels with a covalently cross-linked network structure have generally been prepared via free-radical cross-linking copolymerization of AMPS and a divinyl monomer, typically N,N′-methylenebis(acrylamide) (BAAm) in aqueous solutions [3]. Such hydrogels exhibit, however, insufficient mechanical performances restricting their applications.

An alternative strategy to generate PAMPS hydrogels is the cryogelation technique which is a simple and eco-friendly technique to produce macroporous hydrogels, so-called cryogels [92–96]. Cryogelation bases on conducting the gelation reactions in an apparently frozen reaction system. By this technique, free-radical cross-linking copolymerization reactions are generally conducted in aqueous media below the freezing temperature of the reaction system. As water freezes, monomers expelled from the ice concentrate in the unfrozen domains making them a highly concentrated solution, which is called cryoconcentration [92,94,95]. After attaining thermal equilibrium with the surrounding cold bath, the reaction system consists of unfrozen solution phase containing a high concentration of monomers and initiator, interconnected by ice crystals. Because the cryoconcentration effect generally dominates over the reduced polymerization rates due to the low temperature, cryogels can be obtained even at very low concentration [94,97]. After cryogelation

[3] This chapter is based on the paper "Su, E. and Okay, O. (2019). Cryogenic formation-structure-property relationships of poly(2-acrylamido-2-methyl-1-propanesulfonic acid) cryogels. *Polymer* 178, 121603, 1-9."

followed by thawing the ice crystals acting as a template for the pores, a 3D network of polymers containing μm-sized pores is obtained.

It is worth to mention that the cryoconcentration is a characteristic phenomenon of cryogelation, which distinguishes it from freeze-drying. For instance, freeze-drying of an already formed hydrogel does not lead to materials with cryogel properties due to the formation of ice crystals in a gel network rather than in a solution [94]. The pore wall produced by cryogelation is a dense polymeric gel because of the cryoconcentrated solution of the monomers around the ice crystals. In contrast, the pore wall formed after freeze-drying of a conventional hydrogel is a loosely cross-linked gel due to the absence of cryoconcentration. As a consequence, the porous structures produced during cryogelation are mechanically stable, even under large strain conditions, whereas those produced during freeze-drying are generally brittle in nature. For instance, it was shown that the cryogel scaffolds prepared from frozen aqueous silk fibroin solutions at −18 °C exhibit a Young's modulus of 8 MPa and a compressive fracture stress of 0.22 MPa, which are about 1 order of magnitude higher than those of the corresponding freeze-dried fibroin hydrogels prepared at 50 °C [98].

Thus, cryogelation leads to a significant change in the mechanical performances of the classical first-generation hydrogels. Almost complete squeezability, high-toughness, and superfast responsivity are some of the characteristics of the cryogels which are not observed in the hydrogels [94,98]. Most of the results on cryogels reported so far, however, lack a more detailed analysis to provide real conditions of the cryogelation systems. This includes the true concentration of the monomers in the unfrozen domains during cryogelation and its variation depending on the nominal monomer concentration. We investigate here the correlations between the properties of PAMPS cryogels including their porous structures and mechanical performances with the cryogelation conditions. We prepare PAMPS cryogels from aqueous solutions of AMPS and BAAm at various concentrations in the presence of a redox initiator system at -18 °C. As will be seen below, a clear correlation was found between the morphology of the cryogels and the local conditions during cryogelation including the melting temperature of the reaction solution, the volume of ice template, and the true concentration of the monomers in unfrozen domains. We also show a significant improvement in the mechanical properties of the cryogels with

increasing BAAm content. PAMPS cryogels prepared at 9.1 mol % BAAm exhibit the highest modulus (0.73±0.05 MPa) and could withstand up to 6.0±0.5 MPa compressive fracture stress.

4.1 Experimental

4.1.1 Materials

2-Acrylamido-2-methylpropane sulfonic acid (AMPS, Merck), N, N'-methylenebis(acrylamide) (BAAm, Merck), potassium persulfate (KPS, Merck), N, N, N', N'-tetramethylethylenediamine (TEMED, Merck), and sodium hydroxide (NaOH, Merck) were used as received. To prepare 0.966 M aqueous solution of sodium salt of AMPS (AMPS-Na), AMPS (20 g) was first dissolved in 40 mL distilled water at 23 ± 2 °C under stirring. After addition of 10 mL of 30 w/v % aqueous NaOH, the solution was titrated with 1 M NaOH to pH = 7 and then, the final solution volume was completed to 100 mL with distilled water. For the preparation of the cryogels at a monomer concentration of 24 wt %, 1.18 M aqueous AMPS-Na solution was prepared starting from 24.33 g AMPS. 24 mM KPS stock solution was prepared by dissolving 65 mg KPS in 10 mL distilled water.

4.1.2 Cryogel preparation

PAMPS cryogels were prepared from aqueous solutions of AMPS-Na and BAAm at -18 °C in the presence of 1 mol % KPS (with respect to the monomers) and 0.25 v/v % TEMED as a redox initiator system. To prevent the onset of gelation before freezing of the reaction solution at -18 °C, the solutions were pre-cooled at -196 °C. Two sets of experiments were carried out. In the first set, BAAm content in the monomer feed was varied between 1.2 – 9.1 mol % at a total monomer concentration C_o of 10 wt % whereas in the second set, C_o was changed between 10 – 25 wt % at 1.2 mol % BAAm. A typical synthetic procedure for the preparation of the cryogels at C_o = 15 wt % and 1.2 mol % BAAm follows: BAAm (14 mg) was dissolved in 6.2 mL of 0.966 M AMPS-Na stock solution and the volume of the solution was completed to 7.0 mL with distilled water. After addition of 3 mL KPS stock solution, it was cooled to 0 °C in an ice bath and bubbled nitrogen for 10 min to remove oxygen, TEMED (25 μL) was then added and the solution was transferred into plastic 1 mL-syringes. The syringes were first immersed into liquid nitrogen for 2

min and then transferred into a cryostat at -18 °C to conduct the cryogelation reactions for 24 h.

4.1.3 Determination of unfrozen water content during cryogelation

The The amount of unfrozen water during cryogelation and true monomer concentration in the unfrozen domains were estimated by differential scanning calorimetry (DSC). For this purpose, gelation solutions containing various amounts of AMPS-Na and BAAm were prepared as described above, except that KPS-TEMED initiator system was not included. The solutions in the plastic syringes were immersed into liquid nitrogen for 2 min followed into a cryostat at -18 °C for 24 h. 30 mg of the frozen solution was then transferred in an aluminum pan of the instrument (Perkin-Elmer Diamond DSC). After sealing and weighing of the pan, the solution was frozen within the instrument at -18 °C for 2 h and then heated from to 10 °C with a scanning rate of 1 °C min^{-1}. From the melting enthalpy ΔH of frozen water, the mass fraction f_{unf} of unfrozen water in the apparently frozen solution at -18 °C was calculated as

$$f_{unf} = 1 - \frac{\Delta H}{\Delta H_m} \tag{4.1}$$

where ΔH_m is the melting enthalpy of ice (6.01 kJ mol^{-1}).

4.1.4 Characterization of cryogels

PAMPS cryogels taken out of the syringes after a reaction time of 24 h were cut into small pieces of about 1 cm in length and they were immersed in an excess of water at room temperature to remove soluble species. After reaching equilibrium degree of swelling, which was monitored by recording the mass and the diameter of the gel specimens, they were freeze-dried (Christ Alpha 2e4 LD-plus) for 2 days. The gel fraction W_g ,i.e., the fraction of cross-linked polymer obtained from one gram of AMPS was calculated as

$$W_g = \frac{m_{dry}}{m_o\, w_{AMPS}} \tag{4.2}$$

where m_{dry} and m_0 are the weights of the gel specimens in dried and as-prepared states, respectively, w_{AMPS} is the weight fraction of AMPS in the initial reaction

solution. The equilibrium weight q_w and volume swelling ratios q_v of the cryogels in water were calculated as

$$q_w = \frac{m_s}{m_{dry}} \tag{4.3}$$

$$q_v = \left(\frac{D_s}{D_{dry}} \right)^3 \tag{4.4}$$

where D_{dry} and m_{dry} are the diameter and mass of the specimens in dried state, respectively, and D_{s} and m_{s} are the same quantities but of the equilibrium swollen specimens. To determine the pore volume V_p of the cryogels, dried gel specimens were immersed in an excess of acetone and their equilibrium masses m_{Ace} were recorded. The pore volume V_p, that is, the total volume of the pores in unit mass of dry PAMPS network was estimated using the equation,

$$V_P = \frac{m_{Ace} - m_{dry}}{d_{Ace}\, m_{dry}} \tag{4.5}$$

where d_{Ace} is the density of acetone (0.784 $\mathrm{g \cdot mL^{-1}}$).

For the texture determination of dried cryogels, scanning electron microscopy (SEM) measurements were carried out at various magnifications on Tescan GAIA 3 Field Emission SEM. Prior to the measurements, the specimens were sputter-coated with gold-palladium using Leica ACE 600 instrument. The average pore diameters D were calculated from at least 10 SEM images taken at various magnifications using ImageJ image processing software (US National Institutes of Health, Bethesda, MD).

The morphology of the cryogels was also visualized using micro-computed tomography (μ-CT) scanning performed using a μ-CT Skyscan 1272 instrument (Bruker, Belgium) working at a voltage of 55 kV and a current of 53 μA. All gel specimens were scanned at a 15.3 μm pixel resolution and 180˚ rotation around their vertical axes, with 2 average frames at every 0.20 angle step. The integration time was set to 70 ms and no filter was applied. Reconstructions were carried out using NRecon 1.7.4.2 reconstruction software (Skyscan, Bruker, Belgium) using a full cone beam Feldkamp reconstruction algorithm with grayscale limits defined automatically. Reconstructed data were further processed in the volume of interest (VOI) data-sets within CTAn 1.18.4.0+ software (Skyscan, Bruker, Belgium) to

investigate pore sizes, structure wall thickness, and porosity. To produce binary images for the morphological characterization of the cryogels, thresholding by hysteresis was used as the segmentation method. An optimal threshold for each analysis was chosen and kept consistent throughout all evaluations. To visualize the cryogel samples, reconstructed images were volume-rendered within CTVox 3.3.0 r1403 program (Skyscan, Bruker, Belgium).

Uniaxial compression tests were performed on cylindrical gel specimens at 23 ± 2 °C on a Zwick Roell mechanical test machine using 500 N load cell at a strain rate of 50 mm/min. The stress was calculated as its nominal σ_{nom} value which is the force per cross-sectional area of undeformed specimen, while the strain was given by the elongation ratio ε. Young's modulus E was calculated from the slope of stress–strain curves between 5 and 10% elongation. The compressive fracture stress and strain were calculated from the maxima of true stress–strain curves as detailed before [67].

4.2 Results and Discussion

The PAMPS cryogels were prepared from aqueous solutions of AMPS-Na and BAAm at -18 °C in the presence of KPS-TEMED redox initiator system. To highlight the individual effects of the monomer AMPS-Na and the cross-linker BAAm on the cryogel properties, two sets of experiments were carried out: In the first set, BAAm content was varied between 1.2 - 9.1 mol % at a total monomer (AMPS-Na + BAAm) concentration C_o of 10 wt %. In the second set, C_o was varied between 10 and 25 wt % at a fixed BAAm content of 1.2 mol %. Gel fraction measurements showed that all cryogels reported here exhibit a gel fraction close to unity after a reaction time of 24 h (Figure 4.1), indicating that the monomers in the feed are completely incorporated into the cryogel network.

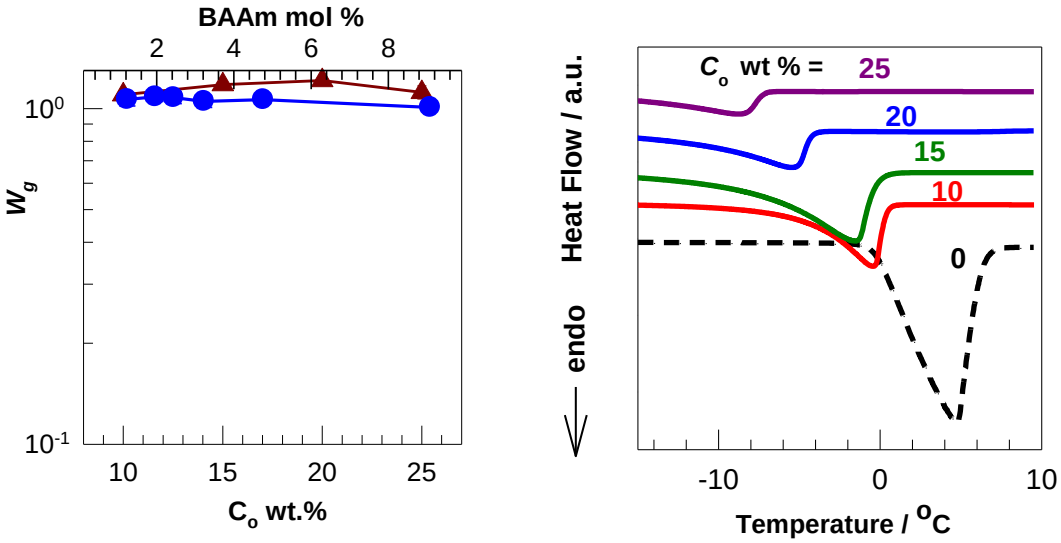

Figure 4.1 : (a) Gel fraction W_g shown as functions of C_o wt % (triangles) and BAAm mol % (circles). Gelation temperature = -18 °C. **(b)** DSC scans of frozen AMPS + BAAm solutions at various monomer concentrations C_o as indicated. The melting temperatures T_m shown in Figure 6a were calculated from the onset temperatures.

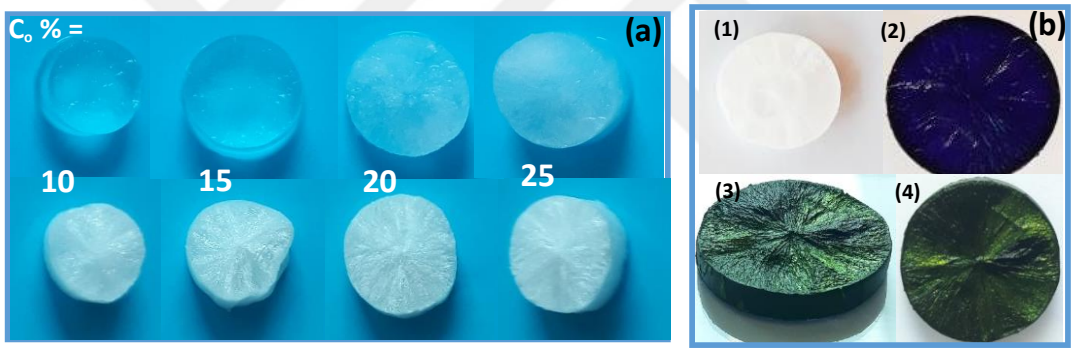

Figure 4.2 : (a) Optical images of PAMPS cryogel specimens formed at 1.2 mol % BAAm and at various C_o in swollen (upper panel) and dry states (bottom panel). **(b)** Optical images of a cryogel specimen before (1), just after immersion in an aqueous solution of crystal violet (2), after 1 h (3) and 24 h (4). C_o = 10 wt %. BAAm =1.2 mol % BAAm.

Figure 4.2a shows typical optical images of the cryogels at 23±2 °C formed at various monomer concentrations C_o in swollen (upper panel) and dried states (bottom panel). At C_o < 20 wt %, swollen cryogels are transparent due to their high water contents (98-99%) whereas those produced at higher concentrations are translucent revealing scattering of light from separate domains. They all become opaque in their dried states reflecting their macroporous structures. Moreover, all cryogels reported here exhibit superfast swelling response when immersed in a good solvent. For instance, Figure 4.2b shows the images of a cryogel specimen before (1) and just after immersion in water colored with crystal violet (2). The specimen immediately

absorbs the solution to attain its equilibrium swollen state and exhibits a blue-violet color which is the typical color of crystal violet (CV) at a neutral pH. After a waiting time of one hour, the color of the cryogel turns to green corresponding to a form of CV with two of the nitrogen atoms positively charged due to the acidic character of PAMPS (images 3, 4 in Figure 4.2b). Thus, swelling of dry gel specimen occurs faster than the chemical equilibration of CV with the gel phase.

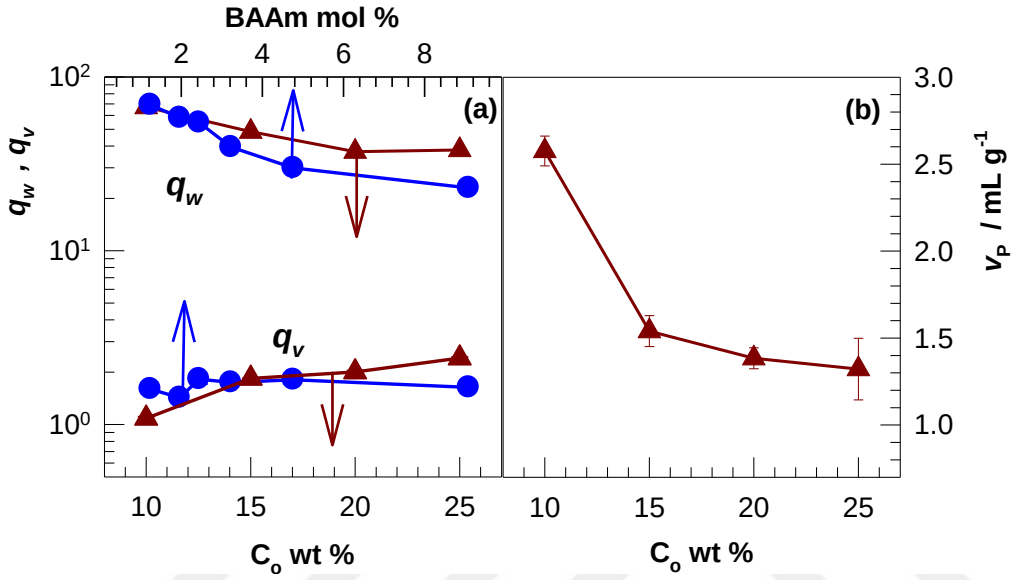

Figure 4.3 : Equilibrium weight q_w and volume swelling ratios q_v (a) and pore volumes V_p (b) of PAMPS cryogels shown as functions of the monomer concentration C_o (triangles) and BAAm content (circles).

Figure 4.3a shows the equilibrium weight q_w and volume swelling ratios q_v of PAMPS cryogels in water as functions of BAAm (circles) and monomer concentrations C_o (triangles). The cryogels exhibit a large weight swelling ratio q_w between 70 and 20, which is a decreasing function of both the cross-linker or monomer concentrations. The volume swelling ratios q_v are 14- to 44-fold smaller than q_w's, and slight increasing functions of BAAm % and C_o. Because the volume swelling is mainly determined by the expansion of the 3D PAMPS network in water due to the favorable PAMPS–water interactions while weight swelling also includes filling of the micro-voids within the gel with the solvent, this finding reflects the existence of an interconnected open porous structure in PAMPS cryogels. The total pore volume of the cryogels was estimated from the uptake of acetone, which is a poor solvent of PAMPS and hence, preferentially enters the open pores of the cryogels. We found that the total pore volume V_p is independent of BAAm % within the limits of the experimental error, i.e., 2.4±0.4 mL·g^{-1}, whereas it decreases from

2.6 to 1.3 $mL \cdot g^{-1}$ as the monomer concentration C_o is increased (Figure 4.3b). This behavior is attributed to the decreasing amount of water in the gelation solution as C_o is increased leading to the formation of a lesser amount of ice acting as a template for the formation of pores.

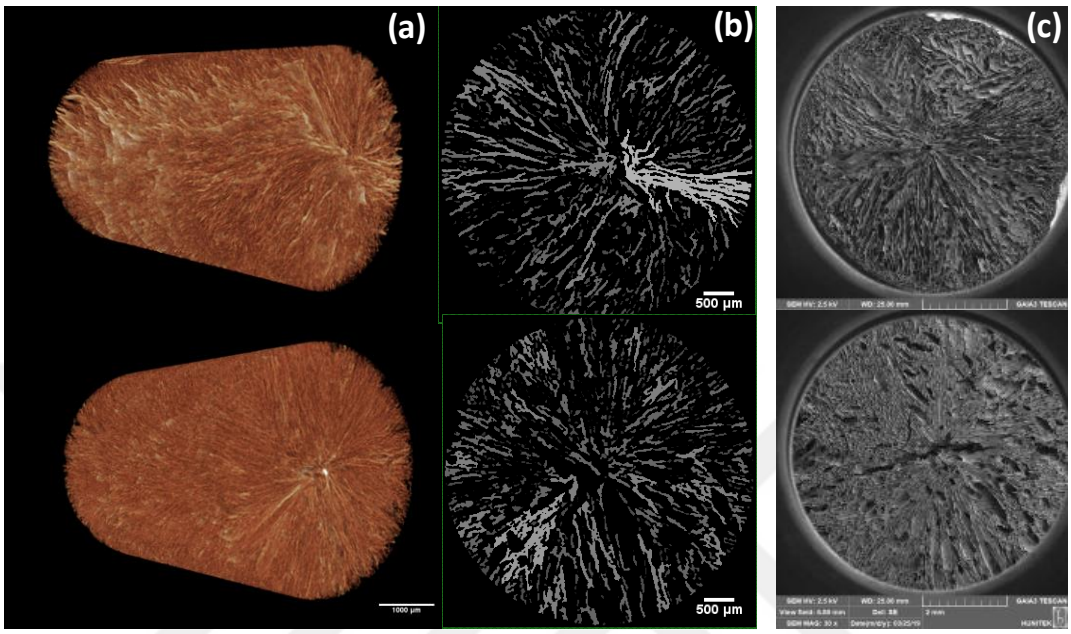

Figure 4.4 : 3D (a), 2D µ-CT (b), and SEM images (c) of cryogels formed at C_o = 10 (upper panel) and 25 wt % (bottom panel). Scale bars are 1 (a), 0.5 (b), and 2 mm (c). BAAm = 1.2 mol %.

To determine the morphology of the cryogels, we used both SEM and µ-CT techniques which are destructive and nondestructive tests, respectively, for the characterization of the porous structures. Moreover, the advantage of SEM is its higher magnification and more precise determination of the pore diameters as compared to µ-CT. Figures 4.4a-c show 3D and 2D µ-CT, and SEM images of the cryogels, respectively, at a low magnification (scaling bars = 0.5-2 mm). The cryogels were prepared at C_o = 10 (upper panel) and 25 wt % (bottom panel). All images show pore channels templated from the growing ice crystals during cryogelation. The channels are aligned in radial directions the extent of which slightly decreases as C_o is increased from 10 to 25 wt %. We attribute the alignment of the pore channels to the pre-cooling step of the reaction solution in liquid nitrogen, as illustrated in Figure 4.5. Fast cooling of the solution in the cold bath at -196 °C results in the rapid growth of ice from the surface of the reactor to the interior, i.e., in the direction of the temperature gradient.

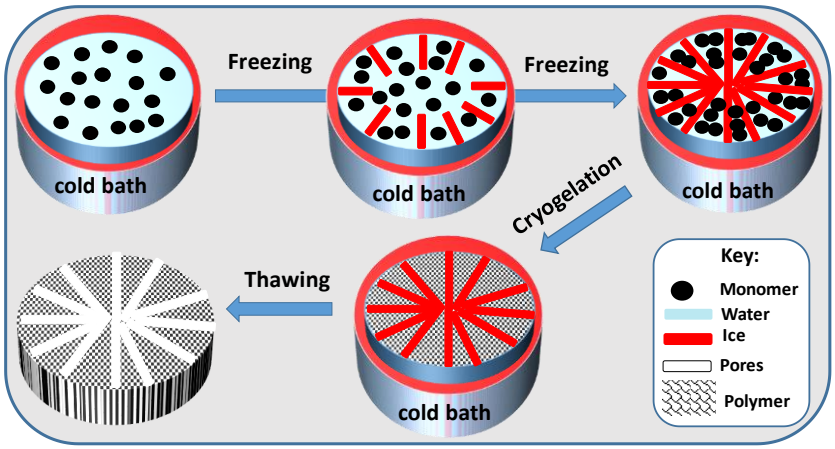

Figure 4.5 : Cartoon showing cryogelation of the monomers under fast freezing condition in a radial direction from surface to the interior.

μ-CT analysis also revealed the existence of less than 0.006% closed pores in the cryogels and hence, they exhibit a highly porous, interconnected open pore structure. Figure 4.6 shows SEM images of the cryogels formed at various concentrations C_o at 300x (upper panel) and 500x magnifications (bottom panel). Aligned pore channels forming a layered structure appear at C_o = 10 and 15 wt %, whereas the degree of alignment decreases above 15 %. Thus, in accord with μ-CT images, cryogels formed below C_o = 20 wt % exhibit an aligned morphology. The existence of an interconnected open pore structure together with an aligned morphology is important for many application areas of macroporous materials including tissue engineering, bioseparation, microfluidics, and organic electronics [99,100]. Spherical pores within the layers together with irregular pores between the layers exist in the cryogels whose number increases with increasing concentration C_o. Moreover, both μ-CT and SEM images show no detectable effect of BAAm content on the morphology and pore size of the cryogels.

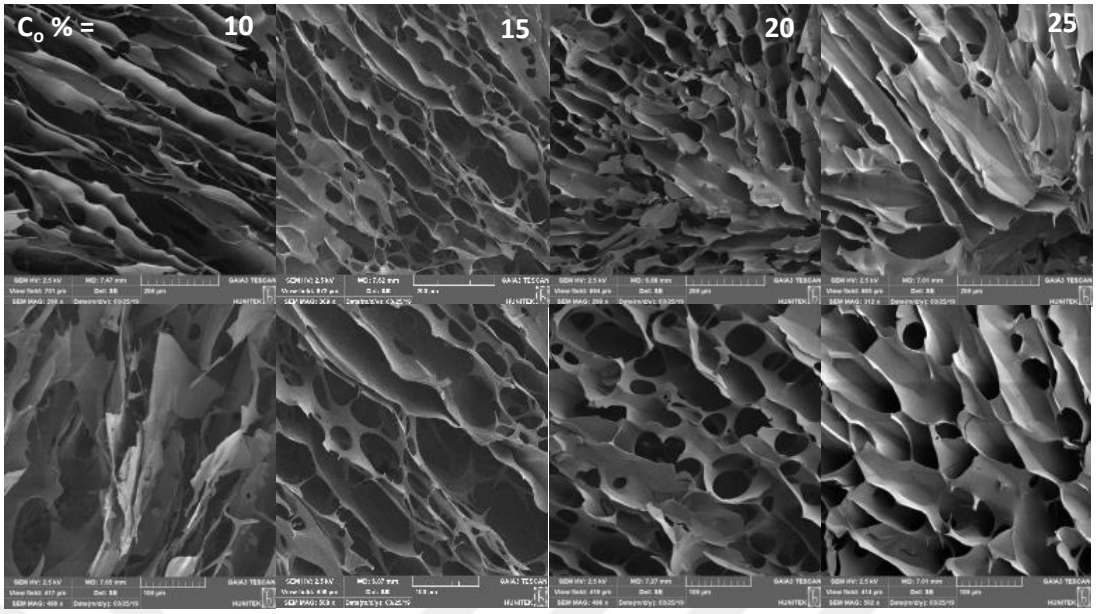

Figure 4.6 : SEM images of cryogels formed at various C_o as indicated. Scale bars are 200 (upper panel) and 100 μm (bottom panel). BAAm = 1.2 mol %.

Figure 4.7a shows average pore diameters (D) and distances (l) between the layers estimated from the SEM images plotted against the monomer concentration C_o. Average pore diameter slightly increases from 34±7 to 50±7 μm whereas layer spacing decreases from 168±23 to 111±10 μm as the monomer concentration C_o is increased from 10 to 25 wt %. Analyzing μ-CT images of the cryogels formed at C_o = 10 and 25 wt % gives a similar trend but somehow larger pore diameters (Figure 4.7b). The average pore diameters estimated from μ-CT are 72±20 and 85±6 μm for C_o = 10 and 25 wt %, respectively, together with large pores of about 0.9 mm in diameter. We should note that the pore diameters using μ-CT are estimated based on the number of pixels present in the pores. Since one pixel corresponds to 15.3 μm, the pore diameters estimated here will be at least 15 μm higher than those obtained from SEM.

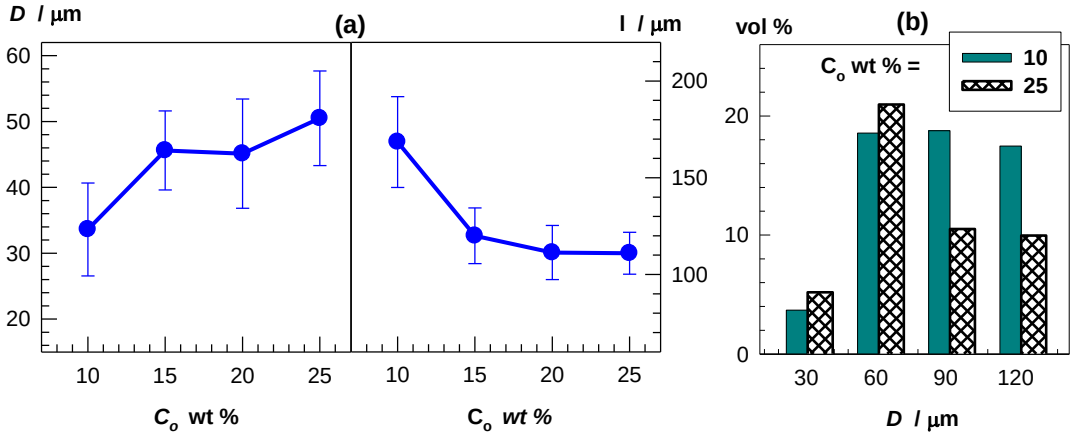

Figure 4.7 : (a): Average pore diameter *D* and layer spacing *l* of the cryogels calculated from the SEM images plotted against the monomer concentration C_o. **(b):** Distribution of the pore diameters *D* estimated from µ-CT of cryogels formed at C_o = 10 and 25 wt %. BAAm = 1.2 mol %.

To explain the observed morphological variations depending on the monomer concentration C_o, one needs to know the local concentrations of the reaction components during cryogelation, i.e., the amounts of frozen and unfrozen water at -18 °C, and the actual concentration of the monomers in the unfrozen domains. To quantify the amount of unfrozen domain during the cryogelation reactions, DSC measurements were conducted by heating frozen AMPS/BAAm solutions from -18 to 10 °C with a scanning rate of 1 °C min^{-1} (Figure 4.1). Melting peak shifted to a lower temperature and the area under the peak became smaller as C_o is increased, reflecting lowering the melting temperature T_m of the monomer solution and decreasing amount of ice in the reaction system. Figure 4.8a shows the melting temperature T_m of the monomer solutions (triangles) and the fraction f_{unf} of unfrozen water at -18 °C (circles) both plotted against C_o. The fraction f_{unf} rapidly increases from 36±2 to 79±5 % whereas T_m decreases from -5.5 to -12.3 °C with increasing C_o from 10 to 25 wt %. Because decreasing T_m means a slower rate of freezing of water in the reaction solution, larger ice crystals will form as C_o is increased leading to the formation of larger pores and hence, a smaller spacing between the pores [94]. Thus, the results are consistent with the experimental finding regarding C_o-dependence of the pore diameters and the distances between pore channels in the cryogels (Figure 4.7). Moreover, decreasing freezing rate of water also leads to a lesser degree of alignment of growing ice crystals, which is in accord with the SEM and µ-CT results.

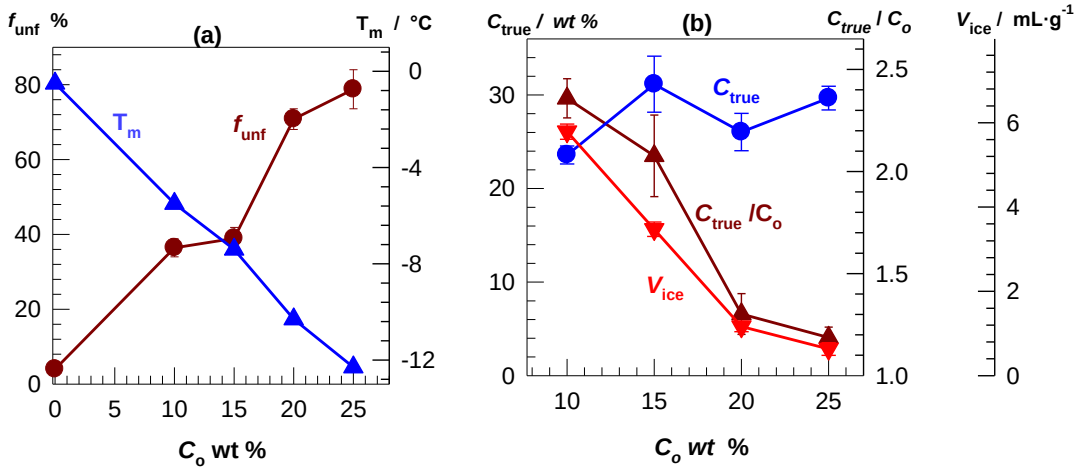

Figure 4.8 : (a): The fraction f_{unf} of unfrozen water at -18 °C (circles) and the melting temperature T_m (triangles) both plotted against C_o. **(b):** True monomer concentration C_{true} in the unfrozen domains (circles), the ratio C_{true} / C_o (triangles up) and the volume V_{ice} of ice per gram of dried cryogel (triangles down) shown as a function of C_o.

The true concentration C_{true} of the monomers in the unfrozen domains and the volume of ice per gram of dry cryogel V_{ice} can be estimated from the fraction f_{unf} of unfrozen water using the equations,

$$C_{true} = \frac{10^2 C_o}{C_o + (1 - C_o) f_{unf}} \tag{4.6}$$

$$V_{ice} = \frac{(1 - C_o)(1 - f_{unf})}{d_1 C_o} \tag{4.7}$$

where d_1 is the density of ice at -18 °C (0.995 g mL^{-1}). Figure 4.8b shows C_{true} (circles), the ratio of true-to-nominal monomer concentration C_{true}/C_o (triangles up), and the volume of ice per gram of dry cryogel V_{ice} (triangles up) plotted against C_o. At the nominal monomer concentration C_o of 10 wt %, C_{true} is 24±1% whereas, at higher concentrations, C_{true} remains constant at 29±3 wt %. Thus, increasing monomer concentration in the reaction solution above 10 wt % does not change its actual concentration C_{true} in the unfrozen solution at -18 °C, revealing that it is a saturated AMPS/BAAm solution. Moreover, the C_{true}/C_o ratio representing the extent of cryoconcentration is the highest at the lowest monomer concentration of 10 wt %, i.e., C_{true} is about 2.4-fold larger than C_o. Increasing C_o continuously decreases the effect of cryoconcentration and the C_{true}/C_o ratio reduces to 1.2 at C_o = 25 wt %. Figure 4.8b also shows a continuous decrease of the ice volume V_{ice} with increasing C_o, which is in accord with the pore volume measurements (Figure 4.3b). All these

findings reveal that DSC measurements conducted on frozen gelation solutions are means for predicting the final properties of the cryogels.

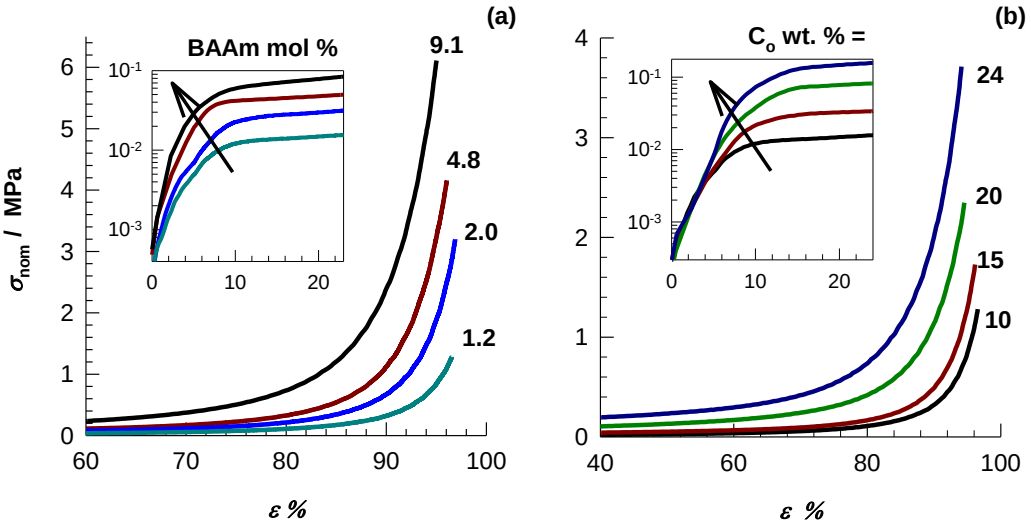

Figure 4.9 : Typical stress-strain curves of dried cryogels as the dependence of the nominal stress σ_{nom} on the strain ε. The data are from cryogels formed at various BAAm (a) and monomer concentrations C_o (b). The insets show the initial portion of the curves in a semi-logarithmic scale.

Mechanical behavior of the cryogels was determined by uniaxial compression tests conducted on cryogels in their dried states at 23±2 °C. Figures 4.9a, b show typical stress-strain curves of the cryogels prepared at various BAAm and monomer concentrations, respectively. The insets to the figures present the initial portion of the curves in a semi-logarithmic scale up to 23% compression. All cryogels could be compressed up to 94-97% strains without any damage. Moreover, the insets reveal that the stress-strain curves first exhibit an elastic region followed by a quasi-plateau regime during which the gel specimens easily deform. Finally, they exhibit hardening behavior at strains above 80%. The appearance of a plateau regime in stress-strain curves suggests the collapse of the porous structure of the cryogels, as also reported before for silk fibroin cryogels [98]. The plateau stress increases with increasing BAAm or monomer concentration indicating increasing mechanical strength of the pore walls constituting the network structure. For instance, the plateau stress increases by one order of magnitude (from 13 kPa to 140 kPa) with increasing monomer concentration C_o from 10 to 24 w/v %.

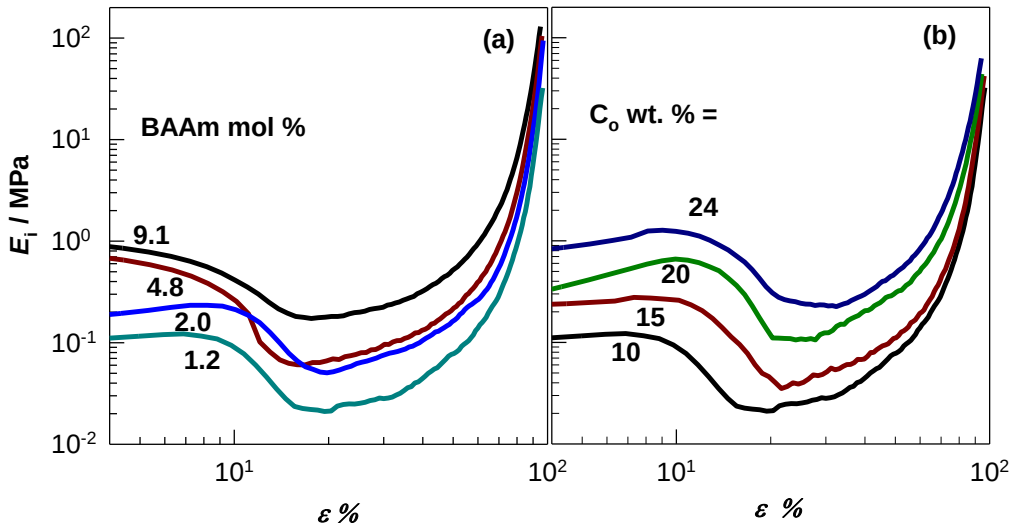

Figure 4.10 : Instantaneous modulus E_i of the cryogels formed at various BAAm (a) and monomer concentrations (b) plotted against the strain ε.

The appearance of three regimes in the stress-strain curves was also reflected from the instantaneous slope of the stress-strain curves corresponding to the instantaneous modulus E_i of the cryogels. Figures 4.10a, b show strain-dependence of E_i of the cryogels formed at various BAAm and monomer concentrations, respectively, calculated from the slope between two consecutive data points in Figure 4.9. To eliminate noise in the data series, they were smoothed using the negative exponential procedure with a sampling proportion of 0.1, i.e., 10 data points for one smoothed value (Figure 4.11) [101]. The modulus E_i decreases and attains a minimum value between 10-20% strains but then continuously increases and approaches to a value of 10^2 MPa, which is in the range of the mechanical strength of bulk polymers. This suggests the disappearance of the pores at high strains and hence compressing bulk PAMPS network. Figure 4.12 shows Young's modulus E and compressive fracture stress σ_f of the cryogels plotted against BAAm and total monomer concentrations C_o. Increasing C_o or BAAm mol % also increases both Young's modulus E and compressive fracture stress σ_f of the cryogels. However, a much significant improvement in the mechanical properties of the cryogels was observed at high BAAm contents. The cryogels prepared at 9.1 mol % BAAm exhibit the highest modulus (0.73±0.05 MPa) and could withstand up to 6.0±0.5 MPa compressive fracture stress.

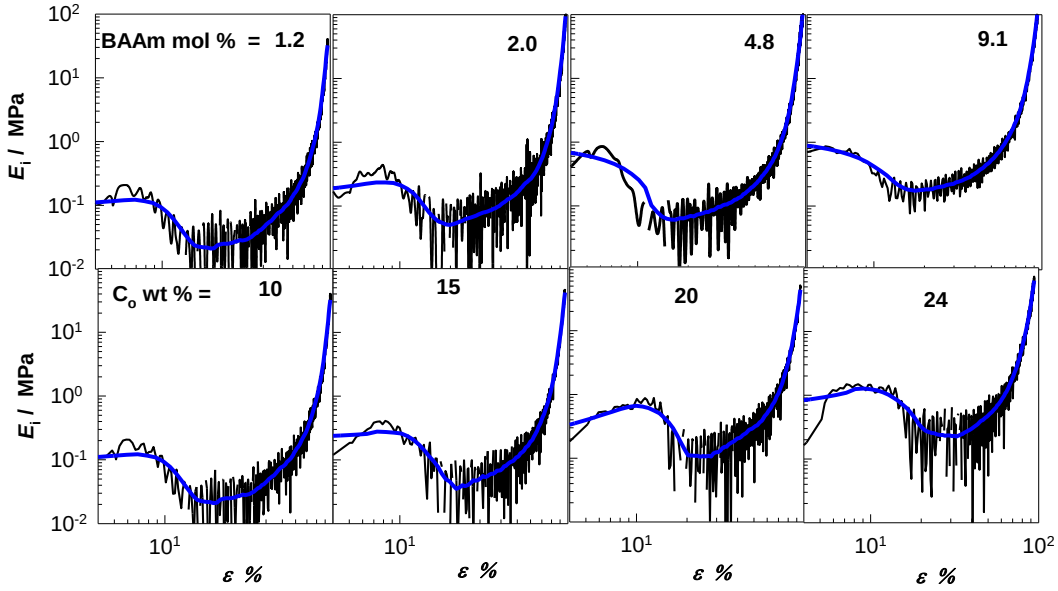

Figure 4.11 : Instantaneous modulus E_i of the cryogels formed at various BAAm (upper panel) and monomer concentrations C_o (bottom panel) plotted against the strain ε. The data are before (solid curves) and after the smoothing procedure (blue curves).

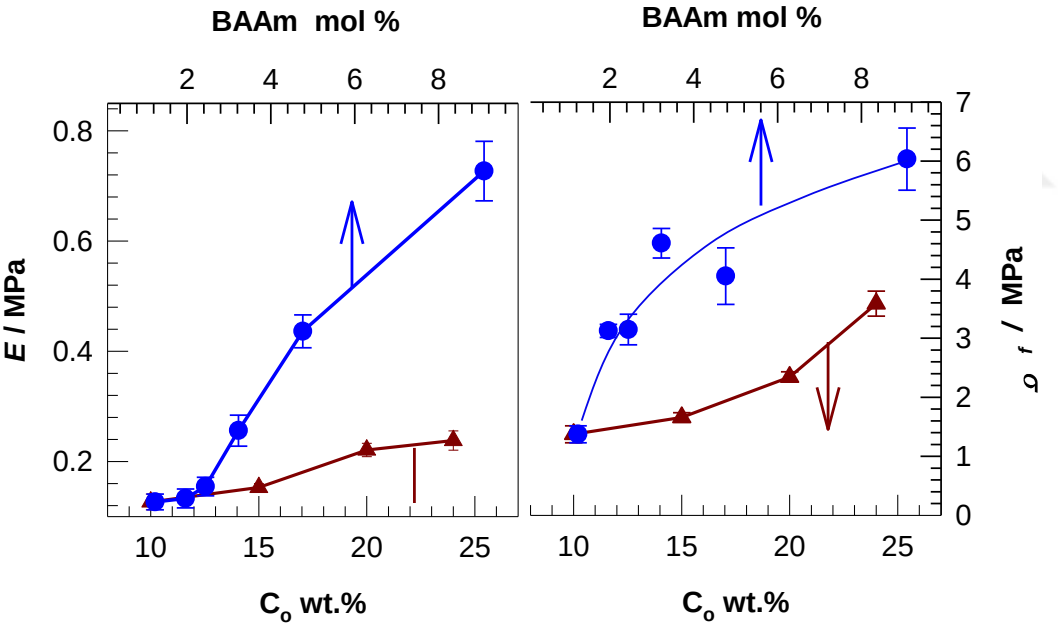

Figure 4.12 : Young's modulus E and compressive fracture stress σ_f of cryogels plotted against BAAm mol % (circles) and C_o wt % (triangles).

All cryogels exhibited superfast swelling behavior when immersed in water (Figure 4.2b). They also exhibited fast responsivity against changes in the solvent quality. Figure 4.14 shows swelling-deswelling kinetics of the cryogels formed at various C_o in water and acetone, respectively, as the dependences of their weight $q_{w,t}$ and volume swelling ratios $q_{v,t}$ on the contact time t. They all attain their equilibrium swollen state in water before the first measurement time of 1 min. When equilibrium

swollen cryogels are immersed in acetone, a poor solvent for PAMPS, they assume an equilibrium collapsed state within 5 min. This swelling-deswelling cycle was totally reversible and independent of BAAm content (Figure 4.13). Another feature of all PAMPS cryogels is their almost complete squeezability, as illustrated in Figure 4.14b using the images of a colored gel specimen. Compressing the specimen under load squeezes water out of the cryogel network (images 1→ 4) whereas, upon unloading, the specimen fully recovers its original shape by sucking back the released water into pores (images 5, 6). The cycles consisting of squeezing and autonomic reswelling steps were repeated 20 times after placing the bottom end of the specimen in contact with water. The swollen cryogels returned to their original shapes and masses after each cycle.

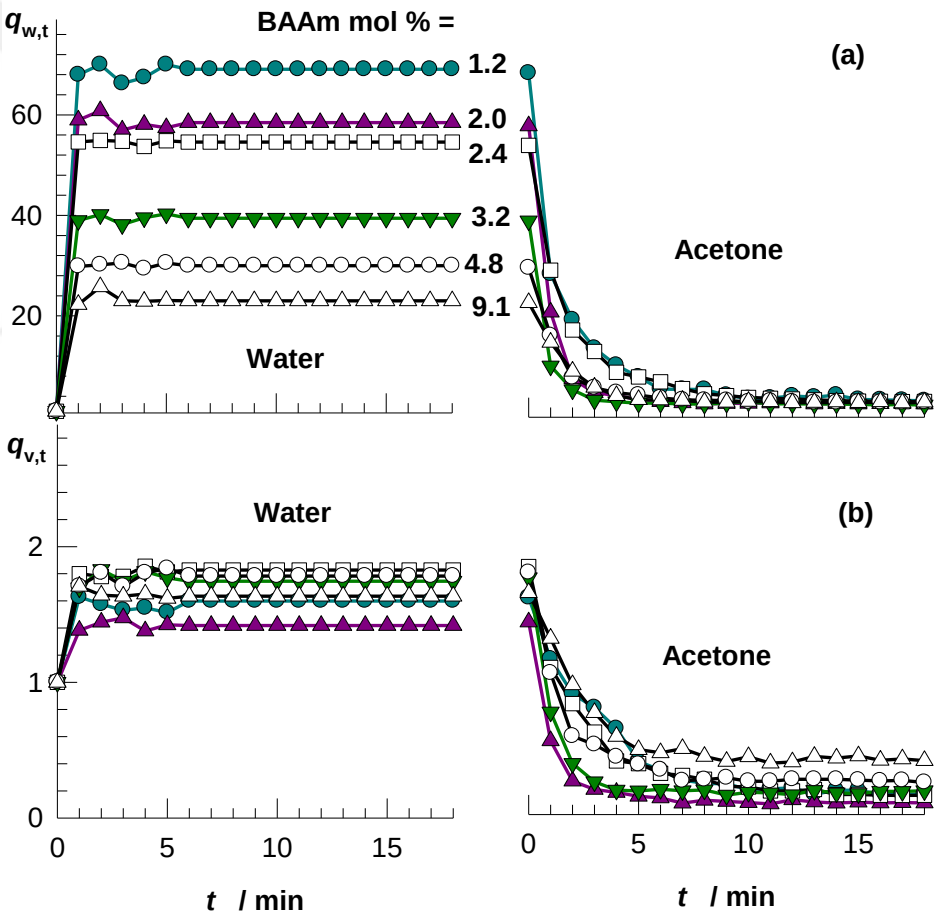

Figure 4.13 : Swelling and deswelling of PAMPS hydrogels in water and acetone, respectively. Weight $q_{w,t}$ (a) and volume swelling ratios $q_{v,t}$ (b) are shown as a function of time t. BAAm concentration is indicated. C_o = 10 wt %.

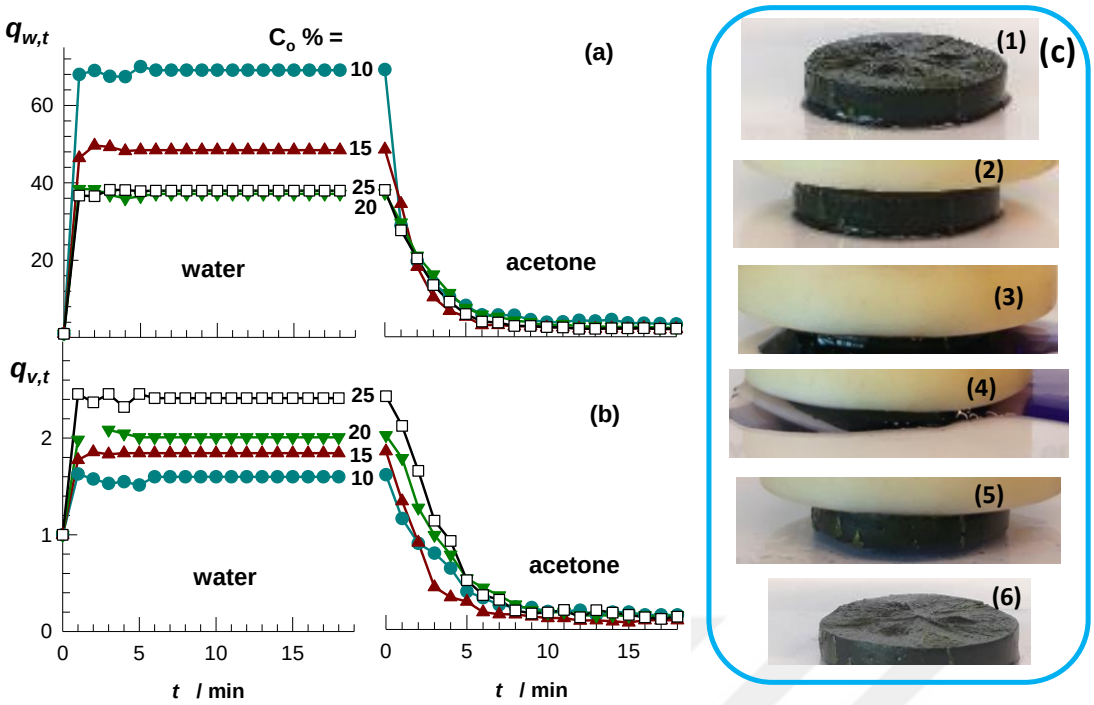

Figure 4.14 : (a, b): Swelling and deswelling of PAMPS cryogels in water and acetone, respectively. Weight $q_{w,t}$ (a) and volume swelling ratios $q_{v,t}$ (b) are shown as a function of contact time t. The monomer concentration C_o is indicated. BAAm = 1.2 mol %. (c): Images of a cryogel specimen under loading and unloading. The specimen was colored with a dye for clarity. C_o = 10 wt %. BAAm = 1.2 mol %.

4. Conclusions

Cryogelation is a simple and eco-friendly technique to produce macroporous hydrogels, so-called cryogels, exhibiting extraordinary properties including large porosity, complete squeezability, high-toughness, and superfast responsivity. Most of the results on cryogels reported so far, however, lack a more detailed analysis to provide real conditions of the cryogelation systems. This includes the melting temperature of the gelation system, the true concentration of the monomers in the unfrozen domains, and the amounts of frozen and unfrozen water during cryogelation. We investigated here the correlations between the cryogel properties and the real conditions of cryogelation. Formation of strong polyelectrolyte PAMPS cryogels was selected for this study because of their wide range of application areas, including water purification, food industry, agriculture, energy and environmental fields, and bioengineering. Cryogelation reactions were conducted in frozen aqueous solutions of AMPS and BAAm at -18 °C in the presence of a redox initiator system at -18 °C. We found that the nominal AMPS concentration C_o affects significantly the porous structure of the cryogels. Both the total volume of the pores and the

distance between pore channels decrease whereas the average diameter of the pores increases with increasing AMPS concentration C_o. These morphological variations depending on C_o could be explained with the local concentrations of the reaction components during cryogelation. The measurements reveal a continuous decrease of the volume of ice acting as a template for the pores in the reaction system with increasing $C_{o,}$ which is in accord with the experimental results. Moreover, the melting temperature T_m of the monomer solution was found to decrease with increasing C_o. Because decreasing T_m means a slower rate of freezing of water in the reaction solution, larger ice crystals will form as C_o is increased leading to the formation of larger pores and hence, smaller spacing between the pores. Further, decreasing freezing rate of water also leads to a lesser degree of alignment of growing ice crystals, which is in accord with the experimental results. The extent of cryoconcentration was found to be the highest at the lowest monomer concentration of 10 wt %, i.e., the true concentration C_{true} of the monomers in unfrozen domains is about 2.4-fold larger than its nominal value C_o. The results also show a significant improvement in the mechanical properties of the cryogels with increasing BAAm content. PAMPS cryogels prepared at 9.1 mol % BAAm exhibit the highest modulus (0.73±0.05 MPa) and could withstand up to 6.0±0.5 MPa compressive fracture stress.

The results of the present study thus reveal that the following parameters of cryogelation systems determine the properties of the final cryogels:

1) The melting temperature T_m of the cryogelation system,

2) the volume of ice after cryogelation

3) the fraction f_{unf} of unfrozen water during cryogelation, and

4) the monomer concentration C_{true} in unfrozen domains.

Because these parameters are determined by DSC, such simple measurements conducted on frozen gelation solutions are means for predicting the final cryogel properties. For instance, decreasing T_m of the cryogelation system also decreases the freezing rate of the solution leading to the formation of larger pores with a lesser degree of alignment. Further, the volume of ice template after cryogelation determines the total volume of the pores. Because the unfrozen domains in the reaction system form the pore walls in the final cryogels, the monomer concentration C_{true} in these domains reflects the polymer concentration of the pores walls. Thus, a

higher C_{true} means a higher polymer concentration of the pore walls and hence, a higher mechanical stability of the porous structure of the cryogels (Figure 4.9). Similarly, increasing the fraction f_{unf} of unfrozen water also increases the amount of polymer in the pore walls contributing to the mechanical strength of the cryogel.

5. CONCLUSIONS

In the current thesis, we focused on synthesizing and improving the mechanical performances of AMPS-based hydrogels. Firstly, PAMPS hydrogels are prepared using thermal and UV photopolymerization methods. In the first two parts of the thesis, studies on the production of PAMPS hydrogels that combine self-healing and high mechanical performance are presented. In the last part, the structural mechanical properties of PAMPS cryogels were investigated. The thesis presented here produced three publications, mainly based on fabricating mechanically strong and self healable PAMPS hydrogels, which are summarized in three sections as given below.

In the first part of the thesis, we present a simple synthetic strategy to prepare mechanically strong poly(2-acrylamido-2-methyl-1-propanesulfonic acid) (PAMPS) hydrogels with self-healing ability. Initiator-free polymerization of AMPS in aqueous solution in the presence of Laponite nanoparticles and N,N′-methylenebis(acrylamide) (BAAm) cross-linker produces hybrid-cross-linked hydrogels with fantastic mechanical properties. The hydrogels exhibit a high modulus (~700 kPa), compressive strength (45 MPa at ~90% strain), good resilience, and self-healing. The results reveal that the incorporation of Laponite and BAAm separately into the physical PAMPS network weakens hydrogen bonding interactions while their combination enhances these interactions and generate water-insoluble hydrogels with a high modulus. The superior properties of hybrid cross-linked hydrogels are attrubuted to the strengthening of the interactions between chemically cross-linked PAMPS chains and nanoparticles. The hybrid approach presented here might enable the preparation of mechanically strong nanocomposite hydrogels consisting of strongly or weakly charged polymer chains of different architecture.

In the second part of the thesis, we present for the first time highly stretchable superabsorbent PAMPS hydrogels formed via H-bonds entirely that are stable in water. UV polymerization of AMPS in aqueous solutions at 23 ± 2 °C without a chemical cross-linker produces hydrogels with large swelling capacities exceeding 1000 times their original mass. Although the hydrogels are stable in water, they

easily dissolve in chaotropic solvents, suggesting that they form via H-bonding interactions between PAMPS chains. We show that the high molecular weight of the primary chains of PAMPS hydrogels formed via UV polymerization contributes to the H-bonding cooperativity and hence is responsible for their stability in water. The incorporation of N,N-dimethylacrylamide (DMAA) segments into the physical PAMPS network further increases the molecular weight of the primary chains, leading to the enhanced mechanical strength of the hydrogels. PAMPS/DMAA hydrogels in their as prepared states exhibit a high modulus (up to 0.41 MPa), tensile fracture stress (up to 0.57 MPa), and high stretchability (~1000%) together with an extraordiinary swelling capacity (up to ~1700 $g \cdot g^{-1}$) and entire self-healing efficiency.

In the last part of the study, we investigate the correlations between the cryogelation conditions and properties of poly(2-acrylamido-2-methyl-1-propanesulfonic acid) (PAMPS) cryogels, which are attractive materials with a wide range of application areas. PAMPS cryogels are prepared by free-radical copolymerization of AMPS and N,N′-methylenebis(acrylamide) (BAAm) in aqueous solutions at −18 °C in the presence of a redox initiator system. The total pore volume of the cryogels decreases whereas the average pore diameter increases with increasing AMPS concentration C_o. The morphological variations depending on C_o could be explained with the local conditions during cryogelation, i.e., the melting temperature of the reaction solution, the ice volume, and the real concentration of the monomers in unfrozen domains. PAMPS cryogels prepared at 9.1 mol % BAAm exhibit the highest modulus (0.73 ± 0.05 MPa) and could withstand up to 6.0 ± 0.5 MPa compressive fracture stress.

In summary, at the end of the studies carried out in the first two parts of the thesis, PAMPS hydrogels, the most frequently encountered hydrogels in the literature, were synthesized that combine two contrasting properties namely a high mechanical strength and self-healing ability, were synthesized. In addition, at the end of the experiments, it was shown that tough and self-healing hydrogels with high mechanical performance could be obtained with only physical interactions such as electrostatic interactions and H-bonds. On the other hand, in the last part of the thesis, the relationship between the actual cryogelation conditions and the final properties of PAMPS cryogels has been clarified.

In follow-up studies, the use of cryogels with multiple network structure is planned. Within the scope of future studies, cryogels with a high swelling rate and capacity will be selected as the first network structure while hydrogel synthesis will be carried out within the pores of the cryogel. It is thought that self-healing cryo-hydrogels can be obtained when hydrogels with purely physical crosslinks are selected as the second network structure.

REFERENCES

[1] **Cordier, P., Tournilhac, F., Soulié-Ziakovic, C., & Leibler, L.** (2008). Self-healing and thermoreversible rubber from supramolecular assembly. *Nature*, *451*, 977.

[2] **Xing, X., Li, L., Wang, T., Ding, Y., Liu, G., & Zhang, G.** (2014). A self-healing polymeric material: From gel to plastic. *J. Mater. Chem. A*, *2*, 11049–11053.

[3] **Durmaz, S., & Okay, O.** (2000). Acrylamide/2-acrylamido-2-methylpropane sulfonic acid sodium salt-based hydrogels: Synthesis and characterization. *Polymer*, *41*, 3693–3704.

[4] **Topuz, F., & Okay, O.** (2009). Macroporous hydrogel beads of high toughness and superfast responsivity. *React. Funct. Polym.*, *69*, 273–280.

[5] **Boonkaew, B., Barber, P. M., Rengpipat, S., Supaphol, P., Kempf, M., He, J., John, V. T., & Cuttle, L.** (2014). Development and characterization of a novel, antimicrobial, sterile hydrogel dressing for burn wounds: Single-step production with gamma irradiation creates silver nanoparticles and radical polymerization. *J. Pharm. Sci.*, *103*, 3244–3253.

[6] **Beuermann, S., Buback, M., Hesse, P., Junkers, T., & Lacík, I.** (2006). Free-radical polymerization kinetics of 2-acrylamido-2-methylpropanesulfonic acid in aqueous solution. *Macromolecules*, *39*, 509–516.

[7] **Fisher, L. W., Sochor, A. R., & Tan, J. S.** (1977). Chain Characteristics of Poly (2-acrylamido-2-methylpropanesulfonate) Polymers. 1. Light-Scattering and Intrinsic-Viscosity Studies. *Macromolecules*, *10*, 949–954.

[8] **Liu, X., Tong, Z., & Hu, O.** (1995). Swelling Equilibria of Hydrogels with Sulfonate Groups in Water and in Aqueous Salt Solutions. *Macromolecules*, *28*, 3813–3817.

[9] **Tong, Z., & Liu, X.** (1994). Swelling Equilibria and Volume Phase Transition in Hydrogels with Strongly Dissociating Electrolytes. *Macromolecules*, *27*, 844–848.

[10] **Yang, C., Liu, Z., Chen, C., Shi, K., Zhang, L., Ju, X.-J., Wang, W., Xie, R., & Chu, L.-Y.** (2017). Reduced Graphene Oxide-Containing Smart Hydrogels with Excellent Electro-Response and Mechanical Properties for Soft Actuators. *ACS Appl. Mater. Interfaces*, *9*, 15758–15767.

[11] **Jones, A., & Vaughan, D.** (2005). Hydrogel dressings in the management of a variety of wound types: A review. *J. Orthop. Nurs.*, *9*.

[12] **Gong, J., P., Kurokawa, T., Narita, T., Kagata, G., Osada, Y., Nishimura,**

G., & Kinjo, M. (2001). Synthesis of hydrogels with extremely low surface friction [4]. *J. Am. Chem. Soc.*, *123*, 5582–5583.

[13] **Nalampang, K., Panjakha, R., Molloy, R., & Tighe, B. J.** (2013). Structural effects in photopolymerized sodium AMPS hydrogels crosslinked with poly(ethylene glycol) diacrylate for use as burn dressings. *J. Biomater. Sci. Polym. Ed.*, *24*, 1291–1304.

[14] **Calvert, P.** (2009). Hydrogels for soft machines. *Adv. Mater.*, *21*, 743–756.

[15] **Zhao, X.** (2014). Multi-scale multi-mechanism design of tough hydrogels: Building dissipation into stretchy networks. *Soft Matter*, *10*, 672–687.

[16] **Tanaka, Y., Fukao, K., & Miyamoto, Y.** (2000). Fracture energy of gels. *Eur. Phys. J. E*, *3*, 395–401.

[17] **Brown, H. R.** (2007). A model of the fracture of double network gels. *Macromolecules*, *40*, 3815–3818.

[18] **Mongondry, P., Tassin, J. F., & Nicolai, T.** (2005). Revised state diagram of Laponite dispersions. *J. Colloid Interface Sci.*, *283*, 397–405.

[19] **Mongondry, P., Nicolai, T., & Tassin, J.-F.** (2004). Influence of pyrophosphate or polyethylene oxide on the aggregation and gelation of aqueous laponite dispersions. *J. Colloid Interface Sci.*, *275*, 191–196.

[20] **Haraguchi, K., & Takehisa, T.** (2002). Nanocomposite hydrogels: A unique organic-inorganic network structure with extraordinary mechanical, optical, and swelling/De-swelling properties. *Adv. Mater.*, *14*, 1120–1124.

[21] **Haraguchi, K., Farnworth, R., Ohbayashi, A., & Takehisa, T.** (2003). Compositional effects on mechanical properties of nanocomposite hydrogels composed of poly(N,N-dimethylacrylamide) and clay. *Macromolecules*, *36*, 5732–5741.

[22] **Klein, A., Whitten, P. G., Resch, K., & Pinter, G.** (2015). Nanocomposite hydrogels: Fracture toughness and energy dissipation mechanisms. *J. Polym. Sci. Part B Polym. Phys.*, *53*, 1763–1773.

[23] **Okay, O., & Oppermann, W.** (2007). Polyacrylamide-clay nanocomposite hydrogels: Rheological and light scattering characterization. *Macromolecules*, *40*, 3378–3387.

[24] **Du, J., Chen, P., Adalati, A., Xu, S., Wu, R., Wang, J., & Zhang, C.** (2014). Preparation and mechanical properties of a transparent ionic nanocomposite hydrogel. *J. Polym. Res.*, *21*.

[25] **Gulyuz, U., & Okay, O.** (2014). Self-healing poly(acrylic acid) hydrogels with shape memory behavior of high mechanical strength. *Macromolecules*, *47*, 6889–6899.

[26] **Wang, H., & Brown, H. R.** (2004). Self-initiated photopolymerization and photografting of acrylic monomers. *Macromol. Rapid Commun.*, *25*, 1095–1099.

[27] **Panagiotopoulou, M., Beyazit, S., Nestora, S., Haupt, K., & Tse Sum Bui, B.** (2015). Initiator-free synthesis of molecularly imprinted polymers by

polymerization of self-initiated monomers. *Polymer, 66*, 43–51.

[28] **Chen, P., Xu, S., Wu, R., Wang, J., Gu, R., & Du, J.** (2013). A transparent Laponite polymer nanocomposite hydrogel synthesis via in-situ copolymerization of two ionic monomers. *Appl. Clay Sci., 72*, 196–200.

[29] **Funke, W., Okay, O., & Joos-Müller, B.** (1998). *Microgels - Intramolecularly Crosslinked Macromolecules with a Globular Structure*. *Adv. Polym. Sci.136*, 139−234.

[30] **Okay, O., Kurz, M., Lutz, K., & Funke, W.** (1995). Cyclization and Reduced Pendant Vinyl Group Reactivity during the Free-Radical Cross-Linking Polymerization of 1,4-Divinylbenzene. *Macromolecules, 28*, 2728–2737.

[31] **Haraguchi, K., Uyama, K., & Tanimoto, H.** (2011). Self-healing in nanocomposite hydrogels. *Macromol. Rapid Commun., 32*, 1253–1258.

[32] **Teodorescu, M., Andrei, M., Turturicə, G., Stənescu, P. O., Zaharia, A., & Sârbu, A.** (2015). Novel Thermoreversible Injectable Hydrogel Formulations Based on Sodium Alginate and Poly(N-Isopropylacrylamide). *Int. J. Polym. Mater. Polym. Biomater., 64*, 763–771.

[33] **D'Este, M., Alini, M., & Eglin, D.** (2012). Single step synthesis and characterization of thermoresponsive hyaluronan hydrogels. *Carbohydr. Polym., 90*, 1378–1385.

[34] **Kundu, M., Mallapragada, S., Larock, R. C., & Kundu, P. P.** (2010). Rheological properties of methylcellulose aqueous gels under dynamic compression: Frequency sweep and validity of scaling law. *J. Appl. Polym. Sci., 117*, 2436–2443.

[35] **Tavsanli, B., & Okay, O.** (2017). Mechanically strong hyaluronic acid hydrogels with an interpenetrating network structure. *Eur. Polym. J., 94*, 185–195.

[36] **Hao, J., & Weiss, R. A.** (2011). Viscoelastic and mechanical behavior of hydrophobically modified hydrogels. *Macromolecules, 44*, 9390–9398.

[37] **Williams, G., & Watts, D. C.** (1970). Non-symmetrical dielectric relaxation behaviour arising from a simple empirical decay function. *Trans. Faraday Soc., 66*, 80–85.

[38] **Gurtovenko, A. A., & Gotlib, Y. Y.** (2001). Dynamics of inhomogeneous cross-linked polymers consisting of domains of different sizes. *J. Chem. Phys., 115*, 6785–6793.

[39] **Ng, T. S. K., & McKinley, G. H.** (2008). Power law gels at finite strains: The nonlinear rheology of gluten gels. *J. Rheol. (N. Y. N. Y)., 52*, 417–449.

[40] **Okay, O.** (2009) General Properties of Hydrogels. In: Gerlach G., Arndt KF. (eds) *Hydrogel Sensors and Actuators. Springer Series on Chemical Sensors and Biosensors (Methods and Applications)*, (Vol 6, pp. 1−14). Springer, Berlin, Heidelberg.

[41] **Ahagon, A., & Gent, A. N.** (1975). Threshold fracture energies for elastomers. *J. Polym. Sci. Polym. Phys. Ed.*, *13*, 1903–1911.

[42] **Creton, C.** (2017). 50th Anniversary Perspective: Networks and Gels: Soft but Dynamic and Tough. *Macromolecules*, *50*, 8297–8316.

[43] **Phadke, A., Zhang, C., Arman, B., Hsu, C.-C., Mashelkar, R. A., Lele, A. K., Tauber, M. J., Arya, G., & Varghese, S.** (2012). Rapid self-healing hydrogels. *Proc. Natl. Acad. Sci. U. S. A.*, *109*, 4383–4388.

[44] **Zhang, H., Xia, H., & Zhao, Y.** (2012). Poly(vinyl alcohol) hydrogel can autonomously self-heal. *ACS Macro Lett.*, *1*, 1233–1236.

[45] **Cui, J., & Campo, A. D.** (2012). Multivalent H-bonds for self-healing hydrogels. *Chem. Commun.*, *48*, 9302–9304.

[46] **Liu, J., Song, G., He, C., & Wang, H.** (2013). Self-healing in tough graphene oxide composite hydrogels. *Macromol. Rapid Commun.*, *34*, 1002–1007.

[47] **Uzumcu, A. T., Guney, O., & Okay, O.** (2018). Highly Stretchable DNA/Clay Hydrogels with Self-Healing Ability. *ACS Appl. Mater. Interfaces*, *10*, 8296–8306.

[48] **Gong, Z., Zhang, G., Zeng, X., Li, J., Li, G., Huang, W., Sun, R., & Wong, C.** (2016). High-Strength, Tough, Fatigue Resistant, and Self-Healing Hydrogel Based on Dual Physically Cross-Linked Network. *ACS Appl. Mater. Interfaces*, *8*, 24030–24037.

[49] **Tuncaboylu, D. C., Sahin, M., Argun, A., Oppermann, W., & Okay, O.** (2012). Dynamics and large strain behavior of self-healing hydrogels with and without surfactants. *Macromolecules*, *45*, 1991–2000.

[50] **Okay, O.** (2015). *Self-healing hydrogels formed via hydrophobic interactions*. *Adv. Polym. Sci. 268*, 101−142.

[51] **Bilici, C., Can, V., Nöchel, U., Behl, M., Lendlein, A., & Okay, O.** (2016). Melt-processable shape-memory hydrogels with self-healing ability of high mechanical strength. *Macromolecules*, *49*, 7442–7449.

[52] **Deringer, V. L., Englert, U., & Dronskowski, R.** (2014). Covalency of hydrogen bonds in solids revisited. *Chem. Commun.*, *50*, 11547–11549.

[53] **Yanagisawa, Y., Nan, Y., Okuro, K., & Aida, T.** (2018). Mechanically robust, readily repairable polymers via tailored noncovalent cross-linking. *Science (80-.).*, *359*, 72–76.

[54] **Perrin, C. L., & Nielson, J. B.** (1997). *"Strong" hydrogen bonds in chemistry and biology*. *Annu. Rev. Phys. Chem. 48*, 511−544.

[55] **Dai, X., Zhang, Y., Gao, L., Bai, T., Wang, W., Cui, Y., & Liu, W.** (2015). A mechanically strong, highly stable, thermoplastic, and self-healable supramolecular polymer hydrogel. *Adv. Mater.*, *27*, 3566–3571.

[56] **Tang, L., Liu, W., & Liu, G.** (2010). High-strength hydrogels with integrated functions of h-bonding and thermoresponsive surface-mediated reverse transfection and cell detachment. *Adv. Mater.*, *22*, 2652–2656.

[57] **Gao, H., Wang, N., Hu, X., Nan, W., Han, Y., & Liu, W.** (2013). Double hydrogen-bonding pH-sensitive hydrogels retaining high-strengths over a wide pH range. *Macromol. Rapid Commun.*, *34*, 63–68.

[58] **Guo, M., Pitet, L. M., Wyss, H. M., Vos, M., Dankers, P. Y. W., & Meijer, E. W.** (2014). Tough stimuli-responsive supramolecular hydrogels with hydrogen-bonding network junctions. *J. Am. Chem. Soc.*, *136*, 6969–6977.

[59] **Jeon, I., Cui, J., Illeperuma, W. R. K., Aizenberg, J., & Vlassak, J. J.** (2016). Extremely Stretchable and Fast Self-Healing Hydrogels. *Adv. Mater.*, *28*, 4678–4683.

[60] **Zhang, Y., Li, Y., & Liu, W.** (2015). Dipole-dipole and h-bonding interactions significantly enhance the multifaceted mechanical properties of thermoresponsive shape memory hydrogels. *Adv. Funct. Mater.*, *25*, 471–480.

[61] **Hu, X., Vatankhah-Varnoosfaderani, M., Zhou, J., Li, Q., & Sheiko, S. S.** (2015). Weak Hydrogen Bonding Enables Hard, Strong, Tough, and Elastic Hydrogels. *Adv. Mater.*, *27*, 6899–6905.

[62] **Ding, H., Zhang, X. N., Zheng, S. Y., Song, Y., Wu, Z. L., & Zheng, Q.** (2017). Hydrogen bond reinforced poly(1-vinylimidazole-co-acrylic acid) hydrogels with high toughness, fast self-recovery, and dual pH-responsiveness. *Polymer*, *131*, 95–103.

[63] **Zhang, X. N., Wang, Y. J., Sun, S., Hou, L., Wu, P., Wu, Z. L., & Zheng, Q.** (2018). A Tough and Stiff Hydrogel with Tunable Water Content and Mechanical Properties Based on the Synergistic Effect of Hydrogen Bonding and Hydrophobic Interaction. *Macromolecules*, *51*, 8136–8146.

[64] **Gundogan, N., Melekaslan, D., & Okay, O.** (2002). Rubber elasticity of poly(N-isopropylacrylamide) gels at various charge densities. *Macromolecules*, *35*, 5616–5622.

[65] **Su, E., & Okay, O.** (2018). Hybrid cross-linked poly(2-acrylamido-2-methyl-1-propanesulfonic acid) hydrogels with tunable viscoelastic, mechanical and self-healing properties. *React. Funct. Polym.*, *123*, 70–79.

[66] **Kazantsev, O. A., Igolkin, A. V., Shirshin, K. V., Kuznetsova, N. A., Spirina, A. N., & Malyshev, A. P.** (2002). Spontaneous polymerization of 2-acrylamido-2-methylpropanesulfonic acid in acidic aqueous solutions. *Russ. J. Appl. Chem.*, *75*, 465–469.

[67] **Carreau, P. J.** (1972). Rheologıcal Equations From Molecular Network Theories. *Trans Soc Rheol*, *16*, 99–127.

[68] **Argun, A., Can, V., Altun, U., & Okay, O.** (2014). Nonionic double and triple network hydrogels of high mechanical strength. *Macromolecules*, *47*, 6430–6440.

[69] **Song, G., Zhang, L., He, C., Fang, D.-C., Whitten, P. G., & Wang, H.** (2013). Facile fabrication of tough hydrogels physically cross-linked by strong cooperative hydrogen bonding. *Macromolecules*, *46*, 7423–7435.

[70] **Kříž, J., Dybal, J., & Brus, J.** (2006). Cooperative hydrogen bonds of macromolecules. 2. Two-dimensional cooperativity in the binding of poly(4-vinylpyridine) to poly(4-vinylphenol). *J. Phys. Chem. B*, *110*, 18338–18346.

[71] **Říž, J., & Dybal, J.** (2007). Cooperative hydrogen bonds of macromolecules. 3. A model study of the proximity effect. *J. Phys. Chem. B*, *111*, 6118–6126.

[72] **Han, S., Cao, S., Wang, Y., Wang, J., Xia, D., Xu, H., Zhao, X., & Lu, J. R.** (2011). Self-assembly of short peptide amphiphiles: The cooperative effect of hydrophobic interaction and hydrogen bonding. *Chem. - A Eur. J.*, *17*, 13095–13102.

[73] **Nowick, J. S.** (2008). Exploring β-sheet structure and interactions with chemical model systems. *Acc. Chem. Res.*, *41*, 1319–1330.

[74] **Uemura, Y., McNulty, J., & Macdonald, P. M.** (1995). Associative Behavior and Diffusion Coefficients of Hydrophobically Modified Poly(N,N-dimethylacrylamides). *Macromolecules*, *28*, 4150–4158.

[75] **Relógio, P., Martinho, J. M. G., & Farinha, J. P. S.** (2005). Effect of surfactant on the intra- and intermolecular association of hydrophobically modified poly(N,N-dimethylacrylamide). *Macromolecules*, *38*, 10799–10811.

[76] **Khokhlov, A. R., & Kramarenko, E. Y.** (1994). Polyelectrolyte/Ionomer behavior in polymer gel collapse. *Macromol. Theory Simulations*, *3*, 45–59.

[77] **Zeldovich, K. B., & Khokhlov, A. R.** (1999). Osmotically active and passive counterions in inhomogeneous polymer gels. *Macromolecules*, *32*, 3488–3494.

[78] **Okay, O., & Durmaz, S.** (2002). Charge density dependence of elastic modulus of strong polyelectrolyte hydrogels. *Polymer*, *43*, 1215–1221.

[79] **Melekaslan, D., & Okay, O.** (2000). Swelling of strong polyelectrolyte hydrogels in polymer solutions: Effect of ion pair formation on the polymer collapse. *Polymer*, *41*, 5737–5747.

[80] **Manning, G. S.** (1969). Limiting laws and counterion condensation in polyelectrolyte solutions I. Colligative properties. *J. Chem. Phys.*, *51*, 924–933.

[81] **Morishima, Y., Nomura, S., Ikeda, T., Seki, M., & Kamachi, M.** (1995). Characterization of Unimolecular Micelles of Random Copolymers of Sodium 2-(Acrylamido)-2-methylpropanesulfonate and Methacrylamides Bearing Bulky Hydrophobic Substituents. *Macromolecules*, *28*, 2874–2881.

[82] **Scott, A. J., Riahinezhad, M., & Penlidis, A.** (2015). Optimal design for reactivity ratio estimation: A comparison of techniques for AMPS/acrylamide and AMPS/acrylic acid copolymerizations. *Processes*, *3*, 749–768.

[83] **Pooley, S. A., Rivas, B. L., Cárcamo, A. L., & Pizarro, G. D. C.** (2008). Hydrogels from N,N′-dimethylacrylamide-co-2-acrylamido-2-methyl-

1- propanesulfonic acid with salt-, temperature- and pH-responsiveness properties. *J. Chil. Chem. Soc.*, *53*, 1483–1489.

[84] **Mukhopadhyay, A., Cole, W. T. S., & Saykally, R. J.** (2015). The water dimer I: Experimental characterization. *Chem. Phys. Lett.*, *633*, 13–26.

[85] **Baker, M. I., Walsh, S. P., Schwartz, Z., & Boyan, B. D.** (2012). A review of polyvinyl alcohol and its uses in cartilage and orthopedic applications. *J. Biomed. Mater. Res. - Part B Appl. Biomater.*, *100 B*, 1451–1457.

[86] **Flory, P. J.** (1953). *In Principles of polymer chemistry*. *Univ. Press*. Ithaca, NY.

[87] **Treloar, L. R. G.** (1975). *The Physics of Rubber Elasticity*. Oxford: University Press.

[88] **Klotz, I. M.** (1993). Solvent water and protein behavior: View through a retroscope. *Protein Sci.*, *2*, 1992–1999.

[89] **Williams, D. H., Searle, M. S., Mackay, J. P., Gerhard, U., & Maplestone, R. A.** (1993). Toward an estimation of binding constants in aqueous solution: Studies of associations of vancomycin group antibiotics. *Proc. Natl. Acad. Sci. U. S. A.*, *90*, 1172–1178.

[90] **Gong, J. P., Katsuyama, Y., Kurokawa, T., & Osada, Y.** (2003). Double-network hydrogels with extremely high mechanical strength. *Adv. Mater.*, *15*, 1155–1158.

[91] **Sahiner, N., & Seven, F.** (2014). Energy and environmental usage of super porous poly(2-acrylamido-2-methyl- 1-propan sulfonic acid) cryogel support. *RSC Adv.*, *4*, 23886–23897.

[92] **Lozinsky, V. I.** (2002). Cryogels on the basis of natural and synthetic polymers: Preparation, properties and applications. *Russ. Chem. Rev.*, *71*, 489–511.

[93] **Lozinsky, V. I.** (2018). Cryostructuring of polymeric systems. 50.† cryogels and cryotropic gel-formation: Terms and definitions. *Gels*, *4*.

[94] **Okay, O., & Lozinsky, V. I.** (2014). *Synthesis and structure–property relationships of cryogels*. *Adv. Polym. Sci. 263*, 103−157.

[95] **Lozinsky, V. I., & Okay, O.** (2014). *Basic Principles of Cryotropic Gelation*. *Adv. Polym. Sci. 263*, 49−101.

[96] **Kudaibergenov, S. E.** (2019). Physicochemical, complexation and catalytic properties of polyampholyte cryogels. *Gels*, *5*.

[97] **Ozmen, M. M., & Okay, O.** (2006). Superfast responsive ionic hydrogels: Effect of the monomer concentration. *J. Macromol. Sci. Part A Pure Appl. Chem.*, *43*, 1215–1225.

[98] **Ak, F., Oztoprak, Z., Karakutuk, I., & Okay, O.** (2013). Macroporous silk fibroin cryogels. *Biomacromolecules*, *14*, 719–727.

[99] **Zhang, H., & Cooper, A. I.** (2007). Aligned porous structures by directional freezing. *Adv. Mater.*, *19*, 1529–1533.

[100] **Yetiskin, B., & Okay, O.** (2017). High-strength silk fibroin scaffolds with anisotropic mechanical properties. *Polymer*, *112*, 61–70.

[101] **Yetiskin, B., & Okay, O.** (2019). High-strength and self-recoverable silk fibroin cryogels with anisotropic swelling and mechanical properties. *Int. J. Biol. Macromol.*, *122*, 1279–1289.

CURRICULUM VITAE

Name Surname **:** Esra SU

EDUCATION **:**

- **B.Sc.** **:** 2013, Anadolu University, Faculty of Science, Chemistry Programme
- **M.Sc.** **:** 2015, Anadolu University, Graduate School of Sciences, Inorganic Chemistry Programme
- **Ph.D.** : 2021, Istanbul Technical University, Graduate School, Chemistry Programme

PROFESSIONAL EXPERIENCE AND REWARDS:

- 2015 −.... Research Assistant, Chemistry, Istanbul Technical University
- 2021−…. Leading Researcher, Republic of Kazakhstan Science Committee of the Ministry of Education and Science (AP09260760)
- 2019 − .... PhD scholarship, TUBITAK 1001 Scientific and Technological Research Projects (218M502)
- 2019− 2020 Academic Advisor, TUBITAK SME R&D Startup Support Projects (7190238)
- 2016 − 2019 Researcher, ITU Scientific Research and Development Support Program Projects (39957)
- 2013− 2015 Researcher, Anadolu University Scientific Research and Development Support Program Projects (1306F010)
- 2017 Best Poster First Prize, 6. Fiziksel Kimya Kongresi
- 2015/2 2211-A General Domestic Doctoral Scholarship
- 2008 Science Faculty First Prize, Anadolu University

PUBLICATIONS AND PRESENTATIONS ON THE THESIS:

- **Su, E.,** and Okay, O. (2018). Hybrid cross-linked poly (2-acrylamido-2-methyl-1-propanesulfonic acid) hydrogels with tunable viscoelastic, mechanical and self-healing properties. *React. Func. Polym., 123,* 70-79.

- **Su, E.,** and Okay, O. (2018). Hibrit Çapraz Bağlı AMPS Esaslı Hidrojeller, *Polimer2018 Uluslararası Katılımlı VII. Polimer Bilim ve Teknoloji Kongresi*, Eskişehir, Turkey. September 09-12.
- **Su, E.,** Yurtsever, M., Okay, O. (2019). A Self-Healing and Highly Strechable Strong Polyelectrolyte Hydrogel via Cooperative Hydrogen-Bonding as Superabsorbent Polymer. *Macromolecules, 52, 9,* 3257-3267.
- **Su, E.,** and Okay, O. (2019). Cryogenic formation-structure-property relationships of poly(2-acrylamido-2-methyl-1-propanesulfonic acid) cryogels. *Polymer, 178,* 121603.
- **Su, E.,** and Okay, O. (2019). Properties of PAMPS cryogels based on cryogelation conditions, *BIOMED 2019 24th International Biomedical Science & Technology Symposium*, İzmir, Turkey. October 17-20.

OTHER PUBLICATIONS AND PRESENTATIONS:

- **Su, E.,** Bilici, C., Bayazit, G., Ide, S., Okay, O. (2021). Solvent-Free UV Polymerization of n-Octadecyl Acrylate in Butyl Rubber: A Simple Way to Produce Tough and Smart Polymer Blends at Ambient Temperature. *ACS Appl. Mater. Interfaces, 13, 18,* 21786–21799.
- Toleutay, G., **Su, E.,** Kudaibergenov, S., Okay, O. (2020). Highly stretchable and self-healable polyampholyte hydrogels via hydrophobic modification. *Colloid Polym. Sci., 298,* 273–284.
- Goktas, H. M., Engiz, G., **Su, E.,** Yangin-Gomec, C. (2019). Comparative evaluation of biogas recovery during anaerobic treatment of aircraft deicing fluids at increased ratios in domestic wastewater. *Desalin. Water. Treat., 172,* 254−259.
- **Su, E.,** Guven, A., Kani, I. (2018). Oxygen bridged Homobinuclear Mn(II) compounds with Anthranilic acid: Theoretical calculations, oxidation and catalase activity. *Appl. Organomet. Chem., 32,* e4105.
- **Su, E.,** and Okay, O. (2017). Polyampholyte hydrogels formed via electrostatic and hydrophobic interactions. *Eur. Polym. J., 88,* 191-204.
- **Su, E.**, and Okay, O. (2017). Hidrofobik ve İyonik Etkileşimlerle Oluşturulan Supramoleküler Poliamfolit Hidrojeller, *6. Fiziksel Kimya Kongresi*, Zonguldak/Turkey. May 15-18.
- Guven, A., **Su, E.,** Kani, I. (2017). A STUDY ON SOME MANGANESE (II) COMPLEXES, *3rd International Conference on New Trends in Chemistry*, Helsinki/Finland. April 28-30.
- **Su, E.**, and Okay, O. (2017). Advancing behaviors of tough polyampholyte hydrogels, *5th International Conference on Multifunctional, Hybrid and Nanomaterials*, Lisbon/Portugal. March 06-10.
- **Su, E.,** and Okay, O. (2016). Supramolecular polyampholyte hydrogels formed via hydrophobic and ionic interactions, *PNG2016 Polymer Networks Group meeting*, Stockholm/Sweeden. June 19-23.
- **Su, E.**, and Kani, I. (2015). DNA-METAL INTERACTION STUDIES with OXYGEN BRIDGED BINUCLEAR Mn(II) COMPLEXES, *DRD2015 International Multidisciplinary Symposium on Drug Reseach & Development*, Eskişehir/Turkey. October 15-17.

- **Su, E.,** and Kani, I. (2015). Catalytic Application of MOF, Binuclear Manganese Complexes**,** *11th Nanoscience and Nanotechnology Conference (NanoTR-11)*, Ankara/Turkey. June 22-25.
- **Su, E.,** and Kani, I. (2015). Synthesis of oxygen bridged binuclear Mn(II) complexes with Anthralinic and 4-fluoro benzoic acid: catalase activity, *FLOHET-2015 Annual Florida Heterocyclic and Synthetic IUPAC-Sponsored Conference*, Gainesville/Florida. March 1-4.